Effective Single-Band Hamiltonians for Strongly Interacting Ultracold Fermions in an Optical Lattice

by
Jason P. Kestner

A dissertation submitted in partial fulfillment
of the requirements for the degree of
Doctor of Philosophy
(Physics)
in The University of Michigan
2009

Doctoral Committee:

Associate Professor Luming Duan, Chair
Professor James W. Allen
Professor Paul R. Berman
Professor Roberto D. Merlin
Professor Georg A. Raithel

To Mom and Dad.

ACKNOWLEDGEMENTS

I am deeply indebted to my advisor, Professor Luming Duan, for mentoring me over the last four years. Whenever I stopped by his office he would put aside what he was doing and welcome me in to talk. I always walked away feeling refreshed and enthused by the clarity and insight that he offered. I cannot adequately express my gratitude for the patience and understanding he showed while supervising my research. I count myself very blessed to have had such a generous and brilliant advisor.

I am also grateful to my undergraduate advisor at Michigan Technological University, Professor Robert Weidman, for introducing me to the wonderful world of quantum mechanics and to Professor Xania Payne at Jackson Community College for luring me into physics in the first place. Both, in their own unique ways, communicated a sense of scientific exhilaration which continues to inspire me.

I have been very fortunate to find myself surrounded by bright and interesting people over the course of my studies at the University of Michigan. However, I would like to particularly thank the people who graciously shared so much of their time and knowledge with me in office discussions and journal club meetings: Wei Yi, Bin Wang, Wei Zhang, Hao Fu, Alejandra Castro, Yong-Jian Han, Rachel Sapiro, Tim Goodman, Zhaohui Wei, Zhangqi Yin, Yang-Hao Chan, Zhe-Xuan Gong, and Chao Shen. I especially thank Guin-Dar Lin, my classmate, officemate, travel companion, and collaborator for the entire five years I have been here. I value his questions,

comments, and advice, but I value his friendship even more.

Finally, I must thank my family for their constant support. I have lived with my parents and siblings and commuted to Ann Arbor the past five years, during which time I have could not have been happier. I thank my parents for teaching me the joy of learning when I was young and for home-schooling me at a time when such a thing was unheard of. Their courage, sacrifice, and commitment merits a greater reward than I can bestow, but to them I dedicate this dissertation as a token of my gratitude. I thank Kendra, Daniel, Grace, Zeke, and Molly for helping me to maintain some semblance of sanity and perspective in my life and for making sure I get a good sunburn now and then. More than anything, I am grateful for my family's love, understanding, counsel, and spiritual encouragement.

TABLE OF CONTENTS

LIST OF TABLES

Table

LIST OF FIGURES

Figure

LIST OF APPENDICES

Appendix

ABSTRACT

In this dissertation, we develop simple single-band effective Hamiltonians for a fermionic gas across a Feshbach resonance in both a quasi-low-dimensional optical trap and a three-dimensional optical lattice. The proper theoretical description of these systems is nontrivial due to the multiband nature of the dimers which form in the ground state of the strongly interacting gas.

For the quasi-low-dimensional case, we show that the ground state of the gas has a significant population in the excited levels of the transverse trap. Hence, the effective low-dimensional (single-band) Hamiltonian must include the effects of this real population frozen in many transverse modes. We accomplish this through the definition of a "dressed molecule" state which incorporates the excited fraction.

For the three-dimensional case, a valid single-band lattice model at first seems impossible for strong interactions. However, we find effective single-band lattice models that remain valid by subtly accounting for the nontrivial structure of the on-site dimer. We perform explicit numerical calculations for two fermions in a double-well to demonstrate the range of validity of the models and their parameter values. In the process of investigation leading to these models we find other interesting results such as a ground state level crossing for three fermions in a single well and a set of Feshbach resonances induced by anharmonicity of the optical potential.

The ultracold neutral atom experiments related to the work presented within provide a flexible and well-controlled tool to observe aspects of quantum physics

not easily accessible or controllable in other systems. The combination of optical lattice trapping techniques with the ability to manipulate the interactions via a Feshbach resonance allows for the study of novel strongly correlated physics. This work addresses an important and fundamentally interesting issue for these systems and serves as a proper starting point for further theoretical studies in conjunction with experiment.

CHAPTER I

Introduction

1.1 Motivation

In only the past 15 years or so, the field of ultracold atomic physics has seen explosive growth spurred on by many exciting experimental achievements such as the observation of Bose-Einstein condensation [1], fermionic superfluidity [2], and the superfluid to Mott insulator transition [3], to name just a few. The ability to load an ultracold gas into an optical lattice potential and to adjust the atom-atom interaction via a magnetic Feshbach resonance creates a system with rich physics of broad interest. Current experimental and theoretical studies have applications in condensed matter, nuclear physics, astrophysics, and quantum information.

The connection between condensed matter systems and the exquisitely controllable optical lattice plus Feshbach resonance atomic system is especially exciting. The large number of experimentally accessible parameters (e.g., lattice depth and geometry and rotation, interaction strength, disorder, population imbalance, atomic properties and statistics, etc.) makes the system a testbed of seemingly boundless versatility. Many seminal models and concepts from condensed matter physics are difficult to thoroughly treat theoretically or computationally, and the extent to which they capture the essence of the complicated material system is in some cases not es-

tablished. Often, however, these models can be cleanly realized in an optical lattice system. This program of research may thus prove invaluable towards understanding exotic quantum behavior in materials, most notably, high-T_c superconductivity. Even more exciting is the prospect of observing new physics in the optical lattice system and using the insight gleaned there to *engineer* materials with previously undreamt behaviors.

1.2 Background

In this section we briefly discuss the basic concepts of the Feshbach resonance and the optical lattice. More detailed discussions can be found in abundance elsewhere (e.g. Refs. [4–6] and [7–11], respectively).

1.2.1 Optical lattices

In the classical picture, the interaction of a neutral atom with an electric field $\mathbf{E}$ is via the induced electric dipole, $\mathbf{d}$, resulting in an energy shift

$$\Delta U = -\mathbf{d} \cdot \mathbf{E} \simeq \alpha |\mathbf{E}|^2 \,. \tag{1.1}$$

where α is the linear polarizability of the atom, and generally depends on the frequency of the field as well as the details of the atom. Already the general idea of optical lattice trapping can be seen from this simple picture, as one can form a spatially periodic electric field using counter-propagating laser beams, resulting in a spatially periodic energy shift.

In a simple quantum picture, we can treat the atom as a two-level system where the atom has been prepared in level 1 and the level most nearly coupled resonantly to it by the laser field is level 2. The energy shift of level 1 induced by the laser field via a virtual absorption/emission process is immediately given by second-order

perturbation theory as

$$\Delta U \simeq \frac{|\langle 1|\mathbf{d}\cdot\mathbf{E}|2\rangle|^2}{\epsilon_1 + N\hbar\omega_L - (\epsilon_2 + (N-1)\,\hbar\omega_L)} = \hbar\frac{|\chi|^2}{\delta}\,, \tag{1.2}$$

where ϵ_i is a bare atomic energy in the absence of the field, N is the photon number, ω_L is the laser frequency, χ is the Rabi frequency, and $\delta \equiv \omega_L - (\epsilon_2 - \epsilon_1)/\hbar$ is the laser detuning from resonance. Once again, we see that a spatially varying electric field gives rise to an effective potential. Here, though, we see that the atom is attracted (repelled) by high-field regions for red- (blue-) detuned light. Of course, we need $|\delta| \gg |\chi|$ so that we can neglect population transfer to the other level, which is shifted by the same amount in the opposite direction. Furthermore, we have neglected spontaneous emission.

More generally, we turn to the steady state density matrix equations. For a standing wave electric field with $\langle 1|\mathbf{d}\cdot\mathbf{E}|2\rangle = \hbar\chi_0^* \cos kz e^{i\omega t} + c.c.$, the coherence ρ_{12} is given in the rotating-wave approximation for a frame rotating at the laser frequency by

$$v_z\frac{\partial\rho_{11}}{\partial z} = -i\chi_0^*\cos kz\rho_{21} + i\chi_0\cos kz\rho_{12} + \gamma_2\rho_{22} \tag{1.3}$$

$$v_z\frac{\partial\rho_{12}}{\partial z} = -i\chi_0^*\cos kz\,(\rho_{22}-\rho_{11}) - (\gamma + i\delta)\,\rho_{12} \tag{1.4}$$

$$v_z\frac{\partial\rho_{21}}{\partial z} = i\chi_0\cos kz\,(\rho_{22}-\rho_{11}) - (\gamma - i\delta)\,\rho_{21} \tag{1.5}$$

$$v_z\frac{\partial\rho_{22}}{\partial z} = i\chi_0^*\cos kz\rho_{21} - i\chi_0\cos kz\rho_{12} - \gamma_2\rho_{22}\,, \tag{1.6}$$

where v_z is the atomic velocity along z, γ_2 is the spontaneous decay rate, and $\gamma = \gamma_2/2 + \Gamma$, with Γ the collision rate. The force on the atom is the opposite of the gradient of the energy shift, so the quantum expectation value of the force is

$$\mathbf{F} = Tr\left[\rho\nabla\left(\mathbf{d}\cdot\mathbf{E}\right)\right] = -\hat{\mathbf{z}}\hbar k\chi_0\sin kz\rho_{12} + c.c. \tag{1.7}$$

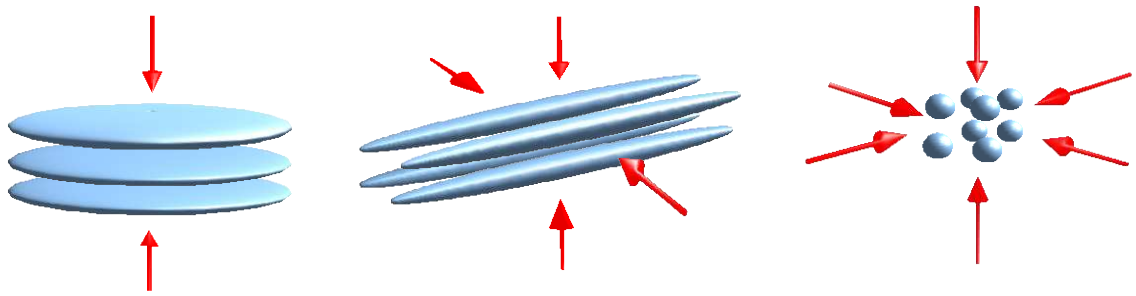

Figure 1.1: Lattices formed by applying orthogonal standing waves in one, two, and three directions.

If the atom is prepared in level 1, one can verify [11] that to first order in χ_0 the steady state solution for the coherence is

$$\rho_{12} = \frac{i\chi^*}{2}\left[\frac{e^{ikz}}{\gamma + i\left(\delta + kv_z\right)} + \frac{e^{-ikz}}{\gamma + i\left(\delta - kv_z\right)}\right]. \tag{1.8}$$

Some algebra then reduces Eq. (1.7) to

$$\begin{aligned}\mathbf{F} &= 2\hat{\mathbf{z}}\hbar k\delta\chi^2 \sin\left(kz\right)\frac{\left(k^2v_z^2 - \gamma^2 - \delta^2\right)\cos\left(kz\right) + 2kv_z\gamma\sin\left(kz\right)}{k^4v_z^4 + 2k^2v_z^2\left(\gamma^2 - \delta^2\right) + \left(\gamma^2 + \delta^2\right)^2} \\ &= \underbrace{\hat{\mathbf{z}}\hbar k\delta\sin\left(2kz\right)\frac{\chi^2}{\gamma^2 + \delta^2}}_{\text{gradient force}} + \underbrace{4\hat{\mathbf{z}}\hbar k\delta\sin^2\left(kz\right)\frac{\gamma\chi^2}{\left(\gamma^2 + \delta^2\right)^2}kv_z + O\left(k^2v_z^2\right)}_{\text{dissipative force}}\end{aligned} \tag{1.9}$$

and we see that in general there is a dissipative force due to spontaneous emission in addition to the conservative force due to the field gradient. (Actually, kinetic energy is dissipated only for red-detuned light; for blue-detuned light, the atoms take on energy from the field.) However, for $|\delta| \gg \gamma, kv_z$, the dissipative force goes as δ^{-3} and so is negligible compared to the gradient force, which goes as δ^{-1} and corresponds to the potential of Eq. (1.2). Thus, in this dissertation we shall always assume the laser field is far-detuned from any atomic resonance so that we may consider the atoms as moving in a conservative potential.

By applying counter-propagating beams along one, two, or three dimensions, one can form a stack of pancake-shaped wells, an array of cigar-shaped wells, or a three-dimensional lattice of spherical wells (see Fig. 1.1). Different interference patterns

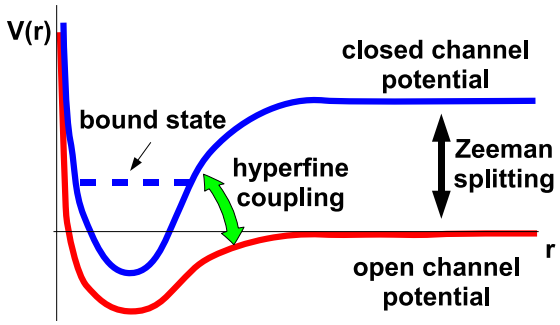

Figure 1.2: Simplified sketch of two collision potentials for atomic scattering in a magnetic field. The closed channel potential is for a predominantly singlet total electronic spin state, and the open channel is predominantly triplet. The bound state can be shifted up or down by tuning the magnetic field.

can be realized by changing the angles, polarizations, intensities, and wavelengths of the laser beams relative to one another, and one can realize a variety of lattice geometries.

1.2.2 Feshbach resonance

A Feshbach resonance occurs when the scattering continuum is coupled to one or more bound (or quasi-bound) states. The low-energy atom-atom scattering is then altered by virtual bound state formation and dissociation processes. One can think loosely of the colliding atoms getting caught in a bound state detuned an energy ΔE from the scattering threshold energy for a time $\Delta t \sim \hbar/\Delta E$ before escaping. When one of the bound state energies is close to the scattering threshold energy, the atoms can spend a long time in the bound state, resonantly enhancing the scattering length. The scattering states are asymptotically free, and are thus said to belong to the open channel. The bound states are not asymptotically free and cannot contribute to the initial or final states, so they are said to belong to the closed channel.

Formally, this can be described by a partition of the Hilbert space, $I = P + Q$, where P and Q denote projectors onto the open and closed channels, respectively.

Then Schrödinger's equation can be written as two coupled equations,

$$H_{PP}|\Psi^P\rangle + H_{PQ}|\Psi^Q\rangle = E|\Psi^P\rangle \tag{1.10}$$

$$H_{QQ}|\Psi^Q\rangle + H_{QP}|\Psi^P\rangle = E|\Psi^Q\rangle\,, \tag{1.11}$$

where $H_{PP} = PHP$, $|\Psi^P\rangle = P|\Psi\rangle$, etc. We can obtain an effective Hamiltonian for the open channel by formally solving the closed channel for $|\Psi^Q\rangle$ and back-substituting it into the open channel equation, yielding $H^{\text{eff}}_{PP}|\Psi^P\rangle = E|\Psi^P\rangle$, where

$$H^{\text{eff}}_{PP} = H_{PP} + H_{PQ}\frac{1}{E - H_{QQ}}H_{QP} = H_{PP} + \sum_i H_{PQ}\frac{|\phi_i\rangle\langle\phi_i|}{E-\epsilon_i}H_{QP}\,, \tag{1.12}$$

with $|\phi_i\rangle$ and ϵ_i the eigenstates and energies of H_{QQ}.

For simplicity, we will ignore direct interactions between open channel atoms and focus on the resonant scattering due to the coupling between channels. In this case, the eigenstates of H_{PP} are plane waves, $|\mathbf{k}\rangle$, with energy $\hbar^2k^2/m$ in the relative frame. Furthermore, we will take only one bound state, $|\phi\rangle$, with energy, ϵ, close enough to the scattering threshold to be important. Relaxing these assumptions does not add anything qualitatively.

The asymptotic outgoing scattered state can then be formally constructed in the usual way as

$$|\psi^+_{\mathbf{k}}\rangle = |\mathbf{k}\rangle + \frac{1}{E + i0^+ - H_{PP}}V^{\text{eff}}_{PP}|\psi^+_{\mathbf{k}}\rangle = |\mathbf{k}\rangle + \int d\mathbf{q}\frac{|\mathbf{q}\rangle\langle\mathbf{q}|H_{PQ}|\phi\rangle\langle\phi|H_{QP}|\psi^+_{\mathbf{k}}\rangle}{(E + i0^+ - \hbar^2q^2/m)\,(E-\epsilon)}\,. \tag{1.13}$$

The two-body T-matrix contains information on all possible two-body processes contributing to the scattering of an incoming plane wave to an outgoing scattered state and is defined such that

$$\langle\mathbf{k}|T\,(E)\,|\mathbf{k}'\rangle = \langle\mathbf{k}|V^{\text{eff}}_{PP}|\psi^+_{\mathbf{k}'}\rangle = \frac{\langle\mathbf{k}|H_{PQ}|\phi\rangle\langle\phi|H_{QP}|\psi^+_{\mathbf{k}'}\rangle}{E-\epsilon}\,. \tag{1.14}$$

By acting on both sides of Eq. (1.13) with $\langle\phi|H_{QP}$, we obtain

$$\langle\phi|H_{QP}|\psi^{+}_{\mathbf{k}'}\rangle = \frac{\langle\phi|H_{QP}|\mathbf{k}'\rangle}{1-\frac{\Sigma(E)}{E-\epsilon}}\,, \tag{1.15}$$

where $\Sigma(E) \equiv \int d\mathbf{q}\frac{|\langle\mathbf{q}|H_{PQ}|\phi\rangle|^2}{E+i0^+-\hbar^2q^2/m}$ can be interpreted as a molecular self-energy due to dressing by uncoupled open channel atoms. Using this result, the T-matrix becomes

$$\langle\mathbf{k}|T(E)|\mathbf{k}'\rangle = \frac{\langle\mathbf{k}|H_{PQ}|\phi\rangle\langle\phi|H_{QP}|\mathbf{k}'\rangle}{E-[\epsilon+\Sigma(E)]}\,. \tag{1.16}$$

The scattering amplitude and s-wave scattering length are related to the T-matrix by $f(\mathbf{k},\mathbf{k}') = -\frac{m}{4\pi\hbar^2}\langle\mathbf{k}|T(\hbar^2k'^2/m+i0^+)|\mathbf{k}'\rangle$ and $a_s = \frac{m}{4\pi\hbar^2}\lim_{k\to0}\langle\mathbf{k}|T(\hbar^2k^2/m+i0^+)|\mathbf{k}\rangle$, which yields

$$a_s = -\frac{m}{4\pi\hbar^2}\frac{|\langle\mathbf{0}|H_{PQ}|\phi\rangle|^2}{\epsilon+\Sigma(0)}\,. \tag{1.17}$$

The scattering length clearly goes through a resonance as the (loosely speaking) dressed bound state energy, $\epsilon+\Sigma(0)$, is somehow tuned through the scattering threshold.

In addition to this striking effect on the scattering physics, the coupling to the closed channel also introduces a bound state comprising a mixture of open and closed channel components. The definition of the T-matrix can be recast in terms of the Green's function as $T = V + VGV = V + V(E-H)^{-1}V$, so the T-matrix has simple poles at the discrete eigenenergies and a branch cut along the continuous eigenenergies. Thus it is evident that an energy that satisfies the self-consistent equation $E = \epsilon+\Sigma(E)$ corresponds to an eigenstate. This state separates from the continuum and becomes bound for $\epsilon+\Sigma(E) < 0$, corresponding to $a_s > 0$. We will have much to say in later chapters about this state, as it has a nontrivial structure and is the ground state of the system (neglecting possible deeply bound states in either channel, against which the system is metastable).

In ultracold atomic experiments, the interatomic potential depends on the total electronic spin, $\mathbf{S}$, of the colliding atoms, so scattering is naturally described by a multichannel model with the hyperfine interaction providing the coupling between channels. A Feshbach resonance occurs when one of the potentials supports a bound state energetically close to the scattering threshold of another potential, provided the two electronic spin states to which they correspond are coupled.

Crucially, turning on a magnetic field, $\mathbf{B}$, shifts the atomic energies by about $2\mu_B \mathbf{S} \cdot \mathbf{B}/\hbar$. Thus, by tuning the magnetic field, any two potentials can be shifted relative to each other such that a bound state of one channel becomes resonant with the scattering threshold of the other, as depicted in Fig. 1.2. It is conventional to recast Eq. (1.17) in terms of more experimentally accessible parameters as

$$a_s = a_{bg}\left(1 - \frac{W}{B - B_0}\right), \tag{1.18}$$

where the first term is the nonresonant background scattering which we neglected in our derivation. The resonance width, W, is related to the coupling strength in Eq. (1.17), and the detuning of the magnetic field from the resonance point, B_0, is linearly related to the bound state detuning from threshold. The s-wave scattering length is sufficient to describe the low-energy interactions, since scattering in higher partial waves is highly suppressed at ultracold temperatures by the centrifugal barrier, which is typically on the order of a few milliKelvin. Furthermore, for fermions this means that only atoms in different internal states have non-negligible interaction at low temperature, since Pauli exclusion forbids s-wave scattering of identical fermions.

Note that the Feshbach resonance mechanism is not the same as that for the familiar shape resonance, which is a one-channel phenomenon occurring when a weakly bound state in the collision potential exists near the scattering threshold. Although

the scattering length displays the same behavior in both cases as the bound state is tuned near threshold, the ground state (setting aside far-detuned deeply bound states) in the two-channel case is generally different from that of the one-channel case in that it contains an admixture of tightly bound closed channel molecules. For a narrow Feshbach resonance or for small, positive scattering length far from a wide Feshbach resonance, this closed channel fraction is significant, and a one-channel model cannot produce the correct ground state. However, for wide Feshbach resonances, the closed channel fraction is generally only a few percent near resonance, and the two-channel model is equivalent to a magically tunable one-channel model there. (There is an exception if the nonresonant open channel background interaction supports a bound state [12, 13].) When this is the case, one is free to neglect the closed channel and simply treat the near-resonant atomic system in a one-channel approximation as interacting via a magnetic field-dependent potential.

1.2.3 Typical values

Even though the laser parameters can be continuously tuned and the Feshbach parameters can be changed by using a different pair of scattering channels or by using a different atomic species, we list some typical experimental orders of magnitude of several characteristic parameters in Table 1.1.

1.3 Dissertation Overview

1.3.1 Conceptual overview

As mentioned in Sec. 1.1, the combination of an optical lattice and a Feshbach resonance leads to experimental flexibility to rival a *gedanken* experiment! This playground for physicists will hopefully lead to a better understanding of strongly interacting many-body physics, a topic which contains many puzzles and mysteries,

laser wavelength/lattice spacing	λ	1 μm
recoil energy	E_R	10 kHz
lattice depth	V_0	100 kHz
Rabi frequency	χ_0	100 MHz
laser detuning	δ	100 GHz
spontaneous decay rate	γ	10 MHz
dipole trapping frequency	ω	100 kHz
background scattering length	a_{bg}	10 nm
resonance width	W	10 G
resonant field	B_0	100 G
number density	n	10^{13} cm^{-3}
temperature	T	100 nK
Fermi temperature	T_F	1 μK

Table 1.1: Typical parameter values for the laser, atoms, and atomic gas in ultracold fermion experiments.

as dramatically illustrated by the enduring riddle of high-temperature superconductivity. A new paradigm becomes necessary to describe these strongly correlated systems, and the controlled environment of ultracold atomic experiments can help provide, or at least test, new insights.

In this dissertation, we consider fermionic atoms with two relevant internal states interacting close to a wide Feshbach resonance in an optical lattice. Our focus is not on the many-body physics, *per se*, but on the correct theoretical description of the interplay between the external potential and the strong interaction. This constitutes a proper starting point for detailed studies of phase diagrams or other many-body calculations.

Around resonance, the interaction energy of the cold atoms can be on the order of the lattice bandgap. This interplay of the energy scales makes even the two-body physics nontrivial, since the open channel continuum splits into a band structure and excited bands can be activated through the resonant coupling with the closed channel. (The closed channel also develops a band structure, but this corresponds to center-of-mass excitations which are usually ignored. We will discuss the consequences of this in detail in Chapter VI.) This multi-band behavior must be accounted for in

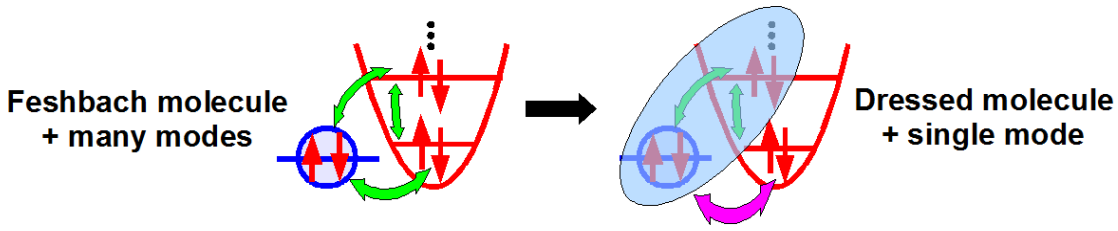

Figure 1.3: Sketch of the dressed molecule concept in a quasi-low-dimensional scenario. A bare molecule coupled to several open channel bands can be thought of as a dressed molecule with an effective coupling to a single open channel band.

any model Hamiltonian. A model Hamiltonian which does not even capture the two-body physics surely cannot accurately capture the many-body physics!

The main concept of the thesis presented herein is that the ground state of two resonantly interacting atoms in an external potential has a significant fraction in excited bands, but this nontrivial two-body state can be written in a single-band form by defining "dressed molecules" which absorb the excited population and act as point bosons. We shall see that when the optical potential is applied along only one or two dimensions, open channel atom pairs in higher transverse bands remain spatially small in all dimensions, so the dressed molecule is defined as the bare closed channel molecule plus the transversely excited atom pairs, as sketched in Fig. 1.3. When the optical potential is applied along all three dimensions, even atom pairs in the lowest band are small and the dressed molecule is simply defined as the on-site dimer state for a single well.

At the two-body level, this is a mere tautology. However, under certain realistic experimental conditions, many-body effects are not strong enough to overcome the bandgap, so multiband physics enter only through the two-body state. The system can then be thought of as single-band atoms coupled to a dressed molecule whose structure is static, fully fixed by two-body considerations. Thus one can write an effective single-band Hamiltonian in terms of open channel atoms and dressed closed

channel molecules. Such a Hamiltonian incorporates the two-body multiband physics through the hidden structure of the dressed molecule.

We pursue this concept along two directions. In the next two chapters, we treat a dilute atomic gas in a strong optical lattice applied along one or two dimensions so that the dynamics in an isolated well are expected to be quasi-low-dimensional (see Fig. 1.1). Low-dimensional systems are particularly interesting because of the enhanced role of quantum fluctuations, leading to physics which are not captured by a mean-field approach. As a result, there have been many recent theoretical proposals to observe interesting strongly correlated phenomena unique to one or two dimensions (e.g. Luttinger liquids, Luther-Emery liquids, or the Berezinskii-Kosterlitz-Thouless phase transition) in transversely trapped ultracold fermionic atoms [14–18]. These proposals typically assume that the atoms are frozen into the lowest transverse band, allowing an obvious low-dimensional description. However, we show that the experimentally relevant situation is actually more subtle, with transverse multiband aspects as mentioned above. Nonetheless, we are able to write an effective low-dimensional Hamiltonian which accounts for multiband population near a Feshbach resonance and justifies prior and ongoing theoretical investigation of low-dimensional physics in this context, albeit with a modified mapping between the parameters appearing in a low-dimensional Hamiltonian and the physical parameters relevant in an experiment.

In the penultimate three chapters, we treat an fermionic gas loaded into a three-dimensional optical lattice at low filling factor. Much attention has been focused on proposing and performing experiments with such a system that realize some lattice Hamiltonian supporting novel strongly correlated physics, such as lattice supersolids, exotic spin liquids, the Fulde-Ferrell-Larkin-Ovchinnikov phase, d-wave superfluidity,

etc. Far from a Feshbach resonance, this system is an ideal realization of the Hubbard model, and the transition to a Mott insulator state has recently been observed [19]. It is natural then to consider possible lattice models applicable near a Feshbach resonance. Single-band lattice models have been considered for this case [20, 21], but these are only valid for extremely weak atom-molecule coupling rates. Brute force multiband Hubbard models sometimes make heuristic appearances in the literature, but they are too unwieldy for any practical purposes and are quickly discarded where calculations begin. This has been an obstacle to obtaining an accurate understanding of experiments performed in the strongly interacting regime. However, a practical and realistic effective single-band lattice model has recently been proposed which accounts for the multiband nature of the onsite dimer [22, 23]. This model resembles the general form of either the Hubbard or $t - J$ model, but contains some novel features. We discuss this proposal and perform explicit calculations to determine where this model is valid and how its parameters are related to the experimental parameters, making it a valuable tool for future calculations. We also discover that the anharmonicity of the lattice couples the atoms to a series of closed channel states and plays an important role near the Feshbach resonance.

1.3.2 Outline

In Chapter II we discuss conditions for the realization of a quasi-low-dimensional system. We show that in the presence of a Feshbach resonance, even for a very deep lattice and/or dilute gas, transverse excited modes cannot realistically be frozen out. We discuss the ground state structure in detail here. The work presented in this chapter is published in Ref. [24].

In Chapter III we discuss how such a system can be considered – and described – as effectively low-dimensional, even in the presence of populated transverse modes.

Here we introduce the dressed molecule mentioned above, accounting for the nonzero, but frozen, excited transverse atomic population distribution. Using this idea, we derive an effective one-band, low-dimensional Hamiltonian. The work presented in this chapter is published in Ref. [25].

In Chapter IV, we address the low-energy physics of three fermions, two in the same internal state and one in another, trapped in a single three-dimensional harmonic well. The motivation for this calculation is to check whether triply-occupied sites contribute to the low-energy physics of a three-dimensional lattice system near resonance in the case where the average number of atoms per site is no greater than two. We show that they do not. In the process, we also find a ground state level crossing, possibly indicating a quantum phase transition for a many-body system. The work presented in this chapter is published in Ref. [26].

In Chapter V, we use the result of Chapter IV and general considerations of the relevant Hilbert space structure to define effective single-band lattice models that remain valid for strongly interacting gases in a three-dimensional lattice. This is contrasted to the single-band Hubbard model derived from considerations of the lowest band only. We show that the anharmonicity of the lattice has some interesting effects near resonance. We also perform some numerical calculations to determine the parameters of our effective models.

In Chapter VI, we consider in more detail the effects on the Feshbach resonance picture of the coupling between the center-of-mass and relative motion due to the anharmonicity of the optical lattice potential. We find that many resonances will be induced by this coupling, permitting greater control of the atomic state via magnetic field sweeps.

CHAPTER II

Conditions of Low Dimensionality for Fermionic Gases in a Transverse Trap

2.1 Chapter Overview

For a dilute atomic gas in a strong transverse trapping potential, one normally expects that, in the ground state, the gas will populate only the lowest transverse level. We show, however, that for the strongly interacting gas under a Feshbach resonance, the ground state includes a large fraction of atoms in excited levels of the trap, even if the gas is in the dilute limit and the trap is very strong. This is because the effective atom-molecule coupling is typically enhanced to many times the trap mode spacing by an induced confinement along the untrapped dimension(s). Thus one cannot "freeze out" the transverse degrees of freedom except under certain highly restrictive conditions.

2.2 Introduction

Recently, the system of interacting atomic gas at low dimensions has attracted considerable interest as it supports a wealth of physics [15, 17, 27–37]. For ultracold atoms, low dimensions are typically achieved by applying a transverse optical lattice potential [3, 38, 39]. With a one- (or two-) dimensional deep optical lattice potential, the atoms trapped at different potential wells basically do not interact with each

other. For a weakly interacting gas, one can then freeze out the transverse degrees of freedom by assuming the system to be in the lowest level of the trap potential. The atomic gas at each individual potential well thus behaves as an effective two- (or one-) dimensional system.

The condition for achieving effective low-dimensionality in an optical lattice becomes more involved if one has a strongly interacting atomic gas. One of the most exciting directions in current atomic physics is to study this strongly interacting atomic gas, where the effective interaction as measured by the atomic scattering length can be tuned in the full range via a Feshbach resonance through control of an external magnetic field [2, 40, 41]. As discussed in Chapter I, the Feshbach resonance comes from the coupling of atoms in the open collision channel to the molecules in the closed channel. If this atom-molecule coupling rate becomes larger than the level spacing of the transverse trapping potential, one cannot assume a low-dimensional system by freezing the transverse mode in the lowest level [22, 42]. On the other hand, intuitively, one may expect that the effective atom-molecule coupling rate always decreases when we make the gas more dilute, and the transverse level spacing increases when we raise the trapping laser intensity. So, for a sufficiently dilute gas under a strong transverse trap, one can still get the transverse level spacing larger than the atom-molecule coupling rate. With this expectation, several recent works have studied properties of low-dimensional strongly interacting gas by (implicitly) assuming the transverse mode in the trap ground state [15, 17].

In this chapter, we want to show that the condition of low-dimensionality for strongly interacting atoms under a transverse trap is more subtle than the above simple picture. In the low-dimensional trap, there exists a bound dimer state for all detunings. Thus we cannot make the effective atom-molecule coupling arbitrarily

weak by diluting the gas, as it will be determined by the dimer length scale rather than the average inter-atom distance. In the dilute limit, the ground state of the system is a gas of independent dimers. We will show that in this limit, for the ground state of the system, we will still have a significant (actually, dominant) fraction of the atomic population in the excited transverse levels under a typical wide Feshbach resonance and realistic confinement. Furthermore, it is very ineffective to reduce the transverse excited fraction by increasing the trapping laser intensity. For realistic atoms such as ^{40}K or ^{6}Li, even if the trapping potential is increased to some completely impractical level, the transverse excited fraction is not yet negligible. The basic reason for this unusual phenomena is that increasing the trap strength increases the binding energy and correspondingly reduces the size of the dimers, even along the untrapped dimension(s). So, although the transverse level spacing increases, the effective atom-molecule coupling is also significantly enhanced. As a net effect, the atomic population in the transverse excited levels becomes pretty insensitive to the magnitude of the trapping potential. Although the result here does not preclude the possibility of an effective low-dimensional Hamiltonian for strongly interacting atoms under the transverse trap, it indeed shows that in general, one cannot neglect the real atomic population in the transverse excited levels and simply renormalize the coupling due to virtual excited populations, so derivation of an effective low-dimensional Hamiltonian is trickier than one might naively expect [22, 25].

In the next section, we give the general formalism for strongly interacting atoms under a transverse trap in the dilute gas limit. In that limit, the basic picture is captured by two-body physics. For the ground state of the system, the atoms form pairs, and interaction between the pairs become negligible. There have been a few works on description of two-body physics of strongly interacting atoms in a trap using

the single-channel model [32–37]. Recently, there have also been descriptions of the problem with a more realistic two-channel model for the Feshbach resonance (in one-dimensional or three-dimensional traps [20, 42–44]). The formalism of Refs. [20, 42, 44], however, neglects the atomic background scattering, while Ref. [43] employs first quantization form. We extend the formalism in second quantization form to include the background scattering, which becomes necessary when the system is outside of the near-resonance region. In addition, our formalism is independent of trap dimensionality and facilitates direct comparison between atoms trapped in one, two, and three dimensions. In Sec. 2.4, we present our main calculation results for the condition of low-dimensionality under one-dimensional or two-dimensional transverse traps. We will also give detailed studies of the atomic population distributions in the transverse levels and in the free dimension(s) for the ^{40}K and ^{6}Li atoms under trapping potentials of various intensities.

2.3 General Formalism

2.3.1 The Hamiltonian

To achieve a D-dimensional ($D < 3$) atomic gas, we assume a $(3-D)$ -dimensional optical lattice applied along the transverse direction. The lattice potential barrier is high so that the atomic interaction between different potential wells becomes negligible. With a strong lattice potential, the atoms at the bottom of the potential wells basically see a transverse harmonic trap. The atomic gas in each well can then be modeled as free in D dimensions ($D = 1, 2$) and trapped by a $(3 - D)$-dimensional harmonic potential of frequency ω along the transverse direction. (A single well of the lattice potential can be well approximated with a harmonic trap.) The atoms are of mass m and possess internal states $\sigma = \{\uparrow, \downarrow\}$. We treat the problem of strongly interacting atoms across a Feshbach resonance using the conventional two-channel

field theory for Feshbach resonance [4, 45], although one could also use a single-channel approach with an energy-dependent pseudopotential [46]. The short range interaction between closed-channel molecules and open-channel atoms is modeled by a delta function, which is entirely appropriate in the low-energy regime where the range of the interaction potential is much smaller than any of the other length scales. For fermions of mass m possessing internal states $\sigma = \{\uparrow, \downarrow\}$, with s-wave contact interactions, the Hamiltonian is

$$H = \sum_{\sigma=\uparrow,\downarrow} \int d^3\mathbf{r} \Psi_\sigma^\dagger \left(-\frac{1}{2}\nabla^2 + \frac{1}{2}\sum_{i=1}^{3-D} x_i^2 \right) \Psi_\sigma + \int d^3\mathbf{r} \Phi^\dagger \left(-\frac{1}{4}\nabla^2 + \sum_{i=1}^{3-D} x_i^2 + \nu_b \right) \Phi$$
$$+ g_b \int d^3\mathbf{r} \left(\Psi_\uparrow^\dagger \Psi_\downarrow^\dagger \Phi + h.c. \right) + U_b \int d^3\mathbf{r} \Psi_\uparrow^\dagger \Psi_\downarrow^\dagger \Psi_\downarrow \Psi_\uparrow \quad (2.1)$$

where $\Psi(\mathbf{r})$ is the atomic field operator and $\Phi(\mathbf{r})$ is the molecular field operator. Above, and throughout this chapter, we use dimensionless quantities with all energies in units of $\hbar\omega$ and all lengths in units of the trap length scale, $a_t = \sqrt{\hbar/m\omega}$. The dimensionless parameters are defined as follows: ν_b is the bare detuning (in units of $\hbar\omega$), g_b is the bare atom-molecule coupling rate (in units of $\hbar\omega a_t^{3/2}$), and U_b is the bare background atomic scattering rate (in units of $\hbar\omega a_t^3$). We refer to them as bare parameters because the use of a delta function interaction introduces unphysical ultraviolet divergences, and one must use a renormalization scheme in order to recover physical results. The bare parameters are related to the physical ones via the standard renormalization relations [45, 47]:

$$U_c^{-1} = \int \frac{d^3\mathbf{k}}{(2\pi)^3} \frac{1}{2E_\mathbf{k}} = \frac{\sqrt{E_c}}{2^{3/2}\pi}, \quad \Gamma^{-1} = 1 - U_p U_c^{-1},$$
$$U_b = \Gamma U_p, \quad g_b = \Gamma g_p, \quad \nu_b = \nu_p + \Gamma g_p^2 U_c^{-1}, \quad (2.2)$$

where the subscript p denotes physical parameters, $E_\mathbf{k} \equiv \mathbf{k}^2/2$, and the integral is taken in three dimensions with an explicit energy cutoff E_c imposed on two dimen-

sions [1]. The physical parameters g_p, U_p, ν_p are determined from the scattering data as

$$U_p = 4\pi a_{bg}/a_t\,, \quad g_p = \sqrt{4\pi \frac{\mu_{co} W}{\hbar\omega} \frac{|a_{bg}|}{a_t}}\,, \quad \nu_p = \frac{\mu_{co}\,(B - B_0)}{\hbar\omega} \tag{2.3}$$

(μ_{co} is the difference in magnetic moments between the two channels) [22], where we have assumed that the s-wave scattering length near resonance has the form [4]

$$a_s = a_{bg}\left(1 - \frac{W}{B - B_0}\right)\,, \tag{2.4}$$

with a_{bg} as the background scattering length, W as the resonance width, and B_0 as the resonance point.

Expanding the field operators $\Psi(\mathbf{r})$ and $\Phi(\mathbf{r})$ in terms of trap eigenmodes in the trapped dimensions and plane waves in the untrapped dimensions yields

$$\begin{aligned} H = &\sum_{\mathbf{mk}\sigma} (\epsilon_{\mathbf{k}} + \varepsilon_{\mathbf{m}})\, a^\dagger_{\mathbf{mk}\sigma} a_{\mathbf{mk}\sigma} + \sum_{\mathbf{mk}} (\epsilon_{\mathbf{k}}/2 + \varepsilon_{\mathbf{m}} + \nu_b)\, b^\dagger_{\mathbf{mk}} b_{\mathbf{mk}} \\ &+ \frac{g_b}{L^{D/2}} \sum_{\substack{\mathbf{mnp} \\ \mathbf{kq}}} \gamma_{\mathbf{mnp}} \left(a^\dagger_{\mathbf{m},\mathbf{k}+\mathbf{q},\uparrow} a^\dagger_{\mathbf{n},-\mathbf{k},\downarrow} b_{\mathbf{pq}} + \text{h.c.} \right) \\ &+ \frac{U_b}{L^D} \sum_{\substack{\mathbf{mnm'n'} \\ \mathbf{kk'q}}} \gamma^{\mathbf{m'n'}}_{\mathbf{mn}} a^\dagger_{\mathbf{m},\mathbf{k}+\mathbf{q},\uparrow} a^\dagger_{\mathbf{n},-\mathbf{k},\downarrow} a_{\mathbf{n'},-\mathbf{k'},\downarrow} a_{\mathbf{m'},\mathbf{k'}+\mathbf{q},\uparrow} \end{aligned} \tag{2.5}$$

where $\mathbf{m}$ indexes trap eigenmodes $\{m_i\}$, $i = 1, \ldots, 3 - D$, and $\mathbf{k}$ denotes the wave vector in the untrapped dimensions $\{k_j\}$, $j = 1, \ldots, D$. The operators $a_{\mathbf{mk}\sigma}$ and $b_{\mathbf{mk}}$ represent the corresponding atomic and Feshbach molecular modes, respectively. The plane wave energy $\epsilon_{\mathbf{k}}$ and the mode energy $\varepsilon_{\mathbf{m}}$ are given by

$$\epsilon_{\mathbf{k}} = \frac{1}{2}\sum_{j=1}^{D} k_j^2\,, \quad \varepsilon_{\mathbf{m}} = \sum_{i=1}^{3-D} m_i \tag{2.6}$$

[for convenience we neglect the constant energy $(3 - D)/2$ in $\varepsilon_{\mathbf{m}}$ as we will measure the two-body bound state energy with respect to the continuum threshold $3 - D$].

[1] We will let this energy cutoff E_c tend to infinity in our final equations as the low-energy physics there is independent of the value of the high energy cutoff [it cancels with the divergence of $S(E)$ in Eq. (2.17)].

L is the dimensionless quantization length in the untrapped dimensions. The form factors appearing in Eq. (2.5) are given by

$$\gamma_{\mathbf{mnp}} = 2^{(3-D)/4} \int d\mathbf{r} \langle \mathbf{m}|\mathbf{r}\rangle \langle \mathbf{n}|\mathbf{r}\rangle \langle \sqrt{2}\mathbf{r}|\mathbf{p}\rangle, \tag{2.7}$$

$$\gamma_{\mathbf{mn}}^{\mathbf{m'n'}} = \int d\mathbf{r} \langle \mathbf{m}|\mathbf{r}\rangle \langle \mathbf{n}|\mathbf{r}\rangle \langle \mathbf{r}|\mathbf{m'}\rangle \langle \mathbf{r}|\mathbf{n'}\rangle = \sum_{\mathbf{p}} \gamma_{\mathbf{mnp}} \gamma^*_{\mathbf{m'n'p}}, \tag{2.8}$$

with

$$\langle \mathbf{r}|\mathbf{m}\rangle = \prod_{i=1}^{3-D} \frac{e^{-r_i^2/2}}{\pi^{1/4}\sqrt{2^{m_i} m_i!}} \, H_{m_i}(r_i)\,, \tag{2.9}$$

where $H_n(x)$ is the Hermite polynomial. The explicit expression for the overlap factor with the lowest molecule mode is

$$\gamma_{\mathbf{mn0}} = \prod_{j=1}^{3-D} \begin{cases} \frac{(-1)^{\left(m_j - n_j\right)/2}}{(2\pi^3)^{1/4}\sqrt{m_j! n_j!}} \, \Gamma\left(\frac{m_j+n_j+1}{2}\right) & m_j + n_j \text{ even} \\ 0 & m_j + n_j \text{ odd} \end{cases}. \tag{2.10}$$

2.3.2 Two-body eigenstates

We assume the gas to be sufficiently dilute so that we need consider only two-body physics within each potential well. At a very low temperature, pairs of atoms interact and form bound dimers. The interaction between the dimers is negligible in the limit of a very dilute gas. The essential physics is then captured by considering the state of two atoms under the above interaction Hamiltonian. For the two-body physics, the center-of-mass degree of freedom is not influenced by the interaction and can be separated under a harmonic potential. So we can assume the center-of-mass mode is in the ground state of the transverse trap and has zero momentum in the free dimension(s).

A general two-body state for the atoms and the molecule can then be expressed as [42]

$$|\Psi\rangle = \left(\beta b^\dagger_{\mathbf{00}} + \sum_{\mathbf{mnk}} \eta_{\mathbf{mnk}} a^\dagger_{\mathbf{mk}\uparrow} a^\dagger_{\mathbf{n-k}\downarrow} \right) |vac\rangle. \tag{2.11}$$

The coefficients in this ansatz state (normalized to unity) are obtained by solving the Schrödinger equation $H|\Psi\rangle = E|\Psi\rangle$, which yields

$$\frac{1}{U_b^{\text{eff}}(E)} = S(E), \tag{2.12}$$

$$\beta^{-2} = 1 - Z_b^2(E)\frac{\partial S(E)}{\partial E}, \tag{2.13}$$

$$\eta_{\mathbf{mnk}} = \frac{\beta\gamma_{\mathbf{mn0}}}{L^{D/2}}\frac{Z_b(E)}{E - 2\epsilon_{\mathbf{k}} - \varepsilon_{\mathbf{m}} - \varepsilon_{\mathbf{n}}}. \tag{2.14}$$

where

$$U_b^{\text{eff}}(E) \equiv U_b - \frac{g_b^2}{\nu_b - E}, \tag{2.15}$$

$$Z_b(E) \equiv g_b - \frac{U_b}{g_b}(\nu_b - E) = 1/\sqrt{\frac{\partial\left[U_b^{\text{eff}}(E)\right]^{-1}}{\partial E}}, \tag{2.16}$$

and

$$S(E) \equiv \frac{1}{L^D}\sum_{\mathbf{mnk}}\frac{\gamma_{\mathbf{mn0}}^2}{E - 2\epsilon_{\mathbf{k}} - \varepsilon_{\mathbf{m}} - \varepsilon_{\mathbf{n}}}. \tag{2.17}$$

Thus, Eq. (2.12) determines the eigenenergy E, and Eqs. (2.13) and (2.14) give us the eigenstate as a function of the eigenenergy. These equations are expressed in terms of the bare parameters, and we need to the use the renormalization relation (2.3.1) to transfer them into the ones with the physical parameters. One can easily check that under the relation (2.3.1),

$$Z_p(E) \equiv g_p - \frac{U_p}{g_p}(\nu_p - E) = Z_b(E) \tag{2.18}$$

for any E, and

$$\left[U_p^{\text{eff}}(E)\right]^{-1} \equiv \left(U_p - \frac{g_p^2}{\nu_p - E}\right)^{-1} = \left[U_b^{\text{eff}}(E)\right]^{-1} + U_c^{-1}. \tag{2.19}$$

The divergence in U_c^{-1} then exactly cancels with the divergence in $S(E)$. As a net result, the above equations (2.12)– (2.15) retain the same form upon renormalization

— all the bare parameters are replaced by their physical counterparts, and $S(E)$ and $\partial S(E)/\partial E$ are replaced by

$$S_p(E) = -\frac{1}{2^{5/2}\pi}\begin{cases}\zeta(1/2,-E/2) & D=1\\ \int_0^\infty ds\left(\frac{\Gamma\left(s-\frac{E}{2}\right)}{\Gamma\left(s+\frac{1}{2}-\frac{E}{2}\right)}-\frac{1}{\sqrt{s}}\right) & D=2\end{cases} \tag{2.20}$$

$$\frac{\partial S_p(E)}{\partial E} = -\frac{1}{2^{7/2}\pi}\begin{cases}\frac{1}{2}\zeta(3/2,-E/2) & D=1\\ \frac{\Gamma(-E/2)}{\Gamma(1/2-E/2)} & D=2\end{cases} \tag{2.21}$$

where $\zeta(s,x) = \lim_{N\to\infty}\sum_{n=0}^{N}(n+x)^{-s} - \frac{(N+x)^{-s+1}}{-s+1}$ is the Hurwitz zeta function and $\Gamma(x)$ is the gamma function. (See Appendix A for details of the summations.) The above set of equations serve as the basic formalism for determining the state of two atoms in a transverse trap across a Feshbach resonance. If we take the one-dimensional case ($D = 1$) and neglect the background scattering (let $U_p = 0$), the above equation for E is reduced to the energy equation in Ref. [20], where it is derived with a different renormalization method.

2.4 Considerations of Transverse Mode Populations for ^{40}K and ^{6}Li

2.4.1 Population distribution among higher modes

In this section, we answer the following basic question: For a dilute gas under a strong transverse trap, can we assume the atoms only populate the lowest transverse level at low temperature so that the system becomes effectively low-dimensional? In the extreme limit of a dilute gas, we can consider only two atoms in each potential well [the density in the free dimension(s) tends to zero in this case, although, due to dimer formation, the local density does not]. We will show that even in this extreme limit the excited fraction is typically still significant, even dominant, for realistic atoms. If the gas density becomes higher, the excited fraction surely cannot

decrease.

To answer this question, we use the above formalism for the two-atom state, and calculate the population distribution in the transverse levels for ^{40}K and ^{6}Li atoms, which are the relevant species for the current experiments. We take the scattering parameters $W \simeq 8\,G$, $a_{bg} \simeq 174\,a_B$, $\mu_{co} \simeq 1.68\mu_B$ for ^{40}K [2, 40, 41] and $W \simeq 300\,G$, $a_{bg} \simeq -1405\,a_B$, $\mu_{co} \simeq 2\mu_B$ for ^{6}Li [48]. With a typical trap frequency $\omega \simeq 2\pi \times 62$ kHz [29, 30], the physical parameters for the atom-molecule interaction are then given by $g_p = 23$ (272), $U_p = 1.7$ (-5.5) for ^{40}K (^{6}Li). To calculate the transverse population distribution in the system ground state, we first determine the binding energy, $-E_B > 0$, between the atoms using Eq. (2.12). Since we have already subtracted out the two-body continuum threshold energy of $(3 - D)$ (in the unit of $\hbar\omega$) by our unusual choice of zero-point energy in Eq. (2.6), E_B is simply the lowest energy satisfying Eq. (2.12). As the binding energy is of interest by itself, we show E_B as a function of the magnetic field detuning $B - B_0$ in Fig. 2.1(a) and 2.1(b) with $D = 1, 2$ for ^{40}K and ^{6}Li, respectively. Throughout this dissertation we refer to the region $B < B_0$ as the BEC region since, in the absence of atom-molecule coupling, the many-body ground state there is a Bose-Einstein condensate of Feshbach molecules, and the region $B > B_0$ as the BCS region since the many-body ground state there in the absence of atom-molecule coupling is a Bardeen-Cooper-Schrieffer superfluid of atomic pairs. In the presence of coupling, there is a smooth crossover from BEC to BCS ground states.

For ^{40}K, the binding energy saturates on the deep BEC side. This effect comes from the positive background scattering length of ^{40}K, and is related to the weakly bound state in the open collision channel. A detailed discussion of the background scattering effects can be found in Ref. [13] (see also Ref. [12]). So, outside of the

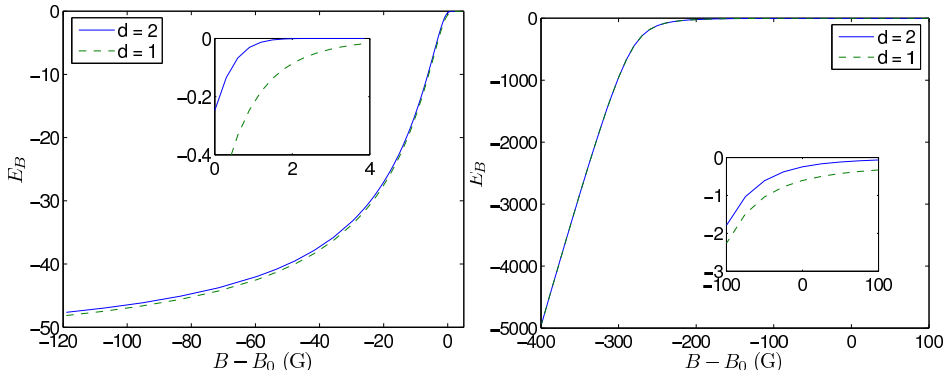

(a) ^{40}K (b) ^{6}Li

Figure 2.1: Binding energy (in units of $\hbar\omega$) vs detuning at $\omega \simeq 2\pi \times 62$ kHz. B_0 is the resonant point in the absence of an optical lattice. The inserts show a close-up of the binding energy in the near-resonance region.

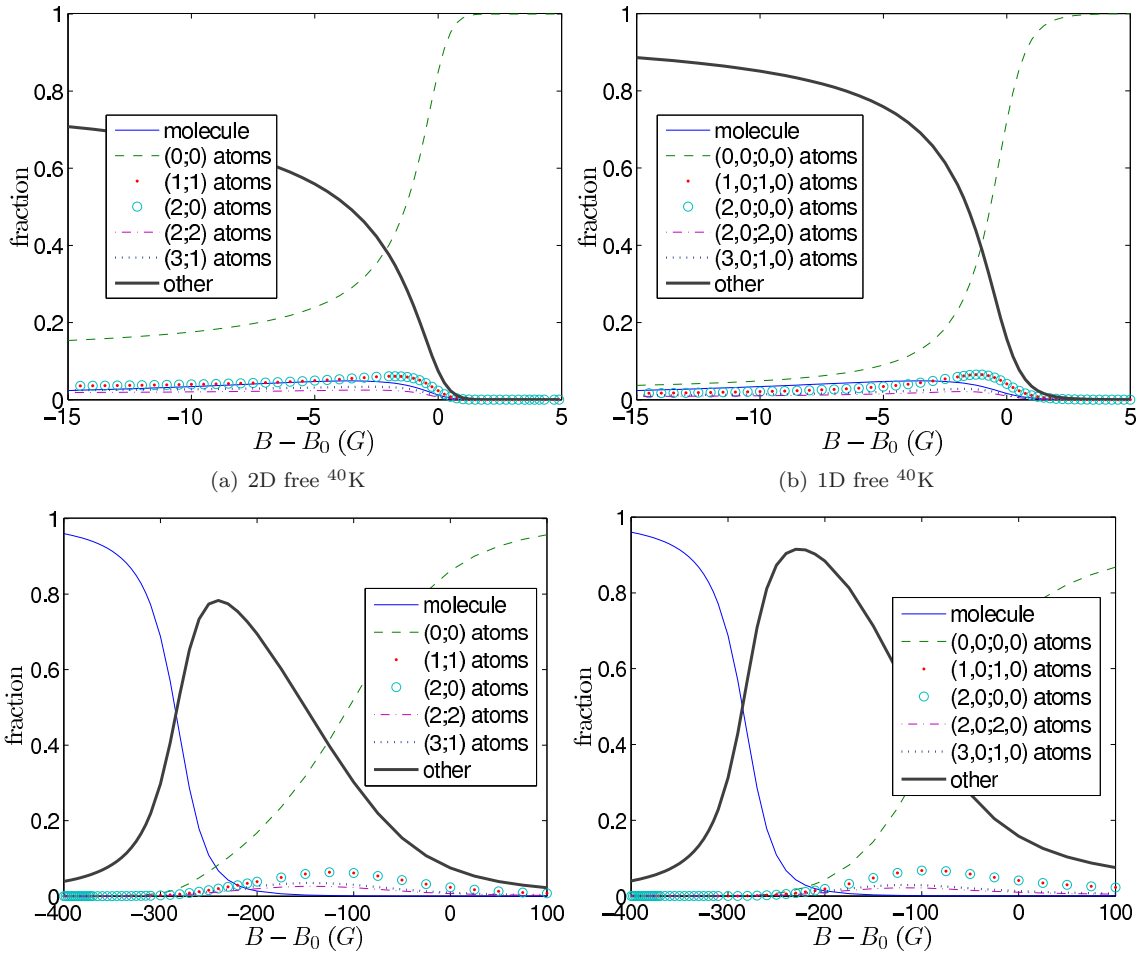

(a) 2D free ^{40}K (b) 1D free ^{40}K

(c) 2D free ^{6}Li (d) 1D free ^{6}Li

Figure 2.2: Ground state composition vs. detuning. Only the six most significant components are shown explicitly. The label $(\mathbf{m};\mathbf{n})$ denotes the sum of $P_{\mathbf{mn}} = \sum_{\mathbf{k}} \eta^2_{\mathbf{mnk}}$ and all components identical by symmetry.

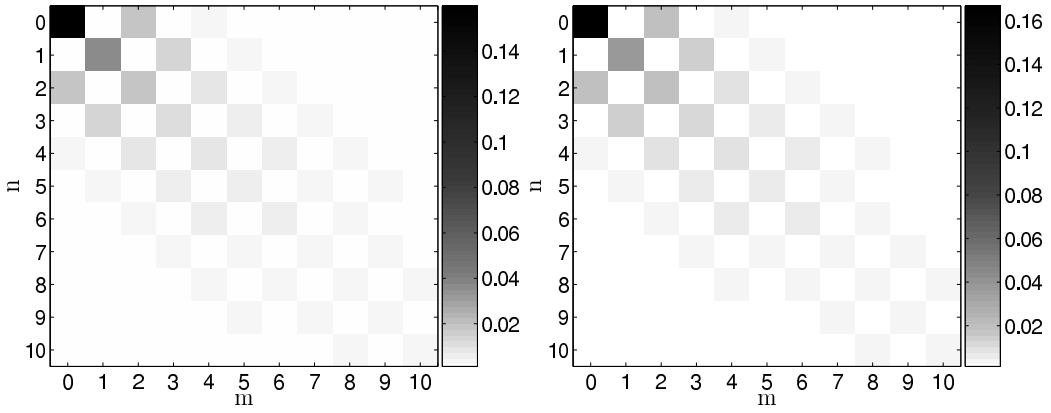

(a) ^{40}K, $B - B_0 = -18\ G$ (b) ^{6}Li, $B - B_0 = -200\ G$

Figure 2.3: The matrix $\sum_{\mathbf{k}} \eta^2_{mn\mathbf{k}}$ for 2D free atoms on the BEC side.

near resonance region, the result here is quite different from the one in Refs. [20, 44], where the binding energy is calculated for the $D = 1$ case without the background scattering contribution. From Fig. 2.1, one can also see that with a transverse trap, the binding energy $|E_B|$ is always positive, and only tends to zero when one goes to the deep BCS limit [20, 29, 30, 32–37, 44] (or when $B - B_0 \to W$ for ^{40}K, where the scattering length goes to zero). This is distinct from the case without traps, where $E_B = 0$ for $B \geq B_0$.

In Fig. 2.2, we show the population distribution in transverse levels for ^{40}K and ^{6}Li in two or one dimensional traps as a function of the magnetic field detuning. The population fraction in the transverse modes $(\mathbf{m}; \mathbf{n})$ is defined as $P_{\mathbf{mn}} = \sum_{\mathbf{k}} |\eta_{\mathbf{mnk}}|^2$. In Fig. 2.3, we show a more complete picture of the population distribution at a fixed detuning on the BEC side for atoms in a one dimensional trap. From the figures, one can see that in general many transverse modes are populated. For a fixed mode, the population still goes down as the energy of the mode goes up, but there are so many excited transverse modes that the total population fraction in the excited levels actually dominates in typical configurations.

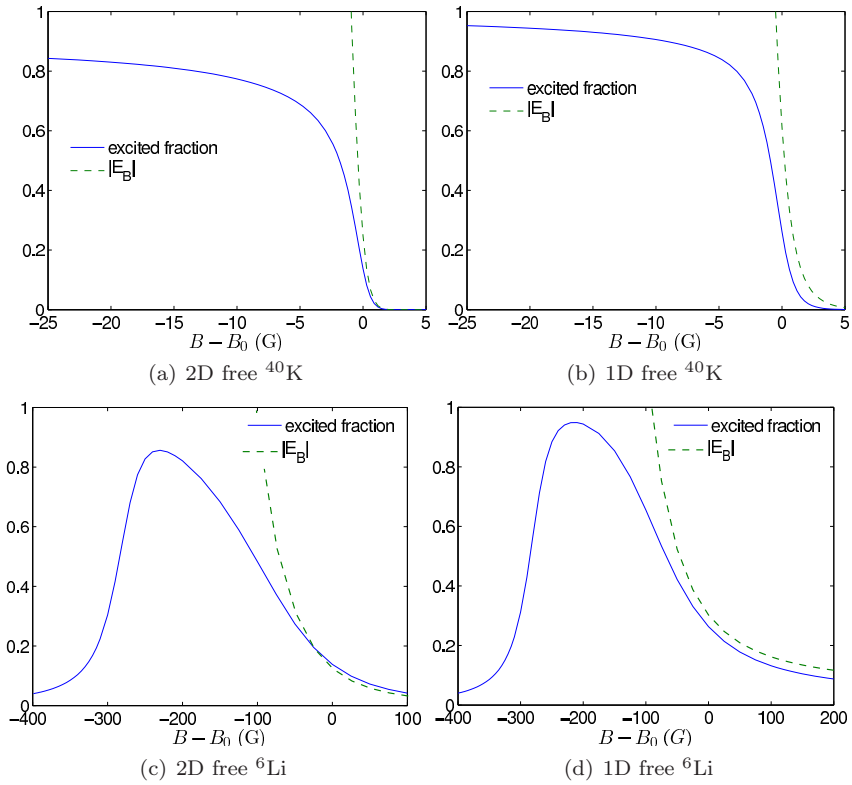

(a) 2D free ^{40}K (b) 1D free ^{40}K

(c) 2D free ^{6}Li (d) 1D free ^{6}Li

Figure 2.4: Excited fraction and binding energy (in units of $\hbar\omega$) vs. detuning for $\omega \simeq 2\pi \times 62\,kHz$.

2.4.2 Conditions of low-dimensionality

In Fig. 2.4, we draw the overall fraction populating the transverse excited levels, which is defined as $P_{ex} \equiv 1 - \beta^2 - \sum_{\mathbf{k}} \eta^2_{\mathbf{00k}}$. This fraction needs to satisfy $P_{ex} \ll 1$ for the assumption that the atoms only populate the lowest transverse level. From the figure, one can see that this condition is in general not satisfied for ^{40}K and ^{6}Li, except in the deep BCS limit with the binding energy $|E_B| \ll 1$. For the case of ^{6}Li, if one goes to the very deep BEC limit with the closed channel population (the bare molecule fraction) $\beta \to 1$, the condition $P_{ex} \ll 1$ is also automatically satisfied. For ^{40}K, because of its positive background scattering length, the bare molecule fraction β remains small even if one goes to the deep BEC limit [12, 13]. So the excited fraction P_{ex} continuously goes up as one increases the negative detuning. From this calculation, it is clear that for the entire region near resonance, which is of particular

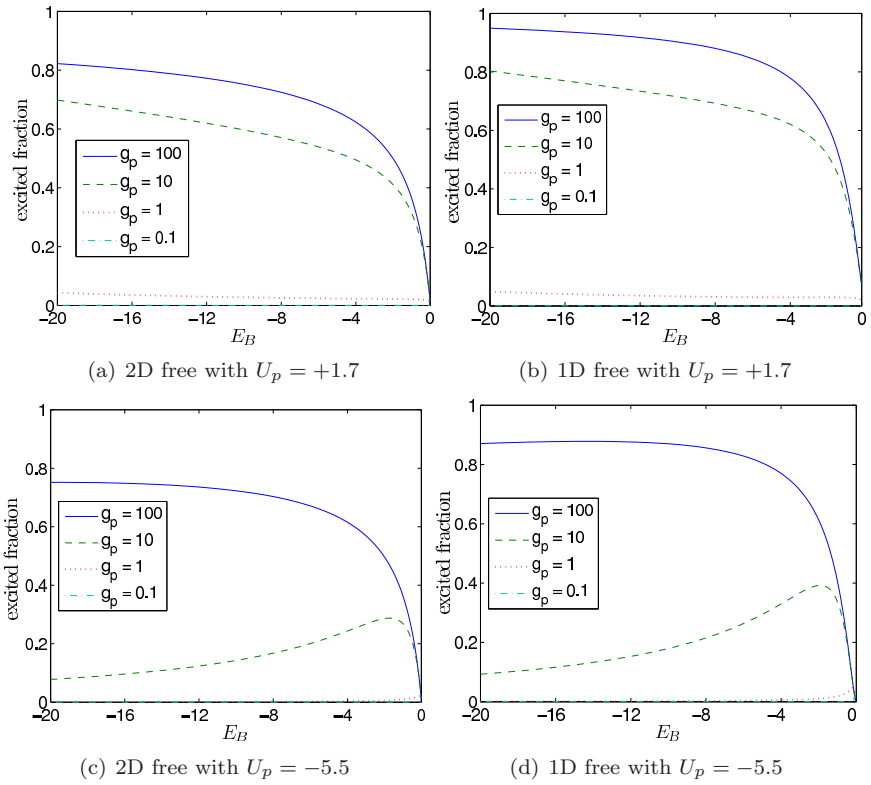

(a) 2D free with $U_p = +1.7$ (b) 1D free with $U_p = +1.7$

(c) 2D free with $U_p = -5.5$ (d) 1D free with $U_p = -5.5$

Figure 2.5: Excited fraction vs. binding energy (in units of $\hbar\omega$) for various coupling rates.

experimental interest, one cannot neglect the transverse excited fractions for any atoms with a wide Feshbach resonance.

The condition $P_{ex} \ll 1$ can only be satisfied in the near resonance region for the narrow Feshbach resonance. In Fig. 2.5, we show the excited fractions for various atom-molecule coupling rates. The background scattering length still takes the positive or negative values corresponding to ^{40}K or ^{6}Li atoms, but we vary the coupling rate g_p (so the resonance width W changes). One can see that the condition $P_{ex} \ll 1$ is satisfied in the whole region only when $g_p < 1$. As $g_p \propto \sqrt{W}$, the condition $g_p < 1$ requires a very narrow resonance with the resonance width $W < 0.01G$. On the other hand, one can also see from the figure that to satisfy $P_{ex} \ll 1$, the background interaction $|U_p|$ can be somewhat larger than 1, but it cannot be arbitrarily larger. We have tested (not shown in the figure) that the condition $P_{ex} \ll 1$ breaks down

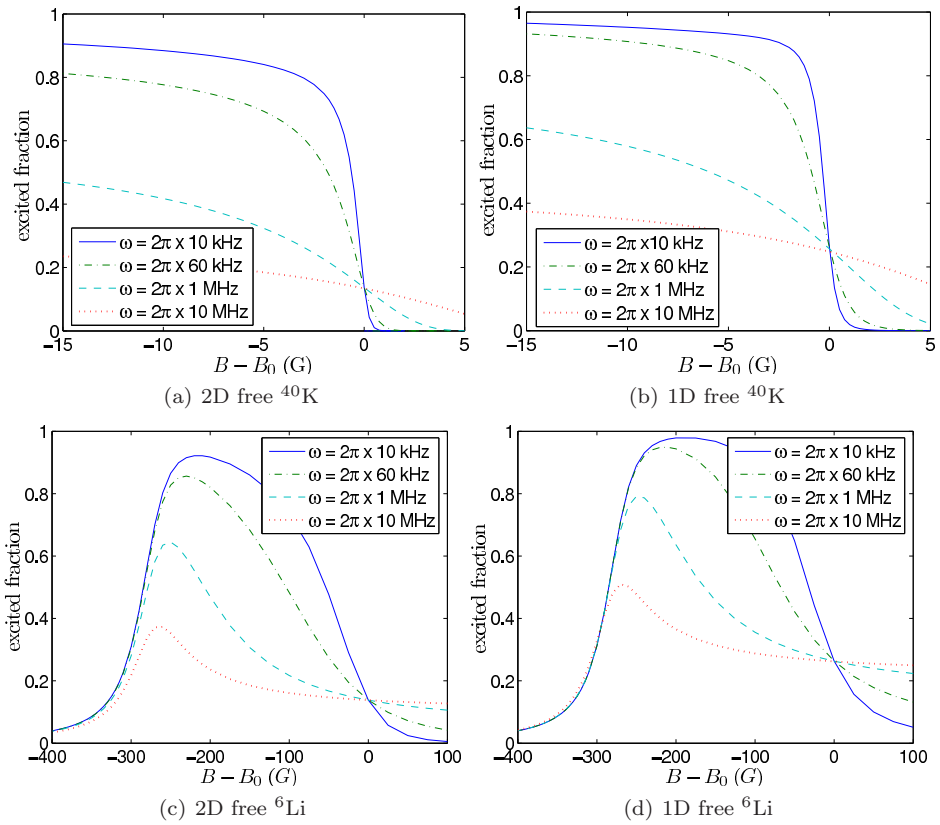

(a) 2D free ^{40}K (b) 1D free ^{40}K

(c) 2D free ^{6}Li (d) 1D free ^{6}Li

Figure 2.6: Excited fraction vs. detuning for various trapping frequencies.

when U_p is on the order of a few tens.

2.4.3 Excited fraction vs. trap frequency

The above calculations are done with a fixed trap frequency $\omega \simeq 2\pi \times 62$ kHz, as it is typical for current experiments [29, 30]. One may expect that if the trap frequency further increases, it will become much easier to suppress the transverse excited fraction and to satisfy the condition $P_{ex} \ll 1$. To test whether this is true, we show in Fig. 2.6 the transverse excited fraction versus the magnetic field detuning for various magnitudes of the trap frequency. One can see that even if the trap frequency increases by several orders of magnitudes, the transverse excited fraction P_{ex} does not change much and remains significant. To understand this puzzling effect, we note that although the transverse level spacing increases a lot, the effective atom-

molecule coupling rate also increases. One cannot assume a constant atom-molecule coupling rate as an increased trapping in the transverse direction will suppress the pair size in all directions including the free dimensions (see Subsec. 2.4.4) to a length scale of $a_t \sim \omega^{-1/2}$. The effective atom-molecule coupling rate increases significantly when the pair size shrinks. As a net effect, the ratio between the atom-molecule coupling and the transverse level spacing is only a slowly-varying function of the trap frequency. The dimensionless parameter g_p, which measures the effective atom-molecule coupling strength in units of $a_t^{3/2}\hbar\omega$, actually characterizes this ratio. From its units, one can verify that g_p goes as $\omega^{-1/4}$. So, the effective ratio only drops by a factor of 10 (it will still be larger than unity for ^{6}Li and ^{40}K) even if the trap frequency increases by four orders of magnitudes from its current value (which is almost impossible). This explains the relative insensitivity of the excited fraction P_{ex} to the trap frequency. We can also conclude here that for any reasonable trap strength one can imagine, it is impossible to neglect the transverse excited fractions for realistic atoms such as ^{6}Li and ^{40}K with a wide Feshbach resonance.

As an aside, we also note that the excited fraction is nearly independent of the trap frequency at resonance. This can be most easily understood from the one-channel picture where one neglects the closed channel molecules and simply models the system as open channel atoms interacting via an effective scattering length. This is valid at resonance because the molecule fraction is still nearly zero there. In that case, when the scattering length goes to infinity, the only remaining energy scale is the trap frequency, so in units of $\hbar\omega$, the energy must be some universal constant. (This point where all scales vanish except for one is often referred to as unitarity.) Since the population distribution of the various modes depends only on the ratio of the binding energy and $\hbar\omega$, the distribution must then be independent of ω as long

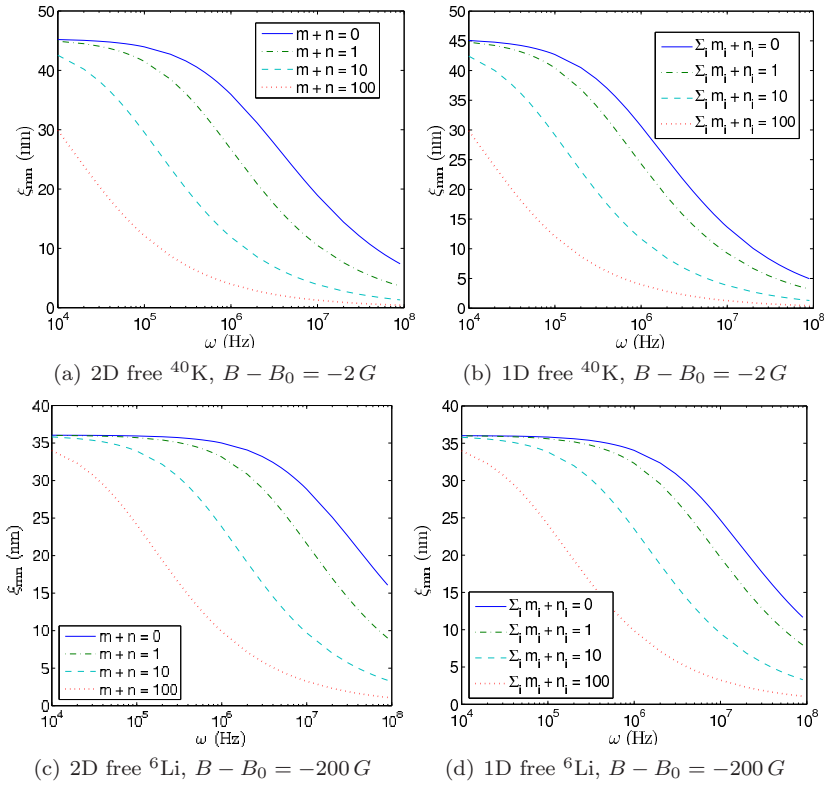

(a) 2D free ^{40}K, $B - B_0 = -2\,G$ (b) 1D free ^{40}K, $B - B_0 = -2\,G$

(c) 2D free ^{6}Li, $B - B_0 = -200\,G$ (d) 1D free ^{6}Li, $B - B_0 = -200\,G$

Figure 2.7: Characteristic atomic pair size vs. trapping frequency for a fixed detuning.

as the single-channel picture is valid.

2.4.4 Extent of the atom pair state

With an increased transverse trapping, it is easy to understand that the pair size along that direction will be suppressed. However, it is not so obvious that the pair size along the free dimension(s), where there is no trap, will correspondingly shrink. Under strong interaction, the pair size cannot change only along one direction. To see the pair size shrinking along the untrapped directions, we can take the Fourier transform of the pair wavefunction $\eta_{\mathbf{mnk}}$ with respect to the momentum $\mathbf{k}$ in the free dimension(s). This Fourier transform, denoted as $\eta_{\mathbf{mn}r}$, yields the real-space wavefunction, which is the probability amplitude for an atom pair in transverse modes $\mathbf{m}$ and $\mathbf{n}$ to be spaced a distance r apart in the free dimension(s). From

Eq. (2.14), $\eta_{\mathbf{mn}r}$ is given by

$$\eta_{\mathbf{mn}r} = \begin{cases} -\frac{1}{2\pi L} g_p \beta \gamma_{mn0} K_0 \left(|r| / \xi_{mn} \right) & D = 2 \\ -\frac{\xi_{\mathbf{mn}}}{2\sqrt{L}} g_p \beta \gamma_{\mathbf{mn0}} e^{-|r|/\xi_{\mathbf{mn}}} & D = 1 \end{cases}, \tag{2.22}$$

where $K_0(x) = \int_0^\infty dt \cos(xt) / \sqrt{t^2+1}$ is a modified Bessel function of the second kind, and

$$\xi_{\mathbf{mn}} = \frac{1}{\sqrt{-E_B + \varepsilon_{\mathbf{m}} + \varepsilon_{\mathbf{n}}}} \tag{2.23}$$

characterizes the pair size in the free dimension(s). Our unit of length, $a_t = \sqrt{\hbar/m\omega}$, is awkwardly frequency dependent, so one can see that the pair sizes scale roughly as $\omega^{-1/2}$. The dependence of $\xi_{\mathbf{mn}}$ on the trapping frequency is shown in Fig. 2.7 for different transverse modes $(\mathbf{m};\mathbf{n})$ on the BEC side. Note that under typical configurations, the atom population is broadly distributed over the transverse modes (as illustrated by Fig. 2.3), so the exact pair size in the free dimension(s) should come from the average of $\xi_{\mathbf{mn}}$ over different $(\mathbf{m};\mathbf{n})$.

From Fig. 2.7, one can see that for typical values of $(\mathbf{m};\mathbf{n})$, the pair size significantly shrinks with increase of the trap frequency, so its average will follow the same trend. As one moves towards the BCS side of resonance, the trend only becomes more dramatic. This provides a physical interpretation of the coupling enhancement: Since an atom pair has twice the zero-point energy of a molecule, and the zero-point energy goes as $\hbar\omega$, strengthening the transverse trap raises the minimum energy of the atom pairs relative to the molecules. Thus, the molecular contribution to the ground state increases. The point-like molecules mix more strongly with small atom pairs than large ones, so the contribution of the small atom pairs correspondingly increases. The net result is a sort of induced pair-wise confinement along the free dimension(s), and this increased local density causes the effective coupling to

increase.

2.5 Chapter Summary

We have shown that for experimentally relevant cases, atoms trapped along one or two dimensions cannot be considered to be in the transverse ground level except when well out of the BCS-BEC crossover region. In the crossover region and for the ground state of the system, a significant fraction of atomic population resides in the excited transverse levels, even if the gas is very dilute. Furthermore, one cannot effectively suppress the transverse excited fraction by raising the trap intensity. Even with an extremely strong trap far beyond the current experimental technology, the transverse excited fraction is still not negligible for realistic atoms such as ^{6}Li and ^{40}K across a wide Feshbach resonance. The conclusion here is that in the experimentally interesting region, one cannot describe strongly interacting atoms under a transverse trap as a low-dimensional system by assuming a fixed transverse mode. Although this result does not exclude an *effective* low-dimensional description of this strongly interacting system, it indeed shows that the effective description will become much more subtle, and such a description needs to take into account the broad population distribution of the atoms in all the transverse modes. The derivation of such an effective description will be the topic of the next chapter.

CHAPTER III

An Effective Low-Dimensional Hamiltonian for Strongly Interacting Fermionic Gases in a Transverse Trap

3.1 Chapter Overview

We derive an effective low-dimensional Hamiltonian for strongly interacting ultracold atoms in a transverse trapping potential near a wide Feshbach resonance. The Hamiltonian includes crucial information about transverse excitations in an effective model with renormalized interaction between atoms and composite dressed molecules. We fix all the parameters in the Hamiltonian for both one- and two-dimensional cases.

3.2 Introduction

As mentioned in Chapter II, cold atomic gases strongly confined via optical lattice techniques along one or two dimensions and placed in an external magnetic field tuned near a Feshbach resonance provide the exciting possibility to study low-dimensional (low-D) strongly correlated physics in a controllable fashion [27, 28, 30, 49–51]. For weakly interacting atoms in a transverse trap, it is easy to get a low-dimensional Hamiltonian by projecting the atomic wave function to the lowest trap mode. However, the situation gets much more complicated for strongly interacting atoms. It is known that virtual excitation of the transverse trap modes during the

atomic collisions could lead to interesting renormalization of the atomic scattering lengths in low dimensions [32, 33, 35, 36, 52]. Furthermore, independent of the detuning from the Feshbach resonance, the atoms can always form dimers (two-body bound states) as their ground state configuration in a transverse trap [24, 32–36, 43, 52]. Because of the formation of dimers, the problem does not simply reduce to atomic scattering with a renormalized scattering length, but instead, we have to take into account the *real population* of the atoms in transverse excited levels, which remains significant even for an extremely strong transverse trap [24], as discussed in detail in Chapter II.

In this chapter, we construct the low-D (both 1D and 2D) effective Hamiltonian by taking into account the atomic population in the transverse excited modes. To describe the transverse excitations, one can introduce a dressed molecule [22, 23], which is part of the dimer state excluding the atomic population in the lowest transverse level. We observe that for realistic atomic densities, the structure of the dressed molecule is largely fixed by the two-body physics and thus almost density independent. This allows us to derive the renormalized interaction between the atoms and the dressed molecules, which gives the effective many-body Hamiltonian. This effective Hamiltonian reproduces the correct two-body state, and from that, we also fix all the parameters in the Hamiltonian at any detuning of the magnetic field.

3.3 Effective Hamiltonian

We again consider a fermionic gas free in D dimensions ($D = 1, 2$) and trapped by a $(3 - D)$-dimensional harmonic potential of frequency ω along the transverse direction. The two-channel Hamiltonian for atoms of mass m and possessing internal states $\sigma = \{\uparrow, \downarrow\}$ in such a potential was given in Eq. 2.5 in terms of dimensionless

quantities with all energies in units of $\hbar\omega$ and all lengths in units of the trap length scale, $a_t = \sqrt{\hbar/m\omega}$. We will continue using those units in this chapter.

The Hamiltonian (2.5) contains many trap modes and is extremely complicated and hard to solve directly. We expect it should reduce to some low-dimensional effective Hamiltonian when the trap confinement is strong enough. In particular, we assume that the many-body energy scale, characterized by the density dependent part of the chemical potential μ_ρ, is much less than the trap energy $\hbar\omega$. This is equivalent to assuming that the 1D (or 2D) atomic density $\rho \ll 1$ measured in units of a_t^{-1} (or a_t^{-2}), which is typically the case for realistic systems. Under this condition, when the atoms are far apart, they should stay in the transverse ground level to minimize the energy. The transverse excited levels get populated only when the atoms come close to strongly interact with each other. However, since $\rho \ll 1$ and there is no n-particle bound state with $n \geq 3$ for two-component fermions, it is rare for three or more atoms to come close (two atoms can approach each other as there exists a bound dimer state at any detuning ν_p from the Feshbach resonance, as seen explicitly in the previous chapter). From this argument, we see that the atomic distribution in the transverse excited modes is determined by the short-range physics, where the latter is fixed through the two-body solution. The two-body state of the Hamiltonian H with energy (relative to the continuum threshold, $3-D$) $E_{2B} < 0$ and momentum $\mathbf{q}$ can be written in the form $|\Psi_2\rangle = \Psi_{2\mathbf{q}}^\dagger |0\rangle$, where $|0\rangle$ denotes the vacuum and

$$\Psi_{2\mathbf{q}}^\dagger = \beta b_{\mathbf{0q}}^\dagger + \sum_{\mathbf{mnk}} \frac{\eta_{\mathbf{mnk}}}{E_{2B} - 2\epsilon_{\mathbf{k}} - \epsilon_{\mathbf{q}}/2 - \varepsilon_{\mathbf{m}} - \varepsilon_{\mathbf{n}}} a_{\mathbf{m},\mathbf{k}+\mathbf{q}/\mathbf{2},\uparrow}^\dagger a_{\mathbf{n},-\mathbf{k}+\mathbf{q}/\mathbf{2},\downarrow}^\dagger \tag{3.1}$$

where the operators $a_{\mathbf{mk}\sigma}$ and $b_{\mathbf{mk}}$ once again represent the atomic and Feshbach molecular modes, respectively, and the coefficients β and $\eta_{\mathbf{mnk}}$ were given in Chapter II, although the actual expressions are not important for the purposes of this discus-

sion. We thus construct the dressed molecular modes $d^\dagger_{\mathbf{q}}$ with the same expression as $\Psi^\dagger_{2\mathbf{q}}$, but excluding the $\mathbf{m} = \mathbf{n} = \mathbf{0}$ term in the summation, and correspondingly normalized to unity. Since the dressed molecule is the part of the two-body bound state which contains atoms in the excited transverse levels, whose energies are at least $\hbar\omega$, the dressed molecule is tightly confined in space to a volume on the order of a_t^3 in the deep BCS regime even though the size of the full two-body bound state diverges there due to the size of the lowest mode pairs, which dominate in the BCS regime. The dressed molecule becomes even smaller in the crossover and BEC regimes, as is evident from Sec. 2.4.4. Note that in this light the requirement $\rho \ll 1$ discussed above is equivalent to requiring that the average interparticle distance is much greater than the dressed molecule size. The dressed molecules can then safely be regarded as point bosons. These modes $d^\dagger_{\mathbf{q}}$ capture the short-range physics and their structure should be basically independent of the atomic density. The coupling between $d_{\mathbf{q}}$ and the atomic modes $a_{\mathbf{0}\mathbf{k}\sigma}$ (which we henceforth denote simply as $a_{\mathbf{k}\sigma}$) in the open channel can be approximated with a contact interaction since $d_{\mathbf{q}}$ is so tightly confined. The general effective Hamiltonian for $d_{\mathbf{q}}$ and $a_{\mathbf{k}\sigma}$ then takes the form

$$H_{\text{eff}} = \sum_{\mathbf{k}\sigma} \epsilon_{\mathbf{k}} a^\dagger_{\mathbf{k}\sigma} a_{\mathbf{k}\sigma} + \sum_{\mathbf{q}} \left(\epsilon_{\mathbf{q}}/2 + \lambda_b\right) d^\dagger_{\mathbf{q}} d_{\mathbf{q}} + \frac{\alpha_b}{L^{D/2}} \sum_{\mathbf{kq}} \left(a^\dagger_{\mathbf{k}+\frac{\mathbf{q}}{2},\uparrow} a^\dagger_{-\mathbf{k}+\frac{\mathbf{q}}{2},\uparrow} d_{\mathbf{q}} + \text{h.c.} \right) + \frac{V_b}{L^D} \sum_{\mathbf{kk'q}} a^\dagger_{\mathbf{k}+\frac{\mathbf{q}}{2},\uparrow} a^\dagger_{-\mathbf{k}+\frac{\mathbf{q}}{2},\downarrow} a_{-\mathbf{k'}+\frac{\mathbf{q}}{2},\downarrow} a_{\mathbf{k'}+\frac{\mathbf{q}}{2},\uparrow} \quad (3.2)$$

where $\epsilon_{\mathbf{k}} = \frac{1}{2}\sum_{j=1}^{D} k_j^2$, λ_b (in units of $\hbar\omega$) is the relative detuning, α_b (in units of $\hbar\omega a_t^{D/2}$) is the coupling rate, V_b (in units of $\hbar\omega a_t^D$) represents the remaining background interaction in the open channel, and L is the dimensionless quantization length in the untrapped dimensions. We introduce "physical" parameters related to the three bare parameters in H_{eff} via a low-D renormalization analogous to Eq. (2.3.1)

in the previous chapter:

$$V_c^{-1} = \int \frac{d^D\mathbf{k}}{(2\pi)^D} \frac{1}{2\epsilon_{\mathbf{k}} + 3 - D}\,, \quad \Omega^{-1} = 1 - V_p V_c^{-1},$$
$$V_p = \Omega^{-1} V_b\,, \quad \alpha_p = \Omega^{-1}\alpha_b\,, \quad \lambda_p = \lambda_b - \Omega\alpha_p^2 V_c^{-1}\,. \tag{3.3}$$

Note that the zero-point energy $3 - D$ appears explicitly in the definition of V_c^{-1}, otherwise there is an artificial infrared divergence. Actually, mathematically this is a completely arbitrary choice since the ultraviolet divergence associated with the contact interaction in two dimensions is removed regardless of the finite, positive energy scale introduced in the denominator to avoid the infrared divergence. No physical observables depend on the value of V_c^{-1}. Denoting the effective parameters defined above as "physical" is a bit of poetic license as they will depend on the details of our renormalization scheme. The only truly physical parameters in the problem are the 3D ones. However, we use the zero-point energy above because there is no other natural energy scale available. In this sense our choice is not arbitrary, and it is reasonable to expect the parameters defined in this way to behave in an intuitive fashion. We will also see that our choice of renormalization is nonarbitrary in that the resulting parameters in the limit as the binding energy goes to zero naturally recover the effective low-D interaction strength derived for the scattering physics via a single-channel treatment with a regularized zero-range pseudopotential [32, 33, 35, 36, 43].

The effective Hamiltonian H_{eff} should reproduce the same physics represented by the 3D Hamiltonian H when the system is near the ground state with the energy per particle close to $E_{2B}/2$ (as $\mu_\rho \ll 1$ in units of $\hbar\omega$). To determine the parameters in H_{eff}, we match the exact two-body bound state obtained from the original H. Specifically, we first determine the effective background scattering V_p by matching

the bound state physics in the deep BCS limit, where the population is entirely atoms in the lowest trap mode. Then, for general detuning, matching the binding energy and the bound state gives two constraints which determine the remaining parameters, λ_b and α_b. Since the composition of the dressed molecule $d_{\mathbf{q}}$ is a function of magnetic field, or equivalently, of the 3D scattering length, so are these two parameters.

3.4 Fixing the Parameters

All the two-body physics contained in a given Hamiltonian are embodied in its T-matrix, defined by $T(E) = H_I + H_I G(E)\, H_I = H_I + H_I G_0(E)\, T(E)$, where H_I is the interaction part of the Hamiltonian H, $G(E) = (E - H)^{-1}$ is the full two-body propagator, and $G_0(E) = (E - H_0)^{-1}$ is the free two-body propagator. Physically, the matrix element $\langle \mathbf{2}|T\,(E)\,|\mathbf{1}\rangle$ is the sum of the direct process whereby a pair of atoms scatters from state $|\mathbf{1}\rangle$ to state $|\mathbf{2}\rangle$ and the indirect processes whereby the atoms scatter into an intermediate state, propagate with energy E, and then scatter into the final state. From its definition, it is clear that the T-matrix has simple poles where E is equal to a two-body bound state of the Hamiltonian. Furthermore, the residue of the diagonal matrix element $\langle \mathbf{1}|T\,(E)\,|\mathbf{1}\rangle$ at such a pole, $E = E_n$, is $|\langle \mathbf{1}|H_I|\Psi_n\rangle|^2 = |\langle \mathbf{1}|H - H_0|\Psi_n\rangle|^2 = (E_n - \epsilon_{\mathbf{1}})^2\, |\langle \mathbf{1}|\Psi_n\rangle|^2$, where $\epsilon_{\mathbf{1}}$ is the noninteracting energy of state $|\mathbf{1}\rangle$. Thus, the residue of a given diagonal matrix element determines the fraction of the bound state in the given basis state. We shall use both of these facts in matching the two-body bound state properties of the exact and effective Hamiltonians.

In Appendix B, we derive the general two-body T-matrix associated with the Hamiltonian H in Eq. (2.5). For a pair of atoms asymptotically in the lowest mode of the trap, the corresponding diagonal T-matrix element (in units of $a_t^D \hbar\omega$) as a

function of the two-body energy E (measured with respect to the continuum threshold, $3-D$) is

$$[T(E)]^{-1} = \gamma_{\mathbf{000}}^{-2}\left(\left[U_p^{\text{eff}}(E)\right]^{-1} - S_p(E)\right), \tag{3.4}$$

where $\gamma_{\mathbf{000}} = (2\pi)^{(D-3)/4}$, $U_p^{\text{eff}}(E) \equiv U_p - g_p^2/(\nu_p - E)$ and, from the normalization in Eq. (2.3.1), $\left[U_p^{\text{eff}}(E)\right]^{-1} = \left[U_b^{\text{eff}}(E)\right]^{-1} + U_c^{-1}$, and the function

$$\begin{aligned} S_p(E) &\equiv \frac{1}{L^D}\sum_{\mathbf{mnk}} \frac{\gamma_{\mathbf{mn0}}^2}{E - 2\epsilon_{\mathbf{k}} - \varepsilon_{\mathbf{m}} - \varepsilon_{\mathbf{n}}} + U_c^{-1} \\ &= \frac{-1}{2^{5/2}\pi} \begin{cases} \zeta(1/2, -E/2) & D=1 \\ \int_0^\infty ds \left[\frac{\Gamma(s-E/2)}{\Gamma(s+1/2-E/2)} - \frac{1}{\sqrt{s}}\right] & D=2 \end{cases}. \end{aligned} \tag{3.5}$$

(See Appendix A.) In the above we have used the gamma function, $\Gamma(x)$, and the Hurwitz zeta function, $\zeta(s,x) = \lim_{N\to\infty}\sum_{n=0}^{N}(n+x)^{-s} - (N+x)^{1-s}/(1-s)$.

The two-body bound state corresponds to a pole of the T-matrix element above with $[T(E_{2B})]^{-1} = 0$ at the binding energy $|E_{2B}|$, which gives the eigen-equation

$$\left[U_p^{\text{eff}}(E_{2B})\right]^{-1} = S_p(E_{2B}) \tag{3.6}$$

to determine E_{2B}, as previously derived in Eq. (2.12) by directly solving Schrödinger's equation. Also, as discussed above, the atom pair population of the lowest trap mode is determined by the residue of the above T-matrix element at this pole and is the same as previously given in Eq. (2.14). Since the bound state of the *effective* Hamiltonian comprises only atom pairs in the lowest trap mode and dressed molecules, specifying the population in the lowest mode is sufficient, in conjunction with normalization, to determine the entire bound state of H_{eff}. Thus, to ensure that the effective and the exact Hamiltonians produce the same two-body bound state, we just need to obtain $[T(E)]^{-1}$ from both H and H_{eff}, and require them to match to first order in $E - E_{2B}$. This is exactly equivalent to solving the effective low-D

Schrödinger's equation for the bound state and energy of H_{eff} in terms of its parameters, and requiring the exact 3D results of the previous chapter be reproduced. However, the T-matrix approach is more elegant and instructive.

Following the same approach as in Appendix B, the corresponding T-matrix element from the effective Hamiltonian H_{eff} is obtained as

$$\left[T^{\text{eff}}(E)\right]^{-1} = \left[V_p^{\text{eff}}(E)\right]^{-1} - \gamma_{\mathbf{000}}^{-2}\sigma_p(E), \tag{3.7}$$

where

$$\left[V_p^{\text{eff}}(E)\right]^{-1} \equiv \left(V_p - \frac{\alpha_p^2}{\lambda_p - E}\right)^{-1} = \left(V_b - \frac{\alpha_b^2}{\lambda_b - E}\right)^{-1} + V_c^{-1}, \tag{3.8}$$

and the function

$$\begin{aligned}\sigma_p(E) &\equiv \gamma_{\mathbf{000}}^2 \int \frac{d^D\mathbf{k}}{(2\pi)^D}\left[\frac{1}{E - 2\epsilon_{\mathbf{k}}} + \frac{1}{2\epsilon_{\mathbf{k}} + 3 - D}\right] \\ &= \begin{cases} \frac{-1}{4\pi\sqrt{-E}} + \frac{1}{2^{5/2}\pi} & D = 1 \\ \frac{\ln(-E)}{2^{5/2}\pi^{3/2}} & D = 2 \end{cases}\end{aligned} \tag{3.9}$$

We require the effective background term alone to reproduce the two-body physics on the deep BCS side, where the dressed molecule population is negligible. Matching Eqs. (3.4) and (3.7) in that region yields

$$V_p^{-1} = (2\pi)^{(3-D)/2}\left(U_p^{-1} - C_p\right) \tag{3.10}$$

where $C_p \equiv \lim_{\nu_p\to\infty} S_p(E_{2B}) - \sigma_p(E_{2B})$. In this way, we obtain an effective single-channel model on the deep BCS side which recovers the low-energy scattering models of Refs. [32, 33, 35, 36, 43] as promised above. However, the single-channel model with a renormalized scattering length ($\propto V_p$) is not adequate near resonance or on the BEC side where the dressed molecule population becomes significant.

To fix the parameters λ_p and α_p, we compare the T-matrix in Eqs. (3.4) and (3.7) at general detuning, and require them to match for the zeroth and the first orders in

expansion with $(E - E_{2B})$ (which are responsible for reproducing the same binding energy and the bound state, respectively). After some algebra, we obtain

$$\lambda_p = E_{2B} - \frac{\sigma_p\left(E_{2B}\right)}{\partial_{E_{2B}}\left[U_p^{\text{eff}-1} - \left(S_p - \sigma_p\right)\right]}\left[1 - \frac{\sigma_p\left(E_{2B}\right)}{U_p^{-1} - C_p}\right] \tag{3.11}$$

$$\alpha_p^2 = \frac{\left(2\pi\right)^{(D-3)/2}}{\partial_{E_{2B}}\left[U_p^{\text{eff}-1} - \left(S_p - \sigma_p\right)\right]}\left[1 - \frac{\sigma_p\left(E_{2B}\right)}{U_p^{-1} - C_p}\right]^2 \tag{3.12}$$

where $\partial_{E_{2B}}$ means $\partial/\partial E\big|_{E=E_{2B}}$. Since the derivative of Eq. (3.5) is not obvious, we write it below explicitly [1].

$$\partial_{E_{2B}} S_p = \frac{-1}{2^{7/2}\pi}\begin{cases} \frac{1}{2}\zeta\left(3/2, -E_{2B}/2\right) & D = 1 \\ \frac{\Gamma(-E_{2B}/2)}{\Gamma(1/2 - E_{2B}/2)} & D = 2 \end{cases} \tag{3.13}$$

Thus, Eqs. (3.10, 3.11, 3.12) along with the low-D renormalization procedure in Eq. (3.3) fix the parameters of the effective Hamiltonian as functions of the two-body binding energy, E_{2B}, which is connected to the physical detuning ν_p through Eq. (3.6). The detuning-dependent parameters are plotted in Fig. 3.1 across resonance, assuming the same typical 3D parameters as in Chapter II. The difference in the sign of U_p between ^{6}Li and ^{40}K gives rise to quite different looking effective parameters. For ^{6}Li, the bare molecule contribution to the dressed molecule quickly vanishes in the BCS limit, leaving only excited atom pairs, so that the effective detuning approaches a constant on the order of the bandgap. For ^{40}K, the bare molecule contribution to the dressed molecule survives and the effective detuning keeps increasing with the magnetic field. However, the relevant combination of parameters for mean-field calculations, V_p^{eff}, is very nearly universal. We plot $V_p^{\text{eff}}\left(2\mu\right)$ across resonance with $\mu = E_{2B}/2 + \mu_\rho$ for small values of μ_ρ (μ has the meaning of the total chemical potential including the per-particle binding energy $E_{2B}/2$, while μ_ρ is the

[1] For $D = 2$, the second term in the integral does not contribute to the derivative, so it can be thrown out and the remaining integral can be differentiated with respect to $-2s$ instead of E.

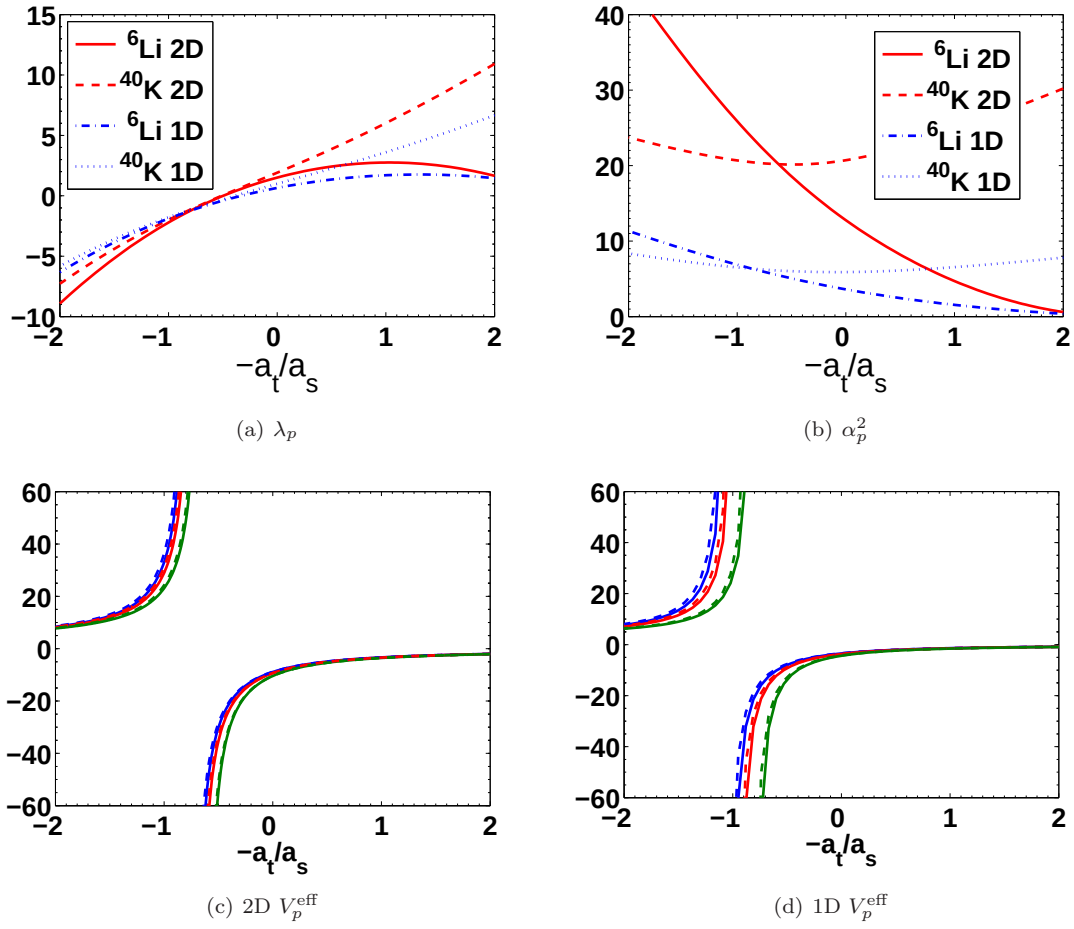

(a) λ_p (b) α_p^2

(c) 2D V_p^{eff} (d) 1D V_p^{eff}

Figure 3.1: (a)-(b): Detuning-dependent effective parameters vs. inverse 3D scattering length, $a_t/a_s = 4\pi/U_p^{\text{eff}}(0)$. (c)-(d): Effective interaction $V_p^{\text{eff}}(2\mu)$ vs. a_t/a_s. Solid lines are for ^{6}Li and dashed lines are for ^{40}K. The curves correspond to $\mu_\rho = 0, 0.05, 0.15$, from left to right.

contribution from many-body effects in units of $\hbar\omega$). The slight difference between the ^{6}Li and ^{40}K curves stems from the slight difference in binding energies as a function of the 3D scattering length. In the low density limit $\mu_\rho \to 0$, V_p^{eff} can approach infinity on the BEC side where $\lambda_p = E_{2B} = D - 3$, corresponding to the position of the well-known confinement induced resonance discussed in Refs. [32, 33, 35, 36, 43]. However, this resonance is for the two-body scattering physics and does not hold any special significance for the bound state physics. The relevant quantity for a typical many-body calculation is $1/V_p^{\text{eff}}(E)$, which is continuous.

3.5 Chapter Summary

We have derived an effective low-dimensional Hamiltonian for a strongly interacting atomic gas trapped in one or two dimensions and free in the other dimensions. Excited trap modes are important to the bound state physics, requiring the effective parameters to assume a highly nontrivial magnetic field dependence. All the parameters in the Hamiltonian have been fixed from two-body considerations. This effective Hamiltonian can provide a starting point to understand the low-dimensional many-body physics when the system is near its ground state configuration (with the chemical potential close to the per-particle binding energy $E_{2B}/2$). In fact, this Hamiltonian is very practical, and has already been used to calculate the Thomas-Fermi radius [53], population imbalanced phase diagram [54], and Berezinskii-Kosterlitz-Thouless transition temperature [55] of a quasi-2D gas. In the first work, the Thomas-Fermi radius was found to smoothly decrease as the gas was swept from the BCS side to the BEC side of resonance, as one would intuitively expect. This contrasts sharply with the unphysical prediction of a constant cloud size from a typical model accounting for the excited trap modes only through a renormalization of the scattering length via virtual transverse excitations. In the last work it was demonstrated that, in contrast to the results from a former 2D model which does not depend on the transverse mode spacing, the BKT transition temperature shows a marked dependence on the transverse trap frequency.

CHAPTER IV

Level Crossing in the Trapped Three-Fermion Problem

4.1 Chapter Overview

We present a solution of the three-fermion problem in a harmonic potential across a Feshbach resonance. We compare the spectrum with that of the two-body problem and show that it is energetically unfavorable for the three fermions to occupy one lattice site rather than two. We also demonstrate the existence of an energy level crossing in the ground state with a symmetry change of its wave function, suggesting the possibility of a phase transition for the corresponding many-body case.

4.2 Introduction

Ultracold atoms, tuned with a Feshbach resonance, offer a great opportunity to study strongly correlated many-body physics in a controlled fashion. For such strongly interacting systems, in general there is no well-controlled approximation method to solve the many-body physics. Exact solution of few-body problems plays an important role in understanding the corresponding many-body systems. Few-body (three- or four-body) problems have been solved for strongly interacting bosons or fermions in free space [56], in a quasi-one-dimensional configuration [57], and in a three-dimensional (3D) harmonic trap for bosons [58] or fermions in the unitary limit [59, 60].

In this chapter, we add to this sort of examples by exactly solving the three-body problem for strongly interacting two-component fermions in a 3D harmonic trap across resonance. This work has two main motivations: Firstly, the situation considered here is relevant for experiments where one loads strongly interacting two component fermions into a deep 3D optical lattice [30, 50]. For each site that can be approximated with a harmonic potential, one could have two identical fermions (spin-$\uparrow$) strongly interacting with another distinct fermion (spin-$\downarrow$). The three-body problem for equal mass fermions turns out to be very different from the corresponding case for bosons. Instead of a hierarchy of bound Efimov states for bosons [58], we show that there is always a significant energy penalty for three fermions to occupy the same lattice site ($\uparrow\uparrow\downarrow$) instead of two ($\uparrow\downarrow + \uparrow$). This result justifies an important assumption made in the derivation of an effective many-body Hamiltonian for this system [22]. Secondly, we analyze the ground-state structure of the three-body problem and show that as one scans the 3D scattering length, there is a level crossing between the lowest-lying three-fermion energy eigenstates, which have s- or p-wave symmetries respectively in the limit as two atoms are contracted to form a dimer. This level crossing with a symmetry change may correspond to a quantum phase transition in the many-body case where one has a spin-polarized fermi gas loaded into an optical lattice. The latter system with polarized fermions has raised strong interest recently in both theory and experiments [61–65].

4.3 Methods

The method here is based on manipulation of a Lippmann-Schwinger equation for the wavefunction, with the formalism similar to the one presented in Ref. [57]. As is standard, we separate the center-of-mass degree of freedom via an orthogonal

transformation of variables from the atomic positions $\{\mathbf{r}_\downarrow, \mathbf{r}_{\uparrow\mathbf{1}}, \mathbf{r}_{\uparrow\mathbf{2}}\}$ to new coordinates

$$\begin{pmatrix} \mathbf{x} \\ \mathbf{y} \\ \mathbf{z} \end{pmatrix} = \begin{pmatrix} 2/\sqrt{3} & -1/\sqrt{3} & -1/\sqrt{3} \\ 0 & -1 & 1 \\ \sqrt{2/3} & \sqrt{2/3} & \sqrt{2/3} \end{pmatrix} \begin{pmatrix} \mathbf{r}_\downarrow \\ \mathbf{r}_{\uparrow\mathbf{1}} \\ \mathbf{r}_{\uparrow\mathbf{2}} \end{pmatrix} \tag{4.1}$$

in which the harmonic trapping potential remains diagonal. The center-of-mass coordinate, $\mathbf{z}$, separates out and the Schrödinger equation for the relative degrees of freedom $\{\mathbf{x}, \mathbf{y}\}$ is

$$\left[-\frac{\hbar^2}{m_0} \left(\nabla_{\mathbf{x}}^2 + \nabla_{\mathbf{y}}^2 \right) + \frac{1}{4} m_0 \omega^2 \left(\mathbf{x}^2 + \mathbf{y}^2 \right) - E \right] \Psi(\mathbf{x}, \mathbf{y}) = -\sum_{\pm} V(\mathbf{r}_\pm) \Psi(\mathbf{x}, \mathbf{y}) \ , \tag{4.2}$$

where m_0 is the atomic mass, ω is the trap frequency, and we have already introduced a new set of relative variables via orthogonal transformation: $\mathbf{r}_\pm = \sqrt{3}\mathbf{x}/2 \pm \mathbf{y}/2$ are the vectors from the $\downarrow$ fermion to each of the two $\uparrow$ fermions. We have shown vectors proportional to the various coordinates introduced, along with some we will introduce in the next paragraph, in Fig. 4.1 in an attempt to maintain some clarity. We approximate the short-range interaction between fermions with the usual zero-range pseudopotential [66]

$$V(\mathbf{r}) = \frac{4\pi\hbar^2 a}{m_0} \delta(\mathbf{r}) \frac{\partial}{\partial r} (r\cdot) \ , \tag{4.3}$$

where a is the 3D s-wave scattering length tunable through the Feshbach resonance.

The above regularized contact interaction is equivalent to imposing boundary conditions

$$\Psi(\mathbf{x}, \mathbf{y}) \underset{\mathbf{r}_\pm \to 0}{\longrightarrow} \mp \frac{f(\mathbf{r}_{\perp,\pm})}{4\pi \mathbf{r}_\pm} \left(1 - \frac{\mathbf{r}_\pm}{a} \right) \ , \tag{4.4}$$

where we have introduced yet another set of variables via an orthogonal transformation: the $\mathbf{r}_{\perp,\pm} = \mathbf{x}/2 \mp \sqrt{3}\mathbf{y}/2$ are proportional to the distances between the center

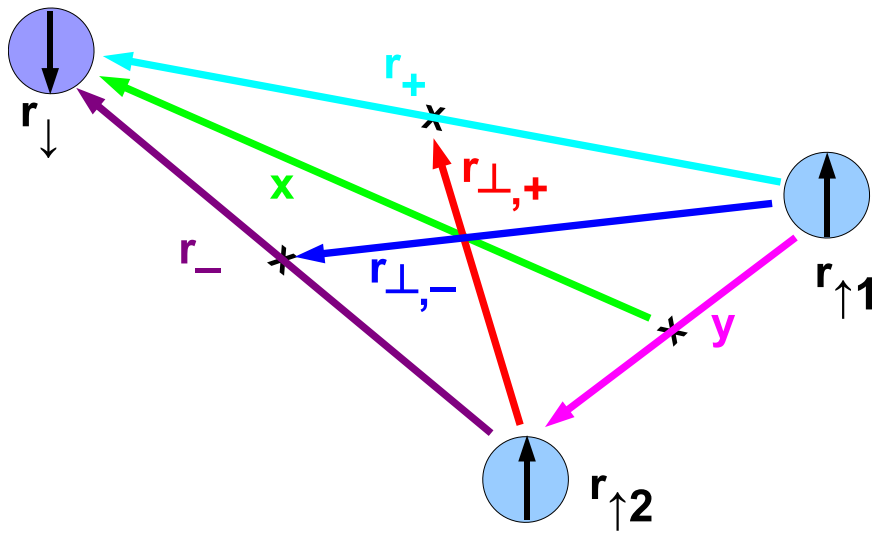

Figure 4.1: Relative coordinates for the three-fermion problem. The vectors referenced in the text are actually typically scaled by some numerical factor, but the directions are as shown.

of mass of an $\uparrow\downarrow$ pair and an $\uparrow$ fermion. The overall $\mp$ sign ensures the antisymmetry of the wavefunction upon swapping the identical fermions. The undetermined function $f(\mathbf{r})$, after a rescaling of the argument, is the relative atom-dimer wavefunction that results when two of the fermions form a tightly bound pair. Solving for this asymptotic wavefunction $f(\mathbf{r})$ fully determines $\Psi(\mathbf{x},\mathbf{y})$.

Since $V(\mathbf{r}_\pm)$ only acts at $\mathbf{r}_\pm = 0$, we use the asymptotic form of Ψ when computing $V(\mathbf{r}_\pm)\Psi$. The formal solution can then be written as

$$\Psi(\mathbf{x},\mathbf{y}) = \int d\mathbf{x}' d\mathbf{y}' G_E^{(2)}(\mathbf{x},\mathbf{y};\mathbf{x}',\mathbf{y}') \sum_\pm \frac{\mp\hbar^2 f(\mathbf{r}'_{\perp,\pm})}{m_0} \delta(\mathbf{r}'_\pm) \,, \tag{4.5}$$

where the two-particle Green's function is given by

$$G_E^{(2)}(\mathbf{x},\mathbf{y};\mathbf{x}',\mathbf{y}') = \sum_{\lambda_1\lambda_2} \frac{\psi_{\lambda_1}(\mathbf{x})\psi_{\lambda_2}(\mathbf{y})\psi^*_{\lambda_1}(\mathbf{x}')\psi^*_{\lambda_2}(\mathbf{y}')}{E_{\lambda_1}+E_{\lambda_2}-E} \,. \tag{4.6}$$

The $\psi_{\lambda_i}(\mathbf{x})$ are the single-particle eigenfunctions with eigenenergies E_{λ_i} for the reduced mass $m_0/2$. Here we use spherical coordinates for the three-dimensional harmonic trap, so the quantum numbers are $\lambda = (n,l,m)$, $n = 0,1,2,...$; $l = 0,1,2,...$; $m = -l,-l+1,...,l-1,l$. The eigenenergies are $E_\lambda = (2n+l+3/2)\hbar\omega$ and the

eigenfunctions are $\psi_\lambda(\mathbf{r}) = R_{nl}(r)\, Y_l^m(\theta,\phi)$, where the $Y_l^m(\theta,\phi)$ are the standard spherical harmonics. The radial wavefunction is given by [67]

$$R_{nl}(r) = \sqrt{\frac{2n!/d^3}{(n+l+1/2)!}} e^{-r^2/2d^2} \left(\frac{r}{d}\right)^l L_n^{l+1/2}\left(r^2/d^2\right) \tag{4.7}$$

where $d = \sqrt{\frac{2\hbar}{m_0\omega}}$ is the length scale of the trap and the $L_n^k(r)$ are associated Laguerre polynomials.

We can make use of the invariance of $G_E^{(2)}$ and the integration measure under an orthogonal transformation of variables to rewrite Eq. (4.5) in terms of $\mathbf{r} \equiv \mathbf{r}_-$ and $\mathbf{r}_\perp \equiv \mathbf{r}_{\perp,-}$,

$$\Psi(\mathbf{r},\mathbf{r}_\perp) = \frac{\hbar^2}{m_0}\int d\mathbf{r}'_\perp f(\mathbf{r}'_\perp)\left[G_E^{(2)}(\mathbf{r},\mathbf{r}_\perp;0,\mathbf{r}'_\perp) - G_E^{(2)}\left(\frac{\mathbf{r}}{2}+\frac{\sqrt{3}\mathbf{r}_\perp}{2},\frac{\sqrt{3}\mathbf{r}}{2}-\frac{\mathbf{r}_\perp}{2};0,\mathbf{r}'_\perp\right)\right] \tag{4.8}$$

We can also decompose the asymptotic atom-dimer wavefunction in terms of the complete set of single-particle wavefunctions, $f(\mathbf{r}_\perp) = \sum_\lambda f_\lambda \psi_\lambda(\mathbf{r}_\perp)$. Then Eq. (4.8) becomes

$$\Psi(\mathbf{r},\mathbf{r}_\perp) = d^2\hbar\omega\sum_\lambda\Bigg[G_{E-E_\lambda}(\mathbf{r},0)\,\psi_\lambda(\mathbf{r}_\perp) - G_{E-E_\lambda}\left(\frac{\mathbf{r}}{2}+\frac{\sqrt{3}\mathbf{r}_\perp}{2},0\right)\psi_\lambda\left(\frac{\sqrt{3}\mathbf{r}}{2}-\frac{\mathbf{r}_\perp}{2}\right)\Bigg] f_\lambda \tag{4.9}$$

where G_E is the single-particle Green's function,

$$G_E(\mathbf{r},0) = \sum_\lambda \frac{\psi_\lambda(\mathbf{r})\,\psi_\lambda^*(0)}{E_\lambda - E} = \frac{e^{-r^2/2d^2}}{2\pi^{3/2}d^3\hbar\omega}\Gamma\left(\frac{\frac{3}{2}-E/\hbar\omega}{2}\right)U\left(\frac{\frac{3}{2}-E/\hbar\omega}{2},\frac{3}{2},\frac{r^2}{d^2}\right) \tag{4.10}$$

[34], and U is the confluent hypergeometric function. Note that the three-fermion wavefunction is fully determined by $f(\mathbf{r}_\perp)$ and that if we consider Eq. (4.9) in the limit as $\mathbf{r} \to 0$, we obtain a self-consistent equation for $f(\mathbf{r}_\perp)$ by using the boundary

conditions. After some work, we obtain

$$\sum_{\lambda'} A_{\lambda\lambda'} f_{\lambda'} = \left[\frac{d}{a} - 2 \frac{\Gamma\left(\frac{3/2+E_\lambda/\hbar\omega - E/\hbar\omega}{2}\right)}{\Gamma\left(\frac{1/2+E_\lambda/\hbar\omega - E/\hbar\omega}{2}\right)} \right] f_\lambda \tag{4.11}$$

where

$$A_{\lambda\lambda'} = \int \frac{d\mathbf{r}_\perp}{4\pi d^3 \hbar\omega} G_{E-E_{\lambda'}}\left(\frac{\sqrt{3}\mathbf{r}_\perp}{2}, 0\right) \psi^*_\lambda(\mathbf{r}_\perp)\, \psi_{\lambda'}\left(\frac{-\mathbf{r}_\perp}{2}\right) \tag{4.12}$$

4.4 Results

We anticipate that the low-energy physics should be contained in a truncated Hilbert space containing only the lowest few asymptotic atom-dimer energy levels. Then Eq. (4.11) is easily solved numerically. We have checked that, indeed, the solution for the ground state and the first excited manifold become insensitive to the cutoff, as long as the first four or five atom-dimer energy levels are included and the binding energy is not too large. In the tightly bound limit, our results are subject to quantitative corrections (discussed in the next paragraph), but still capture the essential physics. For all results presented in this chapter, we have kept the first five energy levels. Because of the degeneracy of the excited levels, Eq. (4.11) then becomes a 35×35 matrix equation. For a given energy, we solve numerically to obtain the corresponding scattering length and eigenstate. By sweeping through a range of energies, we map out the spectrum shown in Fig. 4.2(a). At unitarity, our result for the low-energy spectrum agrees with the analytic result of Ref. [59]. Upon careful inspection, one can discern the presence of level crossings. More usefully, in Fig. 4.2(b) we display the difference between the energy of three fermions in a single lattice site and the energy of two fermions ($\uparrow\downarrow$) in the site and the extra fermion alone in a separate site. Here we have used the well-known exact solution for the

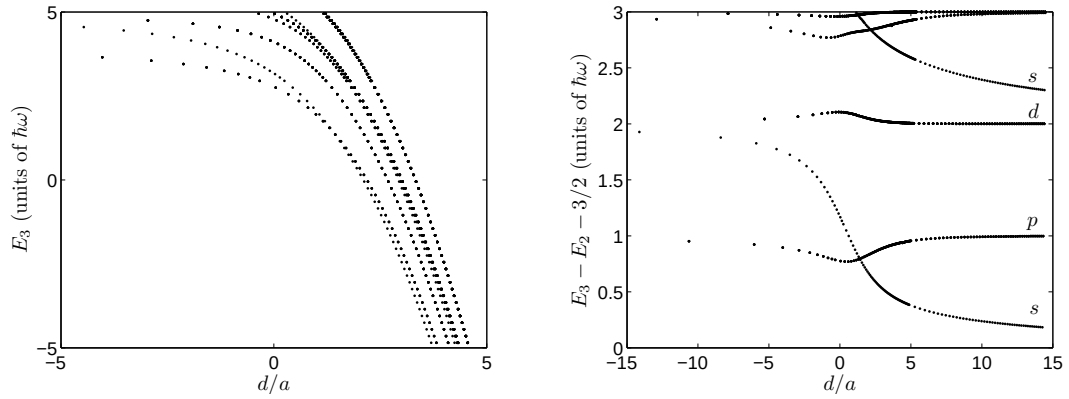

Figure 4.2: (a) Energy vs. inverse scattering length. (b) Difference between three-fermion energy and two-fermion energy plus one-fermion energy vs. inverse scattering length.

two-body energy E_2 [34],

$$\frac{d}{a} = 2\frac{\Gamma\left(\frac{3/2-E_2/\hbar\omega}{2}\right)}{\Gamma\left(\frac{1/2-E_2/\hbar\omega}{2}\right)}. \tag{4.13}$$

After publication of our results, another group performed calculations using a wholly different technique which agree with our results except that their results indicate our s-wave energy is not fully converged in the deeply bound region at small and positive scattering length [68]. We have subsequently confirmed that to attain full convergence in the deeply bound regime for $d/a \sim 7$ we should include on the order of fifty asymptotic atom-dimer energy levels instead of just five, lowering our s-wave energy by about $0.07\hbar\omega$. This is a negligible correction compared to the energy plotted in Fig. 4.2(a), but it results in about a 25% correction to the energy difference plotted in Fig. 4.2(b). However, the general features of the data are unchanged.

Figure 4.2(b) is our main result. There are two main features we would like to point out. First, clearly it is energetically favorable for atoms in a lattice to arrange themselves such that there are less than three atoms per site, regardless of the scattering length. This has already been assumed in the derivation of an effective many-body Hamiltonian for atoms in an optical lattice across a Feshbach resonance

[22], and is confirmed by Fig. 4.2(b). Second, the level crossing in the ground state is now quite evident. On the positive scattering length side of the crossing (the BEC side), the ground state is nondegenerate. On the negative scattering length side (the BCS side), it is triply degenerate. Other crossings appear in the excited spectrum, although to obtain quantitatively accurate results for these one should include higher modes when solving Eq. (4.11).

The origin of the level crossing is the differing symmetries of the eigenstates. For very small, positive scattering length (the deep BEC limit), formation of tightly bound dimers is favorable, so the state should behave as the ground state of the relative atom-dimer motion, which has s-wave symmetry. For very small, negative scattering length (the deep BCS limit), the atoms are essentially non-interacting, so the ground state comprises two atoms ($\uparrow\downarrow$) in the ground state of the trap plus the third in the first excited state of the trap (which is triply degenerate) because of Pauli exclusion. So, on the deep BCS side, the ground state has p-wave symmetry. Due to the rotational symmetry of a spherical harmonic trap, the total angular momentum of the three particles should be a conserved quantity. However, from the above analysis, this quantity has different values for the ground state in the deep BEC and deep BCS limits. Therefore, there must be a ground-state level crossing for this system as one scans the scattering length. If one considers multiple lattice sites with each site having on average two spin-$\uparrow$ and one spin-$\downarrow$ atoms (which could be realized with polarized fermions in an optical lattice with appropriate filling number and population imbalance), as the three-body problem has a level crossing with different ground state degeneracies in the BCS and the BEC limits, there could be a corresponding quantum phase transition for this many-body system (with small tunneling between lattice sites) as one scans the scattering length.

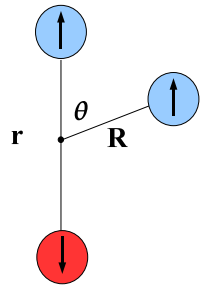

Figure 4.3: Relative coordinates for the three-fermion problem. In terms of variables used in Eq. (4.9), $r = |\mathbf{r}|$, $R = \sqrt{3}\,|\mathbf{r}_\perp|\,/2$.

The wavefunction given in Eq. (4.9) does not generally have definite *relative* angular momentum for any two fermions. However, in the limit as the distance between two distinguishable fermions goes to zero, the wavefunction takes on the symmetry of the asymptotic atom-dimer wavefunction in the remaining coordinates. This is a relative angular momentum eigenstate due to the spherical symmetry of the limiting case. With the relative coordinates defined by Fig. 4.3, the symmetry of the wavefunction as a function of R and θ in the limit as r goes to zero is shown by Fig. 4.4. For finite r, the $m = 0$ wavefunctions are affected by the asymmetry and take nontrivial shapes. We have plotted an example in Fig. 4.5. Note that in this figure we include a factor of $\sin\theta$ since the wavefunction itself diverges at $R = r/2$, $\theta = \pi$ according to the boundary conditions we have imposed. On the BEC side, the lobes are tightly bunched near $\theta = \pi$, but on the BCS side they spread around as expected.

In general, the eigenstates are rather difficult to visualize, since they depend nontrivially on three spatial variables as well as the scattering length. However, one can get some idea of the evolution of the eigenstates from Fig. 4.6, which shows the normalized probability density as a function of the variables introduced in Fig. 4.3 for various scattering lengths. In each subplot we have numerically integrated over

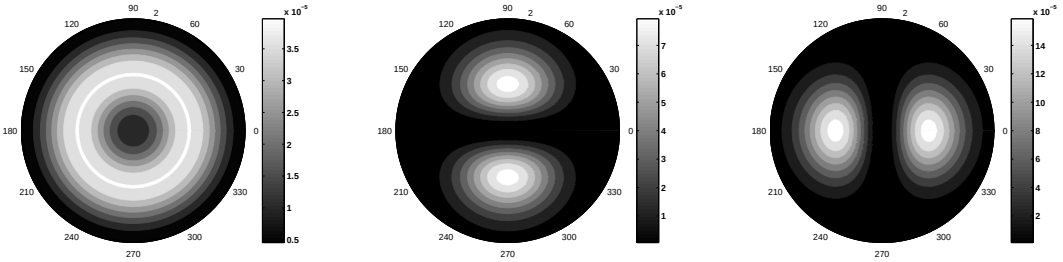

(a) $n = 0$, $l = 0$, $m = 0$ (b) $n = 0$, $l = 1$, $m = \pm 1$ (c) $n = 0$, $l = 1$, $m = 0$

Figure 4.4: Contour plots of $r^2 \left|\Psi\left(r, R, \theta\right)\right|^2_{r\to 0}$ as a function of R and θ for $r/d \simeq 0$ and $d/a \simeq 0$.

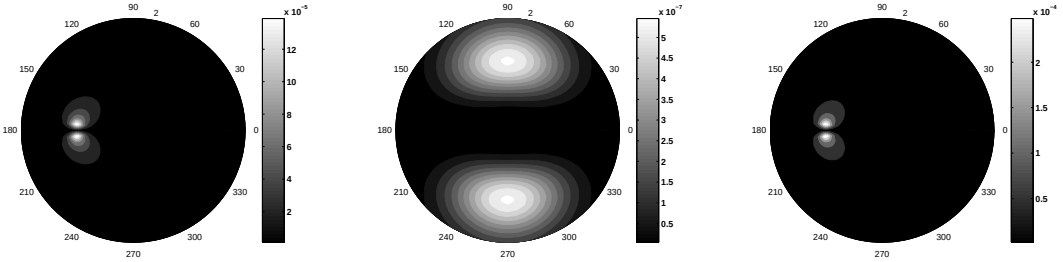

(a) $n = 0$, $l = 0$, $m = 0$ (b) $n = 0$, $l = 1$, $m = \pm 1$ (c) $n = 0$, $l = 1$, $m = 0$

Figure 4.5: Contour plots of $r^2 R^2 \left|\sin\theta\Psi\left(r, R, \theta\right)\right|^2$ as a function of R and θ for $r/d = 2$ and $d/a \simeq 0$.

the other two variables to obtain a one-dimensional function. The dimer size, r, clearly decreases in size as one enters the BEC regime, developing a strong peak at the origin. However, as is clear from Fig. 4.3, there are two ways to form a tightly bound dimer (due to the two identical spin $\uparrow$ atoms) and we have arbitrarily chosen one to define the origin $r = 0$. So it is not surprising that we see a more diffuse second peak at large distance r, corresponding to the dimer forming between the spin $\downarrow$ and the other spin $\uparrow$ atom. This is also the meaning of the spike at $\theta = \pi$ on the BEC side.

4.5 Chapter Summary

We have found the low-lying energy levels of three fermions in a harmonic trap and examined the corresponding wavefunctions. The ground state has s-wave symmetry on the BEC side of Feshbach resonance and has p-wave symmetry on the BCS side.

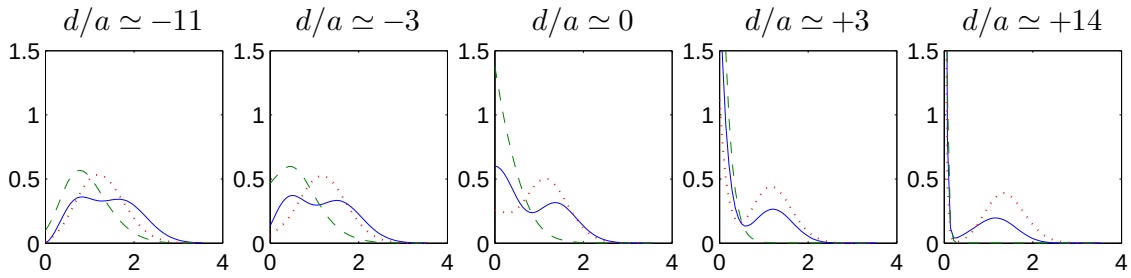

(a) Normalized probability density vs. r/d

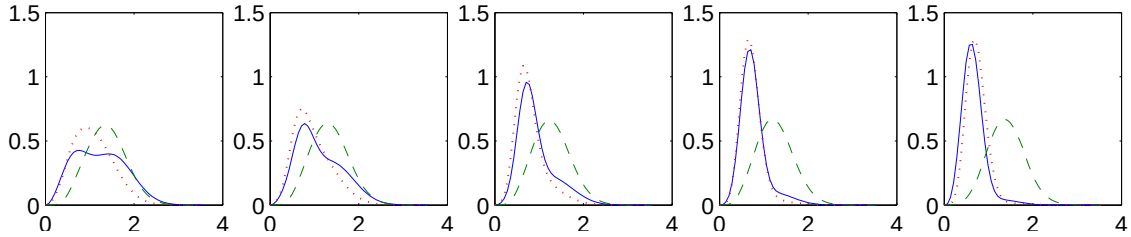

(b) Normalized probability density vs. R/d

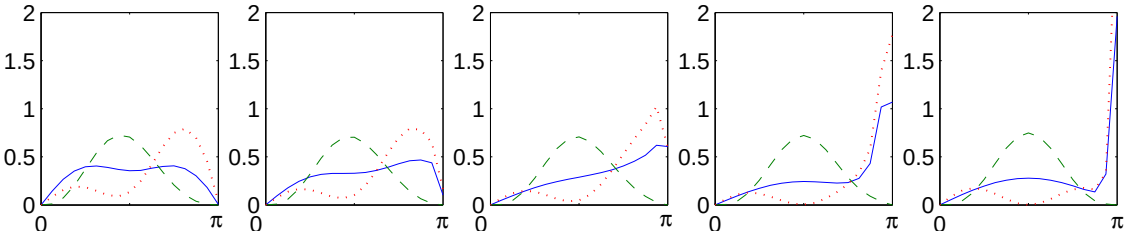

(c) Normalized probability density vs. θ

Figure 4.6: Normalized probability density distribution functions of variables defined in Fig. 4.3 for various scattering lengths. The solid line is for the $n = 0$, $l = 0$, $m = 0$ state; the dashed line is for the $n = 0$, $l = 1$, $m = \pm 1$ state; and the dotted line is for the $n = 0$, $l = 1$, $m = 0$ state.

In the resonance region there is a level crossing, which may indicate a phase transition in the corresponding many-body case. We also note that, in the vicinity of resonance, the energy of three atoms in a single site is greater than their energy if they are in two sites, with a gap on the order of the trap energy, validating the approximation in Ref. [22].

After completion of this work, we became aware of a work which treats the trapped three-fermion problem with a different approximation method [69] and also mentions the possibility of a ground state level crossing.

CHAPTER V

Effective Single-Band Lattice Models for Fermions in an Optical Lattice at Low Filling Factors

5.1 Chapter Overview

We numerically find the energy spectrum for two fermions interacting across a Feshbach resonance in a double well potential. From the spectrum we determine the range of detunings for which a many-body system loaded into an optical lattice at low filling factor can be described by a lattice model, and how the model parameters are related to the experimental parameters. We find that for a range of strong interactions the system is well described by an effective $t - J$ lattice model, and the effective superexchange term, J, can be smoothly tuned through zero on either side of unitarity. Right at and around unitarity, an effective one-band Hubbard model is appropriate, with a finite and small on-site energy, due to a lattice-induced anharmonic coupling between atoms at the scattering threshold and a weakly bound Feshbach molecule in an excited center of mass state.

5.2 Introduction

Systems of ultracold fermionic atoms interacting in an optical lattice potential via a Feshbach resonance provide seemingly boundless opportunities to realize a zoo of lattice Hamiltonians in an extremely clean and controllable fashion [22, 70–

72]. This allows a new tool to study many lattice models familiar from condensed matter physics such as the Hubbard, $t-J$, and XXZ models, to name a few. In addition to the prospect of studying these paradigmatic models experimentally in the absence of complications such as phonons and impurities, ultracold gases provide the especially exciting possibility of gaining new insight into the proper description of strongly correlated systems. While it is well-known that a weakly interacting gas in an optical lattice can be described by the one-band Hubbard model [71], a similarly simple model for strongly interacting gases has remained elusive.

In the strongly interacting regime, the conventional one-band Hubbard model for two-component fermions (and the $t-J$ model derivable from the Hubbard model for large U) obviously no longer applies, since the on-site interaction energy becomes greater than the bandgap of the lattice. In this case, two atoms on the same site will form a dressed molecule which populates many excited bands [22, 42], as discussed in Chapters II and III in a low-dimensional context. The dressed molecule is defined somewhat differently in this case, though, since the atoms in the lowest band are now tightly confined and there is no longer any need to separate them from the other components of the two-body state. Here we can safely denote the entire on-site dimer state as the dressed molecule, a point boson. Since multi-band effects are not negligible [73], a simple description appears impossible.

However, in the case where the average number of atoms per site $\bar{n} \leq 2$, we saw in Chapter IV that configurations with sites occupied by more than two atoms are energetically unfavorable due to Pauli exclusion and are irrelevant to the low-energy physics. Thus the Hilbert space is severely restricted: each site may be empty, or populated with either one atom or one dressed molecule. The most general Hamiltonian for this Hilbert space, assuming SU(2) symmetry for the two components

and number conservation for each, is a one-band two-channel model (corresponding to atoms and dressed molecules) with slave bosons (corresponding to empty sites) necessary to enforce the Hilbert space restriction [23]. The actual details of the Hamiltonian are irrelevant at this point; our focus is simply on the structure of the Hilbert space.

This model can be rewritten in a one-band one-channel form, without slave bosons, by mathematically treating the dressed molecules as if they were simply an on-site atom pair in a single band [23]. Pauli exclusion then enforces the restriction on the Hilbert space automatically – each site now can be empty, or populated with either one atom or one "atom pair" – with no need for slave bosons. Note that although the actual physical state of two strongly interacting atoms in a single site is much different than a one-band pair, we have simply made a one-to-one mapping between the bosonic dressed molecule and the one-band fermion pair in order to take advantage of fermion statistics to generate the correct Hilbert space structure. We will refer to this one-band one-channel model as the general Hubbard model, because it has the same Hilbert space structure as the conventional one-band Hubbard model, although it may contain additional processes such as occupation-dependent tunneling, direct off-site interaction, etc. However, we emphasize that while the one-band Hubbard model includes only lowest band physics, the general Hubbard model includes on-site multi-band physics via the hidden structure of the dressed molecule, which will determine which processes are important and what values the parameters must take.

Similar to the above discussion, but more straightforward, is the strongly interacting case when the average number of atoms (dimers) per site is ≤ 1 and sites are doubly (singly) occupied only virtually because the dressed molecule energy is far detuned from the atomic energy. Then the most general Hamiltonian, keeping

only nearest neighbor terms, is a one-band one-channel $t-J$ (XXZ) model. In this chapter we consider models for the energy range around the scattering threshold and not deeply bound energies, so we will not consider an effective XXZ model here, but we will discuss an effective $t-J$ model. Note, though, that here the $t-J$ model does not arise from the Hubbard model via perturbation theory, as is usually the case [74]. Instead, it is fundamental, and may be valid even when a general Hubbard model is not.

Although the lattice models discussed above resemble familiar models, here they arise from very general considerations rather than microscopic ones. We have also made an implicit assumption that at most one dressed molecule state is relevant, i.e., close to the lowest atomic band. In order to determine the range of scattering lengths for which this assumption is valid, as well as to determine the proper values of the model parameters in terms of the experimental ones, detailed calculations are necessary.

In this chapter, we numerically solve the strongly interacting two-body problem in a double-well potential simulating a three-dimensional optical lattice. We examine the resultant spectrum and find regions where there is a low-lying set of energy levels that is well isolated from both deeply bound levels and higher excited levels. The number of isolated levels determines the type of lattice model that is applicable, and the model parameters are extracted by requiring the model to correctly reproduce those levels. Although we only treat the two-body case, our results are applicable to the many-body case since we have already assumed $\bar{n} \leq 2$ and configurations with more than two atoms per site are unfavorable. The only relevant information inaccessible to a two-body calculation is the values of the tunneling rate for an atom hopping from a doubly occupied site to a singly occupied site (a three-body process)

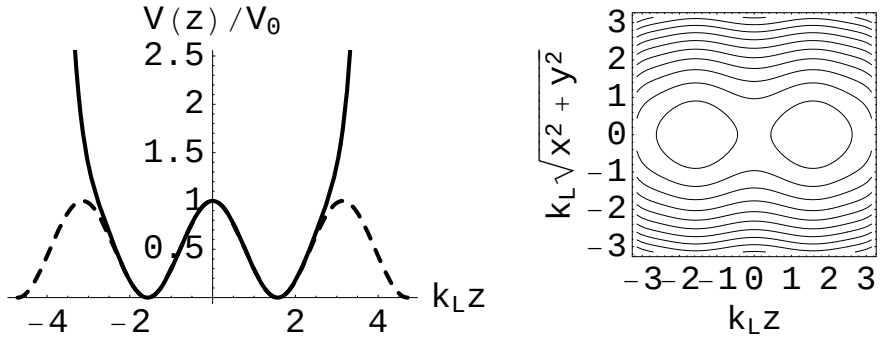

Figure 5.1: (a) The double-well potential along z modeling a periodic potential; (b) contour plot of the locally isotropic 3D double-well potential.

and the dimer-dimer off-site interaction (a four-body process).

5.3 Methods

We consider two distinguishable fermions of mass m in an external potential $V(\mathbf{x})$, interacting via a short range potential $U(r)$ characterized by its s-wave scattering length, a_s. In experiments, the external potential is typically the sum of a periodic potential $V_0 \prod_{i=1}^{3} \cos^2 k_L x_i$ and a harmonic confining potential. To make our calculations easier we will model this by considering a double-well potential along the z-axis (formed by Taylor expanding $\cos^2 k_L z$) and a harmonic potential in the other two directions, with the frequency, ω, chosen such that the potential is locally isotropic at the bottom of each well, as shown in Fig. 5.1. In fact, this double-well problem is interesting in its own right, as it is relevant to experiments with gases confined in optical superlattices [75]. Since the barrier is the same as for the full lattice, the hopping rates should be nearly unaffected. Also, the on-site interaction energy should not be affected qualitatively. The only relevant information that the double-well approximation renders inaccessible is rates for any next-nearest neighbor process.

Due to the harmonicity of the transverse trap, the center of mass (c.m.) motion

in the transverse direction separates out and is thus neglected in the rest of the discussion. However, along the axis of the double-well, the c.m. motion is not separable from the relative motion. The two atom system then has three relevant coordinates: the relative coordinates z and ρ, along the axial and transverse directions, respectively, and Z, the axial c.m. coordinate. In terms of these coordinates, the external potential approximating an optical lattice of depth V_0 is

$$V(\rho, z, Z) = V_0 \left[\frac{1}{2} k_L^2 \rho^2 + \sum_{\substack{n=0 \\ \pm}}^{6} \frac{(-4)^n \Gamma(1-2n)}{\Gamma(1-4n)\Gamma(1+4n)} \left(\frac{k_L (Z \pm z)}{2} \right)^{2n} \right] \tag{5.1}$$

where $\Gamma(x)$ is the Euler gamma function.

The exact form of the interaction, $U\left(\sqrt{\rho^2 + z^2}\right)$, is irrelevant in the low-energy limit as long as its range is much smaller than the average interatomic distance and the trap length scale, and most analytical treatments use a zero-range pseudopotential. Numerically, it is easiest to use a finite-range attractive gaussian interaction $U(r) = -U_0 \exp(-r^2/r_0^2)$, where we typically take $r_0 = 0.05\sqrt{\hbar/m\omega}$. Finite-range effects should be negligible for such small values of r_0, and we have verified this by repeating the calculations with $r_0 = 0.1\sqrt{\hbar/m\omega}$. The free space scattering length is varied by adjusting the strength of the interaction, U_0. We have calculated the mapping between the two and plot it in Fig. 5.2.

Adopting units such that $k_L = 1$ and $E_R = \hbar^2 k_L^2 / 2m = 1$, the Hamiltonian may be written as

$$H = -2\partial_\rho^2 - 2\partial_z^2 - \frac{1}{2}\partial_Z^2 + V(\rho, z, Z) - U_0 e^{-\left(z^2+\rho^2\right)/r_0^2}. \tag{5.2}$$

We find the low-lying states of the system using a stochastic variational method [76] recently introduced to the ultracold gas community by von Stecher and Greene

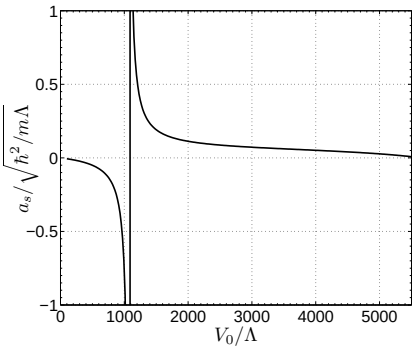

Figure 5.2: Free space scattering length vs. attractive gaussian interaction strength with range $r_0 = 0.05\sqrt{\hbar/m\Lambda}$. The unit of energy, Λ, is arbitrary.

[77]. In this approach, the variational wavefunction takes the form

$$\Psi_{abc}(\rho, z, Z) = \sum_i^N \alpha_i \exp\left(-\rho^2/a_i^2 - z^2/b_i^2 - Z^2/c_i^2\right), \tag{5.3}$$

where α is a linear variational parameter, $\{a, b, c\}$ are nonlinear variational parameters which define the basis elements, and N is the size of the basis set. The nonlinear parameters are selected from stochastically generated pools of candidates to minimize the variational energy $\langle\Psi_{abc}|H|\Psi_{abc}\rangle/\langle\Psi_{abc}|\Psi_{abc}\rangle$. Details of the method can be found in Appendix C and Ref. [76].

We typically achieved fairly good convergence for $N \sim 300$. Although in principle the nonlinear basis optimization must be performed for each value of a_s, actually the basis set does not change too much as one sweeps across resonance except to include narrower and narrower gaussians for positive a_s where deeply bound molecules form. Apart from deeply bound states, the change in the wavefunction is mainly due to changing the expansion coefficients, α. To save computational time then, we performed the nonlinear basis optimization for four different values of a_s across resonance, joined the four optimized basis sets, and simply minimized the energy with respect to α using the resultant basis set of about 1200 elements for all values of a_s. As a result, very deeply bound energy levels may not be fully converged, but

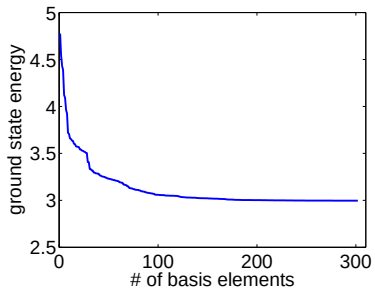

Figure 5.3: Typical plot of the convergence of the ground state energy vs. basis size.

we are only interested in the energy range around the lowest noninteracting levels. In this range, our results appear to be converged, as shown in Fig. 5.3.

5.4 Results

5.4.1 Regions of model validity

In Figs. 5.4 and 5.5, we show the spectrum of two atoms interacting in a double-well potential across a Feshbach resonance for $V_0 = 8E_r$ and $V_0 = 10E_r$. For clarity, we have plotted a diabatized spectrum for $-1/k_L a_s < -4$, omitting the plunging levels. We have also omitted the exactly flat, noninteracting levels. In the absence of trap anharmonicity, there are three kinds of curves present: plunging levels corresponding to tightly bound molecules in motionally excited states, flat levels corresponding to atoms in separate wells, and sigmoidal levels corresponding to atomic pairs interacting in the same well. Levels corresponding to states of similar parity never cross, instead undergoing a rich set of narrow avoided crossings. This is due to the coupling of the center of mass and relative motion by the anharmonic potential. (We will discuss this point further in Chapter VI.) Away from unitarity, these avoided crossings become even narrower and are irrelevant. We note that some of our calculations of highly excited even molecule states are apparently not as well converged as the corresponding calculations for the odd states, since the even states (solid lines) should be the lowest of each plunging doublet as the molecules become

tightly bound and act as a point particle. However, this is not important for our purposes.

To approximate the two-atom, double-well physics with a general Hubbard model requires a separation of energy scales such that there is a manifold of four energy levels well-separated from all the others, corresponding to a doublet of doubly occupied states and a doublet of singly occupied states. This condition is satisfied far from unitarity on either side. (On the scale of the plots, it may be hard to distinguish the two levels in the doubly occupied doublet, as their splitting is on the order of the tunneling energy. The levels in the singly occupied doublet are likewise very close, but we have only shown one since the other is odd in the relative coordinate and is independent of the interaction.) We have marked the low-energy regions where the ratio of the energy range of the low-lying manifold and its separation from the nearest level outside the manifold is greater than five. Actually, in enforcing this requirement, we have taken into account that the discrete levels turn into bands of width $\sim 4t$ when extending the two-site potential to an infinite lattice.

The small disconnected regions near unitarity where a general Hubbard model is applicable, shown in Figs. 5.4(b) and 5.5(b), are qualitatively different from the weakly interacting regions. Here the on-site dimers correspond to Feshbach molecules in an excited center of mass band. The usual ground band Feshbach molecules are far-detuned and irrelevant. The coupling to the relevant singly occupied states (which are in the lowest center of mass band) is facilitated by the anharmonicity of the potential. This is a very interesting phenomenon whereby the lattice-induced coupling turns the unitary regime on its head: the on-site energy becomes arbitrarily small instead of arbitrarily large. As higher excited molecular bands become relevant, eventually the molecule bandwidth becomes comparable to the bandgap and one can no longer

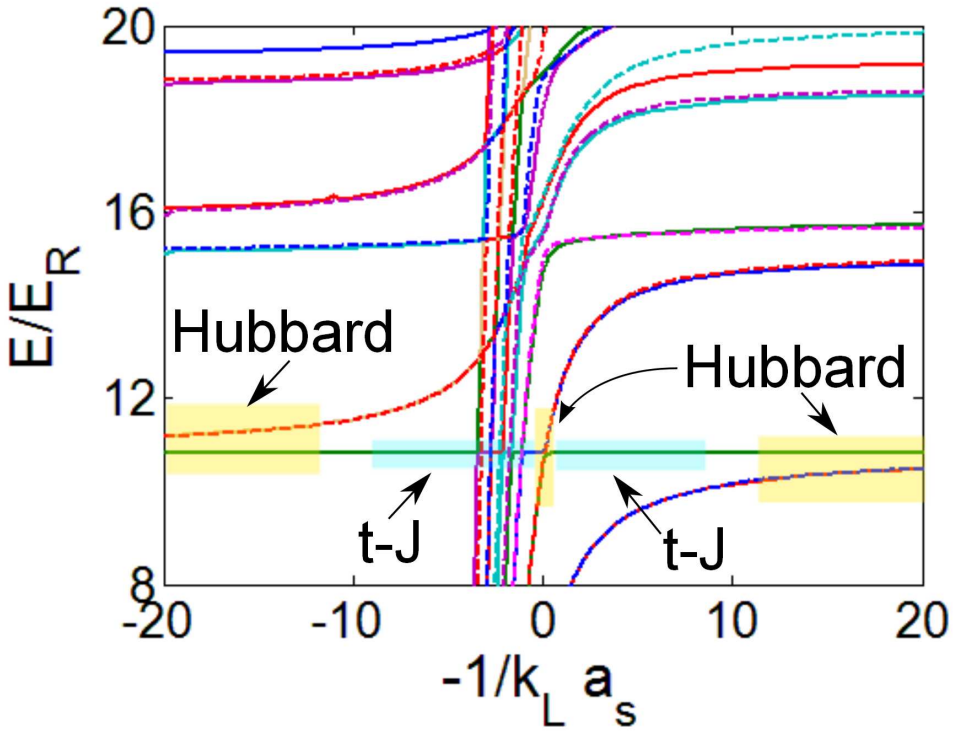

(a)

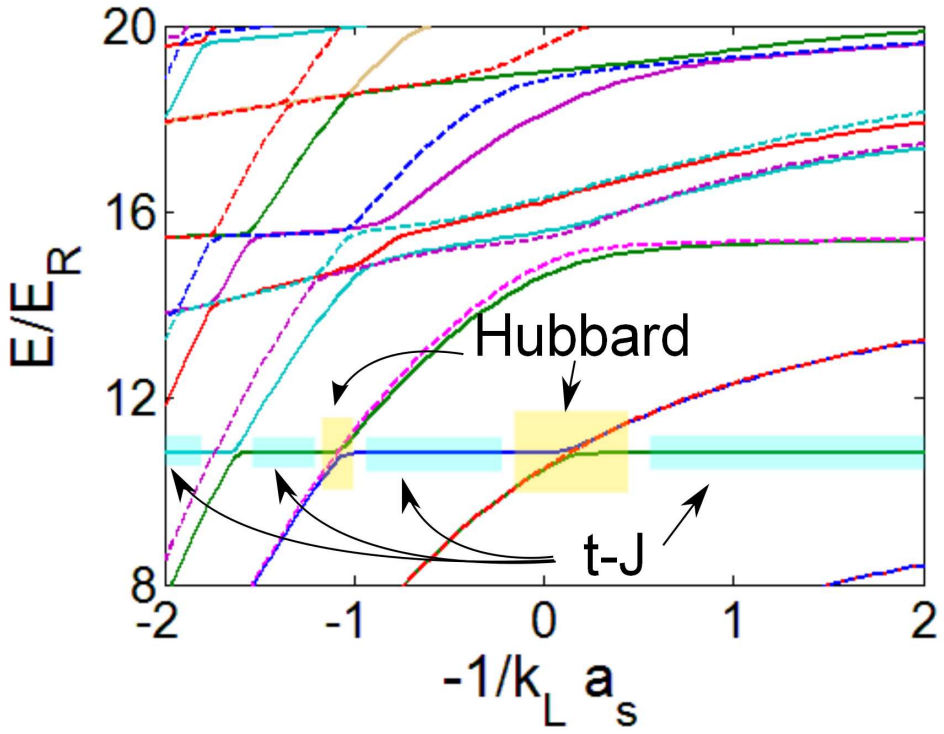

(b)

Figure 5.4: (a) Spectrum of two interacting atoms in a three-dimensional double-well potential vs. inverse free space scattering length with $V_0 = 8E_R$. Solid (dashed) lines correspond to states of even (odd) symmetry in Z. Only the first few plunging levels are shown. (b) Close-up of the strongly interacting region. The noninteracting states odd in z are not shown.

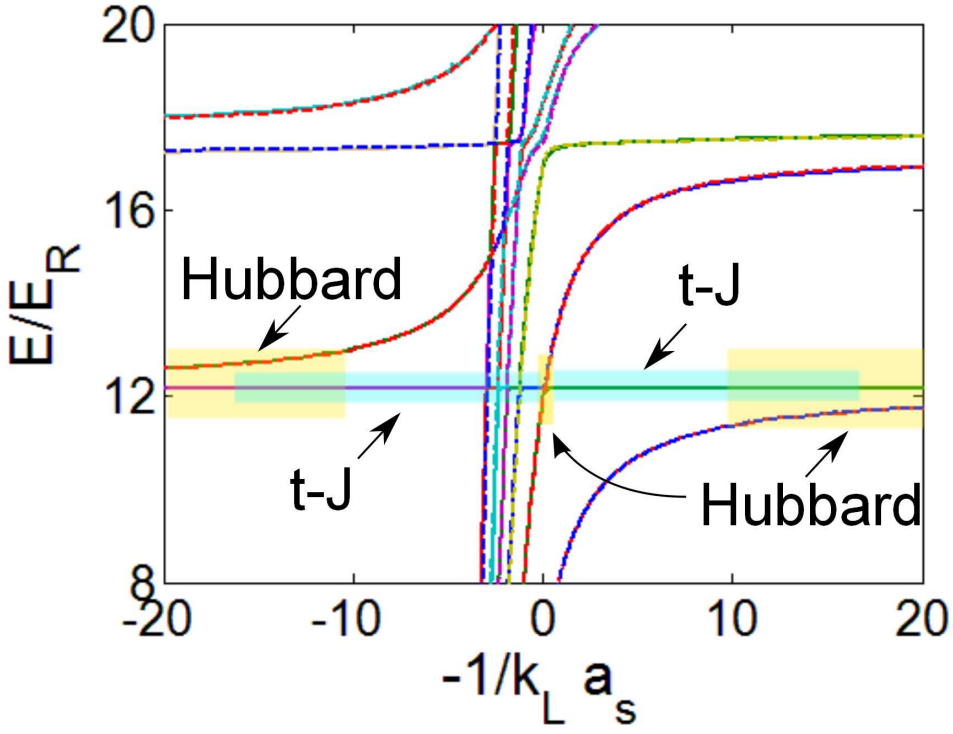

(a)

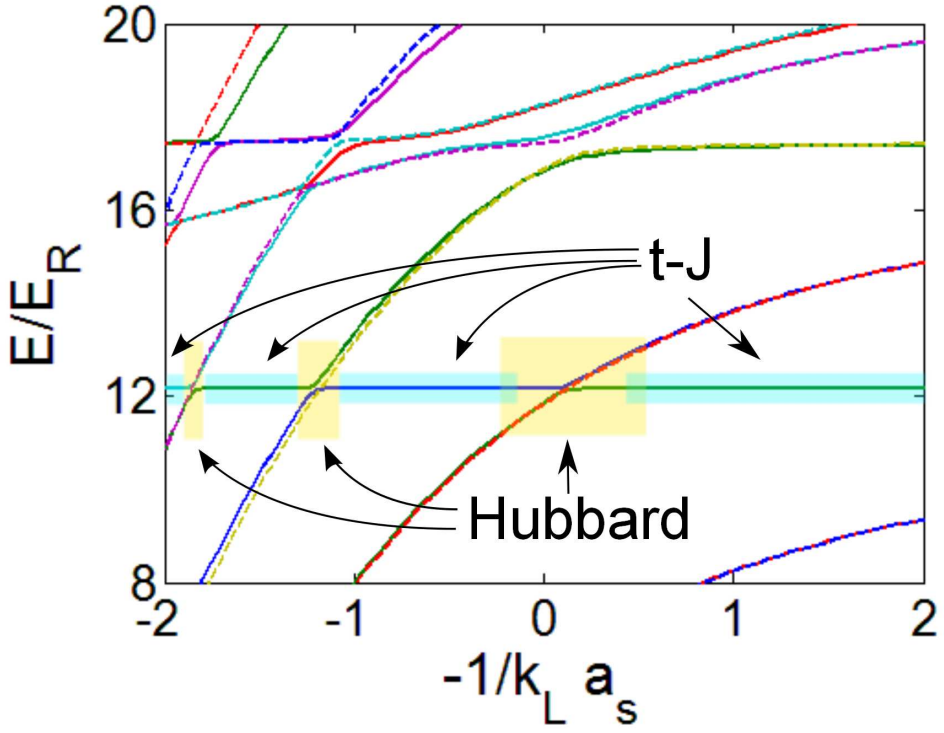

(b)

Figure 5.5: Same as Fig. 5.4 but for $V_0 = 10E_R$.

apply a general Hubbard model. This is the case in Fig. 5.4(b) at $-1/k_L a_s \sim -1.7$.

Likewise, approximation by a $t-J$ model requires that two singly occupied states are well-separated from the others, and these regions are also marked in Figs. 5.4 and 5.5. (Again, one of these states is not shown and would be indistinguishable anyway on the scale of the plot.) Note that the form of the $t-J$ model is valid at detunings where the general Hubbard model is not. There the $t-J$ model does not come from the usual perturbative treatment of the Hubbard model for $|U| \gg t$, which gives $J = 2t^2/U$ [74]. Instead it is the fundamental model in that region and there are no *a priori* constraints on the parameters. The regions of validity shown in Figs. 5.4 and 5.5 for the two types of lattice models are the main result of this chapter.

We have performed the calculations for lattice depths of $V_0 = 2 - 10E_R$. For $V_0 \leq 4E_R$, a lattice model is not valid for any value of the scattering length. At $V_0 = 6E_R$, the bandgap has increased enough that the lattice models become valid in regions, similar to those plotted in Fig. 5.4, but narrower. These regions quickly widen when the lattice depth is increased to $V_0 = 8E_R$. As the lattice is deepened to $V_0 = 10E_R$, the $t-J$ model continues to quickly expand its validity further into the weakly interacting regime, overlapping with the regions where a general Hubbard model is valid. It expands only slightly closer to unitarity. A general Hubbard model also becomes valid over only a slightly larger region.

5.4.2 Model parameters

Above we have determined the structure of the relevant model Hamiltonians across unitarity. Now we consider the details of the Hamiltonians and their parameters. Neglecting off-site interactions, the most general Hubbard-type model takes the form

[23]

$$H_{GHM} = \sum_{i,\sigma} \left(n_{i\bar{\sigma}}\Delta - \mu\right) n_{i\sigma} - \sum_{i,j,\sigma}{}' \Big[t + (g-t)\left(n_{i\bar{\sigma}} + n_{j\bar{\sigma}}\right) + \left(t_{da} + t - 2g\right) n_{i\bar{\sigma}} n_{j\bar{\sigma}} \Big] a^{\dagger}_{i\sigma} a_{j\sigma} - t_d \sum_{i,j,\sigma}{}' a^{\dagger}_{i\sigma} a^{\dagger}_{i\bar{\sigma}} a_{j\bar{\sigma}} a_{j\sigma} \quad (5.4)$$

where the prime on the sum means that only nearest neighbor terms are included, σ denotes a fermion component $\{\uparrow, \downarrow\}$ and $\bar{\sigma}$ denotes the other component, $n_{i\sigma} = a^{\dagger}_{i\sigma} a_{i\sigma}$, Δ is the on-site interaction energy, μ is the chemical potential, g is the particle-assisted tunneling rate, t_{da} is the rate for an atom to hop from a doubly occupied site to a singly occupied site, and t_d is the dimer tunneling rate. For just two atoms on two sites, the Hamiltonian can be written as the matrix

$$H^{(2,2)}_{GHM} = \begin{pmatrix} \Delta & -g & -g & -t_d \\ -g & 0 & 0 & -g \\ -g & 0 & 0 & -g \\ -t_d & -g & -g & \Delta \end{pmatrix} - 2\mu I \quad (5.5)$$

in the basis $\{|\uparrow\downarrow, 0\rangle, |\uparrow, \downarrow\rangle, |\downarrow, \uparrow\rangle, |0, \uparrow\downarrow\rangle\}$.

From the spectrum we can extract the model parameters as a function of the experimental parameters by choosing them such that the lattice model correctly reproduces the four energy levels. The resulting values depend on the scattering length and are shown in Fig. 5.6 for $V_0 = 8E_R$. The model is not valid in the hatched regions, in accord with Fig. 5.4. The particle-assisted hopping rate, g, generally differs from the single-particle hopping rate, t, by about 10%. (We use the value of t obtained from the one-atom spectrum.) Away from resonance, the on-site interaction energy, Δ, is 25% larger than the standard Hubbard U computed from the overlap of the lowest Wannier functions, but this is no doubt due in part to the additional confinement compared to the infinite lattice case. We have not shown the

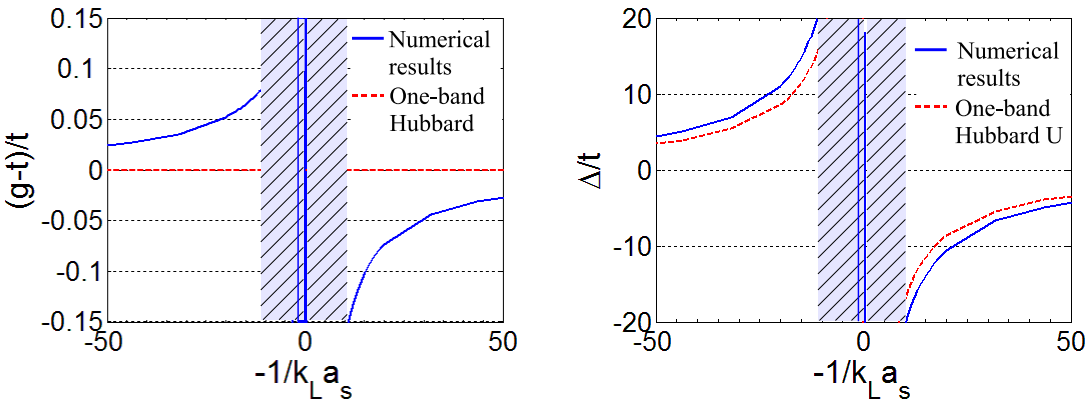

(a) (b)

Figure 5.6: (a) Particle-assisted hopping rate and (b) on-site interaction energy vs inverse scattering length for $V_0 = 8E_R$. Dimer hopping is negligible and not shown.

dimer hopping rate away from resonance, as it is negligible – less than 1% of the single-particle hopping rate in this case. Far from unitarity, where the interaction is too weak to populate higher bands, the general Hubbard model reduces to the one-band Hubbard model. In general, except for within the sliver of validity around resonance, Fig. 5.6 shows that the general Hubbard model is qualitatively similar to the standard Hubbard model with some quantitative corrections as one begins to approach the strongly interacting region.

Around unitarity, though, the general Hubbard model is strikingly different than the single-band Hubbard model, as shown in Fig. 5.7. Of course, the physical single-band approximation is not expected to hold in this region and it does not even make sense to compare the two, but it is still interesting to contrast them. Most notably, the effective on-site interaction does not become unbounded near resonance. That is not too surprising, as the relevant on-site dressed molecule state is only weakly bound at resonance, completely different from the lowest dressed molecule state. Likewise, the dimer tunneling is no longer negligible, as might be expected for an excited dimer in a relatively weak lattice. Only the particle-assisted hopping is qualitatively similar

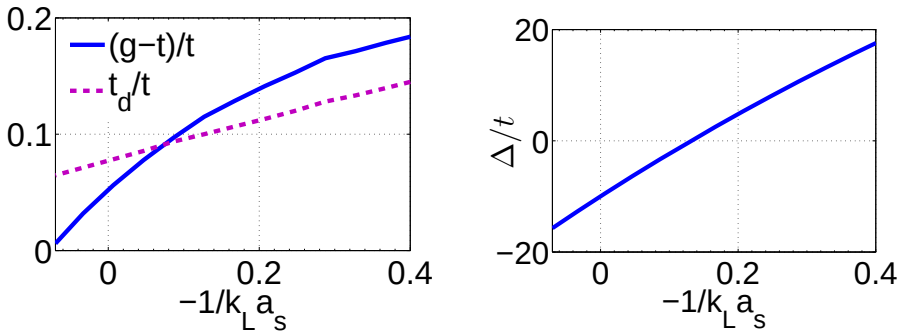

(a) (b)

Figure 5.7: (a) Particle-assisted hopping rate, dimer hopping rate, and (b) on-site interaction energy vs inverse scattering length in the narrow region around resonance where a general Hubbard model is valid for $V_0 = 8E_R$.

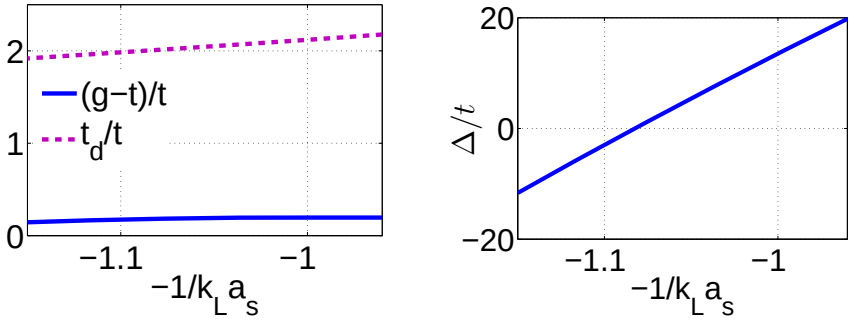

(a) (b)

Figure 5.8: Same as Fig. 5.7 but in the validity region around $-1/k_L a_s \sim -1$.

to that plotted away from unitarity.

Similarly, for the small region around the crossing of the second excited molecule state and the lowest atomic state, one can obtain the general Hubbard model parameters shown in Fig. 5.8. The particle-assisted hopping and the on-site interaction energy are much the same as in Fig. 5.7. However, here the dimer tunneling rate is much larger, twice as large as the atom tunneling rate, due to the excited nature of the relevant molecule state.

The effective $t - J$ model has the familiar form

$$H_{t-J} = -\mu \sum_{i,\sigma} n_{i\sigma} - {\sum_{i,j}}' \left[t \sum_{\sigma} P_a a^{\dagger}_{i\sigma} a_{j\sigma} P_a - J \left(\mathbf{s_i} \cdot \mathbf{s_j} - n_i n_j / 4 \right) \right], \tag{5.6}$$

where P_a is a projector onto the subspace with at most one atom per site, J is the superexchange energy, $n_i = \sum_\sigma n_{i\sigma}$, and $\mathbf{s_i} = \sum_{\sigma,\sigma'} a^\dagger_{i\sigma}\sigma_{\sigma,\sigma'}a_{i\sigma'}/2$, with σ denoting the Pauli matrices. For just two atoms on two sites, the Hamiltonian can be written as the matrix

$$H^{(2,2)}_{t-J} = -\begin{pmatrix} J & J \\ & \\ J & J \end{pmatrix} - 2\mu I \tag{5.7}$$

in the basis $\{|\uparrow,\downarrow\rangle, |\downarrow,\uparrow\rangle\}$. We extract from the spectrum the effective superexchange energy relevant for the regions where a $t-J$ model is valid. We have plotted this in Fig. 5.9, along with the result of $2t^2/U$ one would derive from the single-band Hubbard model. Again, this is just for reference, as there is no expectation that the physical single-band approximation is valid in the strongly interacting regime. It is interesting to note that J does not vanish at unitarity, but in fact passes through zero on both sides of unitarity (in fact, more than once on the positive-a_s side). This implies that one may find some transition to an exotic phase there, where the interaction is dominated by higher-order or next-nearest neighbor processes. A similar zero-crossing has previously been found on the positive a_s side of resonance in a completely different calculation [78].

As the lattice depth is adjusted, the behavior of the parameters remains qualitatively unchanged. Even the maximum values of the particle-assisted hopping rate and the superexchange energy remain more or less the same. The only exception is that t_d/t decreases quickly as the lattice becomes deeper, as expected. Where both models are valid, the $t-J$ model can be derived from the general Hubbard model and $J \simeq 2g^2/\Delta$.

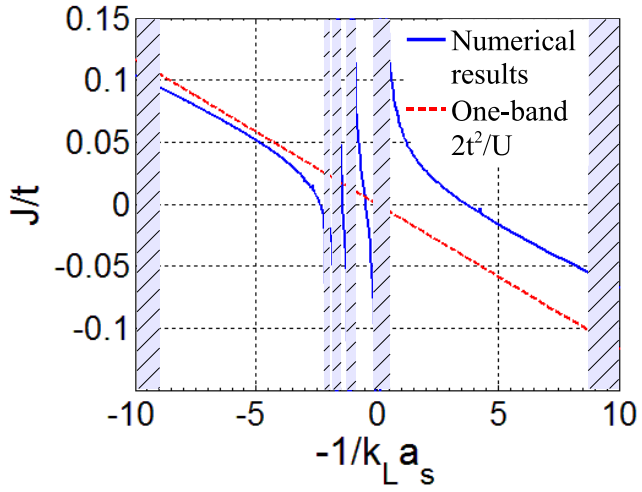

Figure 5.9: Superexchange energy vs. inverse scattering length for $V_0 = 8E_R$.

5.5 Chapter Summary

We have discussed the basic form of candidate single-band lattice Hamiltonians to describe the low-energy physics of ultracold fermionic atoms in an optical lattice. General considerations of the relevant Hilbert space and system symmetry [23] lead to two possibilities: an effective single-band generalized Hubbard model and a $t - J$ model.

We have performed numerical calculations of the spectrum of two interacting fermions in a double-well potential to determine under what conditions one of these lattice models is a good description of a physical system in a periodic optical potential. By requiring the lattice models to reproduce the low-energy two-site two-atom physics in their respective regions of validity, we have determined the one- and two-body on-site and nearest-neighbor parameters of the models. We find that at unitarity there exists a valid effective single-band Hubbard model with counterintuitive weak on-site interaction. We also find that near unitarity there exists a valid $t - J$ model whose superexchange energy can be tuned through zero on either the

attractive or repulsive side of resonance.

These models should prove useful starting points for future theoretical or experimental considerations of strongly correlated many-body physics in an optical lattice. In particular, the ability to tune J through zero suggests an interesting phase diagram in the vicinity of the crossing, and the effect of the lattice potential on the unitary regime is rather intriguing and will be further discussed in Chapter VI.

CHAPTER VI

Anharmonicity-Induced Resonances and Their Detection

6.1 Chapter Overview

When two atoms interact in the presence of an anharmonic potential, such as an optical lattice, the center of mass motion cannot be separated from the relative motion. In addition to generating a confinement-induced resonance (or shifting the position of an existing Feshbach resonance), the external potential changes the resonance picture qualitatively by introducing new resonances where molecular excited center of mass states cross the scattering threshold. We demonstrate the existence of these resonances, give their quantitative characterization in an optical superlattice, and propose an experimental scheme to detect them through controlled sweeping of the magnetic field.

6.2 Introduction

In recent years, there has been much progress in the study of ultracold atoms in optical lattices, which can cleanly emulate important models in condensed matter, hold promise for quantum computing schemes, and offer the prospect to observe many interesting new phenomena [71, 79, 80]. The versatility of this line of research is due in no small part to the control of the atomic interactions afforded by tuning an external magnetic field near a Feshbach resonance [4–6]. In addition to a mag-

netic field, a confining potential can also be used to tune the scattering length via a Feshbach-type mechanism, typically referred to as a confinement-induced resonance [32, 33, 37] or a trap-induced shape resonance [81, 82] depending on the trap configuration. The trap-induced resonance is basically caused by a shift of the free-space Feshbach resonance point by the confining potential [29]. In this chapter we point out a new effect whereby anharmonic confinement, e.g., from an optical lattice, not only shifts the free-space resonance point, but also induces a series of additional resonances. We characterize these anharmonicity induced resonances in an optical superlattice and propose an experimental scheme to detect their consequences.

To understand the basic mechanism of the anharmonicity induced resonances, let us first compare it with the free-space Feshbach resonance. The free space Feshbach resonance is caused by coupling between the scattering state of the atomic pair and a highly excited molecular level (the Feshbach molecule), as depicted in Fig. 6.1(a). When the energy of the Feshbach molecule, tuned by the external magnetic field, crosses the lowest scattering state, a resonance in the scattering length is signaled [4–6]. In free space, the center of mass (c.m.) and relative motions are decoupled during the atomic scattering, and the c.m. momentum forms a continuum which is not altered by the scattering process.

In the presence of an optical lattice, the continuum spectrum for the atomic and the molecular c.m. motion both split in a series of energy bands. We consider scattering of the atoms in the lowest bands, and only this lowest atomic band in shown in Fig. 6.1(b). However, even for this lowest-band atomic scattering, the excited bands for the c.m. motion of the Feshbach molecule still plays a significant role due to the anharmonicity of the optical lattice potential. In a harmonic potential, the c.m. motion of two colliding atoms is separated from their relative motion, and thus

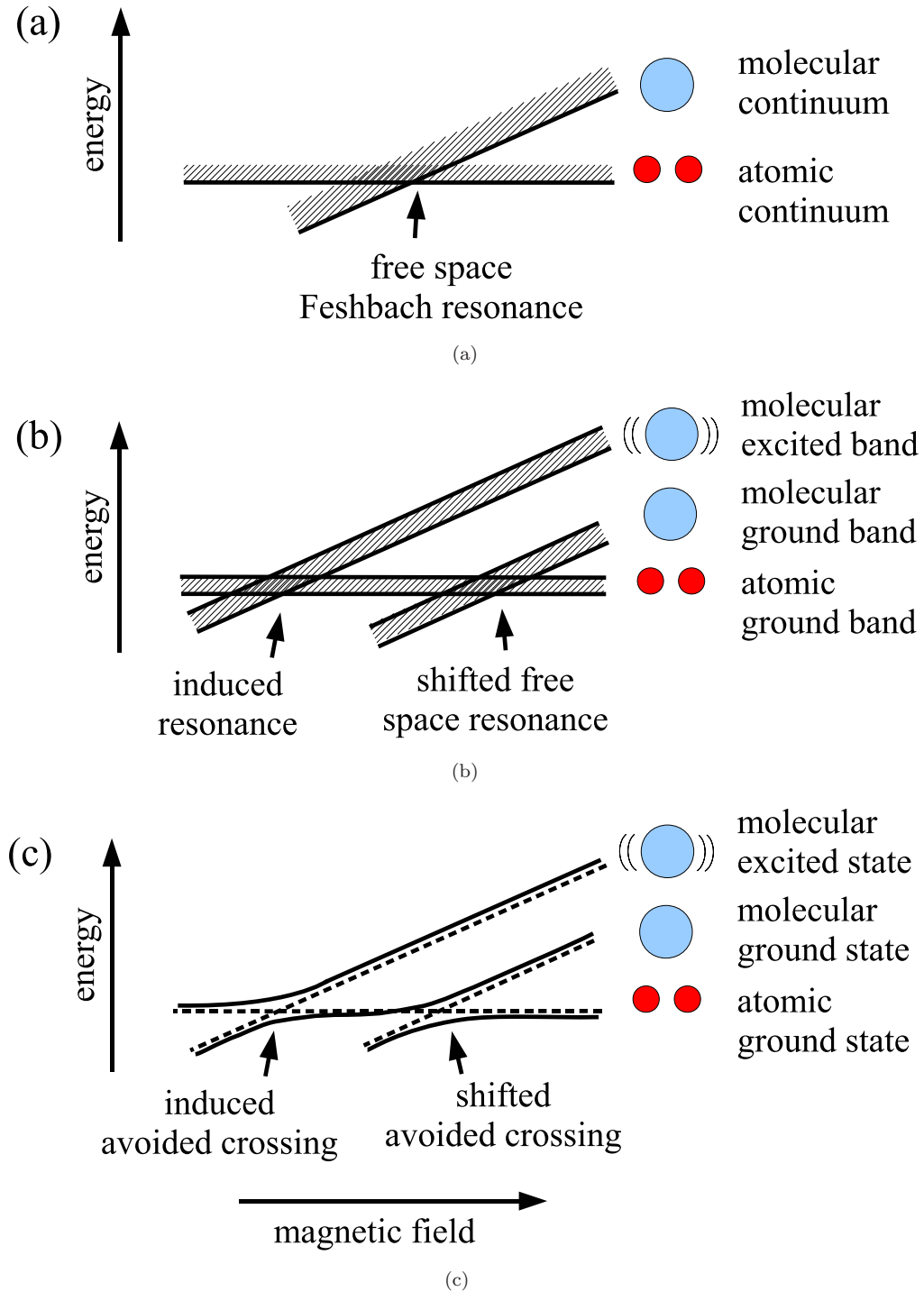

Figure 6.1: Sketches of the Feshbach type of resonances (a) in free space; (b) in an optical lattice with additional anharmonicity induced resonances; (c) in a confining potential where the resonances are signalled by the avoided level crossings.

remains in the lowest band during the collision and does not couple to the Feshbach molecule in the excited bands. However, the anharmonicity of the potential mixes the c.m. and the relative motions, and the lowest band scattering state of the atoms is coupled to the Feshbach molecule in *each band*, as depicted in Fig. 6.1(b). As one can see from this figure, all the bands for the Feshbach molecule, no matter how excited, eventually cross the atomic scattering threshold as one lowers the magnetic field. This will lead to many resonances for the atomic scattering. In practice, the anharmonic coupling between a Feshbach molecule in the excited band and the atomic pair state in the lowest band will decrease as the band becomes more excited, and the resonances become progressively narrower as one lowers the magnetic field, so only the first few of these resonances are broad enough to be experimentally observable. We also note that the coupling between the c.m. and the relative motions of the atomic pair in an anharmonic potential has been noticed recently for discussion of different physical process [83, 84].

In order to quantitatively characterize the anharmonicity induced resonances, we consider the atoms in an optical superlattice potential, as in Chapter V. In an optical lattice, direct calculation of the scattering length between two atoms is challenging as one can not separate the c.m. and the relative motion and solution of an equation with all six degrees of freedom is numerically demanding. Instead, here we consider the atoms in a deep superlattice potential [75, 85, 86], which separates the periodic optical lattice into a series of double well potentials. This has several motivations: first, by adding an confining trap, as illustrated in Fig. 6.1(c), the resonance in the continuum scattering spectrum caused by the emergence of a new Feshbach molecular level becomes an avoided level crossing in the discrete spectrum of the trapped atoms. By calculating the width and the position of the avoided level

crossing, we can approximately characterize the resonance properties for the atomic scattering. Numerically, it is more convenient to deal with the discrete spectrum in a trap which allows application of specific calculation techniques presented below. Second, the optical superlattice potential has been realized in experiments [75, 85, 86], which allows direct detection of consequences of the anharmonicity induced resonances in this kind of trap. We will propose an experimental scheme to test the quantitative predictions from the anharmonicity induced resonances in a superlattice. Third, the anharmonicity induced resonances also affect the effective many-body Hamiltonian for strongly interacting atoms in an optical lattice [22, 23], as we have seen in the previous chapter. In the derivation of such a Hamiltonian we showed it was natural to consider the effective interaction for atoms in double-well potentials realized with a deep optical superlattice.

6.3 Results

As in the previous chapter, we assume that the superlattice potential is along the axial direction z which separates the system into a series of double wells [75, 85, 86]. We consider two distinguishable fermions of mass m in each double well potential $V(z)$, numerically fixed by Taylor expanding $\cos^2 k_L z$ to 12^{th} order in z. The atoms are interacting via a short range potential $U(r)$ characterized by its s-wave scattering length a_s. For ease of calculation, the lattice wells in the transverse directions are approximated by harmonic potentials, with the frequency, ω, chosen such that the potential is locally isotropic at the bottom of each well.

In Fig. 6.2, we show the energy spectrum of two particles interacting near a free space Feshbach resonance ($1/k_L a_s = 0$) in the double-well potential. This calculation was performed using a stochastic variational method with correlated gaussian

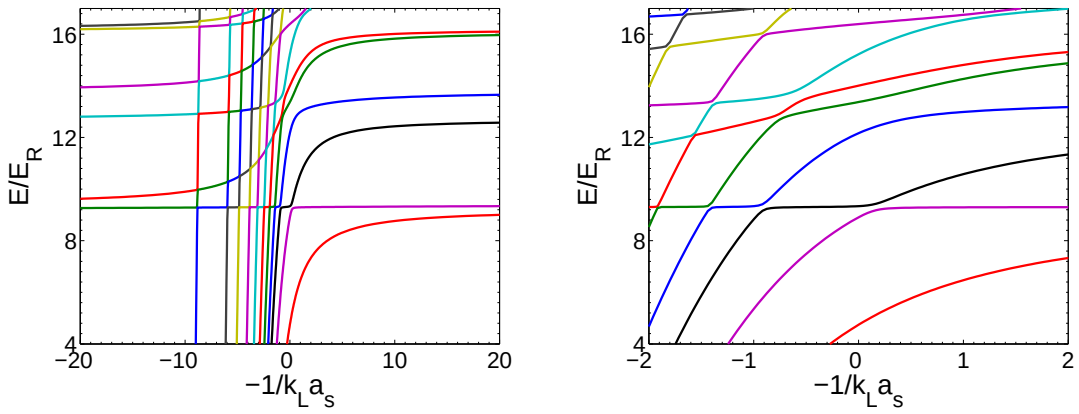

Figure 6.2: (a) Spectrum of two strongly interacting atoms in a three-dimensional double-well potential with $V_0 = 6E_R$. Only states even in Z have been plotted. Only the first few plunging levels are shown. (b) Close-up of the strongly interacting region.

basis states as in Chapter V. See Appendix C for details. For clarity, we have omitted the levels corresponding to wavefunctions of odd parity in z or Z (which have no contribution to the anharmonicity induced resonances) and plunging levels for $-1/k_L a_s < -10$. In the absence of anharmonicity, there are three kinds of curves present: plunging levels corresponding to tightly bound molecules, flat levels corresponding to atoms in separate wells, and sigmoidal levels corresponding to on-site dimers. The anharmonicity induces a rich set of avoided level crossings, each of which signals an induced resonance. The resonances become weaker away from $1/k_L a_s = 0$, so that only the first few are observable.

To characterize the anharmonicity induced resonance, we estimate the time required to adiabatically sweep across the avoided level crossing, transferring population between atomic and molecular states. In the Landau-Zener approximation [87], the probability of an adiabatic transfer at sweep rate v is $P_{ad} = 1 - \exp(-v_{LZ}/v)$, where the Landau-Zener parameter $v_{LZ} = \pi\Delta^2/2\hbar|\partial\Delta/\partial B|$, Δ is the minimum energy gap between the two levels in question, and $\partial\Delta/\partial B$ is the rate at which the

	$-1/k_L a_s$	$\Delta/\hbar$ (kHz)	t_{min} (μs)	v_{LZ} (G/s)
^{6}Li	0.2	50	40	2×10^6
	-0.9	50	70	3×10^5
	-1.4	30	100	6×10^4
	-1.9	8	200	2×10^3
	-2.5	2	1×10^3	40
^{40}K	0.2	8	600	800
	-0.9	8	600	400
	-1.4	5	1×10^3	100
	-1.9	1	2×10^3	6
	-2.5	0.3	1×10^4	0.1

Table 6.1: Induced resonance data for $V_0 = 6E_R$.

energy gap changes with the magnetic field away from the avoided crossing. The energy splitting Δ for the avoided level crossing should be proportional to the width of the corresponding anharmonicity induced resonance in a periodic optical lattice. This parameter Δ is listed in Table 6.1 for the various avoided crossings between excited molecular states and the lowest atomic level for ^{6}Li (^{40}K) atoms. To connect our results to experiment, we assume the scattering length is related to the magnetic field via the usual relation $a_s = a_{bg}\left[1 - W/\left(B - B_0\right)\right]$, where a_{bg} is the background scattering length, W is the resonance width, and B_0 is the resonance point. We take $k_L \sim 2\pi/1\mu m$ and consider ^{6}Li (^{40}K) near the free space Feshbach resonance at 834 G [48] (202 G [2]). In Table 6.1, we have also listed an estimate of the minimum time, t_{min}, required to ramp across the avoided crossing at the critical rate, v_{LZ}. If the time available in the experiment to perform the ramp is on the order of a few milliseconds, appreciable adiabatic transfer is feasible across the first five (four) avoided crossings for ^{6}Li (^{40}K) atoms.

We have performed the same kind of calculations for several lattice depths. In Fig. 6.3 we show how the energy splitting Δ and the Landau-Zener parameter v_{LZ} for the first few resonances listed in Table 6.1 change as V_0 is varied for ^{40}K. Generally, the energy splitting for the avoided level crossing decreases for deeper wells, as one

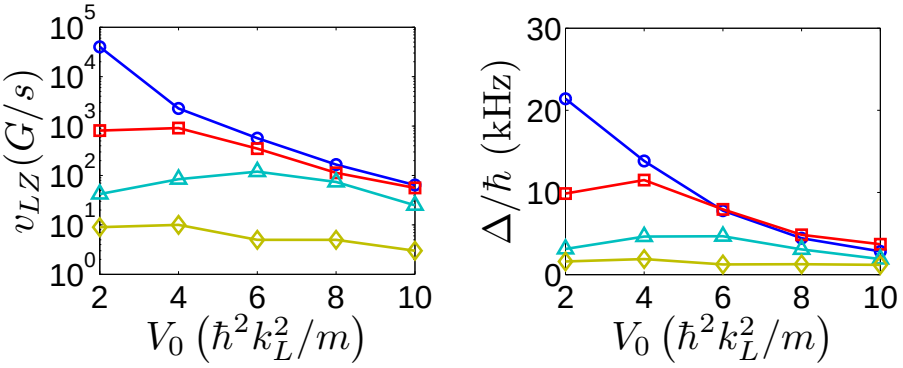

(a) (b)

Figure 6.3: (a) Energy gap and (b) Landau-Zener parameter for the first four avoided crossings vs. well depth for ^{40}K.

would expect due to suppression of the anharmonicity in a deep lattice (the harmonic approximation becomes better for a deep lattice well). For very shallow wells, though, the potential apparently cannot couple the higher c.m. states of Feshbach molecules to the lowest atomic state as efficiently, and the energy splitting Δ actually increases with the lattice depth at first for small V_0. As the potential wells are deepened, the resonance positions shift slightly to lower magnetic fields.

6.4 Detection

To experimentally detect the avoided level crossings associated with the anharmonicity induced resonances, one can take the following steps: first, one loads the optical superlattice in the weakly interacting region with two fermionic atoms of different spins in each double well [75, 85, 86, 88]. The inter-well barrier is kept high so that one has a Mott state with one atom per well. Second, one ramps the system to the strongly interacting region with $-1/k_L a_s = \pm 2$, and then quickly lower the inter-well barrier to the desired value (with $V_0 = 6E_R$ in our example), leaving the atoms still in the Mott state at this moment. The magnetic field is then adiabatically ramped across the anharmonicity induced resonances, and one detects the resulting

population distribution after the ramp. To do the detection, the inter-well barrier is quickly tuned back up to freeze the system evolution again before the magnetic field is ramped to the deep BEC side ($-1/k_L a_s \ll -1$), separating the molecular levels from the atomic levels. One can then selectively take absorption images of either the atoms or the molecules [89], and measure their distribution over different bands through a band-mapping procedure [75, 85, 86]. The presence of the anharmonicity induced level crossings can then be inferred from the final population distribution.

As an example, in Fig. 6.4(a), we show the calculation results (in the Landau-Zener approximation) of a sweep at $V_0 = 6E_R$ from $-1/k_L a_s = -2$ to $-1/k_L a_s = 2$ starting with ^{40}K atoms in the Mott state (which corresponds to the 6^{th} even eigenstate at $-1/k_L a_s = -2$). For fast sweeps, the atoms remain in the same Mott state in the lowest band (which is now the 2^{nd} even eigenstate at $-1/k_L a_s = 2$), as would be expected in the absence of anharmonicity. In the adiabatic limit, all the atoms end up in the 6^{th} even eigenstate, which corresponds to atoms in the first excited band at $-1/k_L a_s = 2$. At intermediate speeds, several excited atomic bands become populated. A sweep in the opposite direction, from $-1/k_L a_s = 2$ to $-1/k_L a_s = -2$, starting again with atoms in the Mott state, is shown in Fig. 6.4(b). When sweeping in this direction, population can be transferred to Feshbach molecules in several excited bands (the $2^{nd} - 5^{th}$ eigenstates at $-1/k_L a_s = -2$) as well as diabatically to the atomic Mott state in the lowest band (the 6^{th} state).

6.5 Chapter Summary

We predict the existence of several Feshbach-type resonances induced by the anharmonicity of the optical lattice, which couples the Feshbach molecules in the excited bands and the atomic states in the lowest bands. We have characterized the corre-

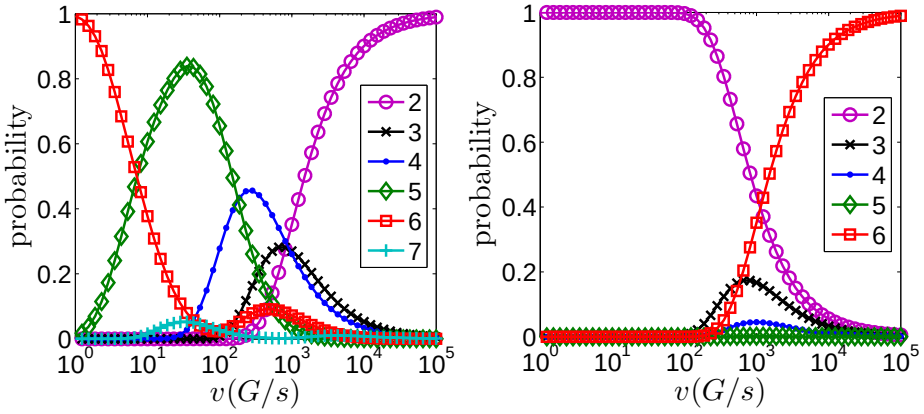

Figure 6.4: Final population distribution vs. ramp speed of the magnetic field (a) from the 6^{th} even eigenstate at $-1/k_L a_s = -2$ to the $2^{nd} - 7^{th}$ even eigenstate at $-1/k_L a_s = 2$ or (b) from the 2^{nd} even eigenstate at $-1/k_L a_s = 2$ to the $2^{nd} - 6^{th}$ even eigenstate at $-1/k_L a_s = -2$. Both plots are for ^{40}K atoms with $V_0 = 6E_R$.

sponding set of avoided level crossings in the calculated spectrum of two fermions interacting in a superlattice potential, and proposed an experimental scheme to observe these avoided crossings through slow sweeps of the magnetic field. The anharmonicity induced resonances may prove to be a useful tool for manipulation of interaction between ultracold atoms in optical lattice potentials.

CHAPTER VII

Conclusions

7.1 Summary

In this dissertation, we have explored the effect of strong interactions in combination with an optical lattice potential on the physics of a dilute fermionic gas. This is currently a topic of great interest as such a system is already experimentally attainable [50], and there are still many open questions regarding its proper description and phase diagram. The fact that the interaction can be comparable to the lattice bandgap poses a unique set of challenges and the opportunity to observe new behaviors.

We have shown that for two-component fermions interacting in an isolated anisotropic potential well near a Feshbach resonance, many bands of the trap are populated, even for a very strong trap and/or dilute gas. This is due to the formation of bound dimers for any scattering length in the presence of a trapping potential. Each dimer comprises a mixture of a tightly bound closed channel Feshbach molecule and open channel atomic Cooper pairs in various bands. No matter how dilute the atomic gas, the many-body ground state is actually a dilute gas of dimers, each having binding energy on the order of the bandgap (and length on the order of the shortest trap length, a_t, even in the weakly trapped direction), so the short-range interaction still

populates the excited bands. Also, although strengthening the trap increases the bandgap, it also decreases the dimer size, with the result that excited bands cannot be frozen out by increasing the trap depth. Thus, in a highly anisotropic trap near resonance, one cannot simply obtain a low-dimensional Hamiltonian by renormalizing the atomic scattering length with virtual transverse excitations. The real population in the transverse bands must be accounted for in the construction of an effective low-dimensional Hamiltonian.

To accomplish this, we have defined a highly localized "dressed molecule" (with characteristic length scale a_t) throughout the entire BEC-BCS crossover, composed of the Feshbach molecule dressed with atomic Cooper pairs in excited bands such that the transverse excitations of the two-body bound state are explicitly built into the structure of the dressed molecule. Furthermore, in the many-body case when the one- (two-) dimensional atomic number density is small compared to a_t^{-1} (a_t^{-2}), the transverse structure of the many-body wavefunction is fully determined by the two-body physics, because the probability for three fermions to come close to each other and populate some transverse excited band is negligible since there is no three-body bound state for two-component fermions with equal mass.

Thus, although the transverse motion is not frozen in the lowest band, it is frozen in a configuration fixed by the two-body physics and incorporated into the definition of the dressed molecule. We have accordingly described the low-energy, dilute, many-body physics via a simple low-dimensional effective Hamiltonian in terms of dressed molecules coupled to atoms in the lowest band. By matching the two-body physics emerging from the effective Hamiltonian with the exact two-body results from the full three-dimensional Hamiltonian, we have determined the parameters of the effective Hamiltonian as functions of the three-dimensional scattering length.

Leaving quasi-low-dimensional systems to consider three-dimensional optical lattices, we have numerically found the three-fermion ($\uparrow\uparrow\downarrow$) spectrum and wavefunctions across the BEC-BCS crossover in a single well (approximated as harmonic) using a Green's function method. We find that the energy of a triply occupied well is always greater than the sum of the energies of a doubly occupied well and a singly occupied well. Near resonance, the difference is on the order of the bandgap. Thus, we are justified in assuming, for a deep optical lattice with average occupation of two or less per site, that configurations with greater than double occupancy do not contribute to the low energy physics across resonance.

In addition, we have discovered an energy level crossing in the ground state, going from s-wave symmetry in the BEC regime to p-wave in the BCS regime. This crossing was independently noted at the same time by others [69], and later confirmed using more sophisticated numerical methods [68]. The abrupt change in ground state angular momentum as the magnetic field strength is adiabatically adjusted is readily explained: In the deep BEC regime, two distinguishable fermions form a tightly bound dimer and the three-body ground state is the s-wave ground state of the relative atom-dimer motion. In the deep BCS regime, the fermions are essentially noninteracting, so the three body ground state simply has two distinguishable fermions in the lowest (s-wave) band and the extra fermion in the first excited (p-wave) band because of Pauli exclusion, so the state has p-wave symmetry. Thus, there must be a ground state level crossing in the crossover region, and this may indicate a quantum phase transition in the corresponding many-body lattice system with an average of two identical and one unique fermion per site.

To determine a lattice model which properly describes the full periodic optical potential, we have presented very general arguments leading to an effective $t-J$ model

or an effective general Hubbard model with tunable on-site attraction/repulsion, dimer hopping, and occupation-dependent atom hopping [23] assuming only i) global SU(2) symmetry for the two fermion components, ii) sites are at most doubly occupied, and iii) only one on-site dimer state lies energetically close to the noninteracting state. However, these *effective* single-band models retain the multi-band physics which enter through the structure of the on-site dimer, in sharp contrast to a *physical* single-band model arising from microscopic considerations of only the lowest band. This offers a valuable tool to analyze the many-body problem in an optical lattice near a Feshbach resonance.

Assumptions (i) and (ii) are satisfied automatically in experiments with spin-independent potentials and densities of less than two atoms per site (as shown by our three-fermion calculation). We have further determined the regions where assumption (iii) is valid and the connection between the model parameters and the actual experimental parameters by explicit calculation. We have used a stochastic variational approach assuming a correlated gaussian wavefunction (see Appendix C) to obtain a numerical solution for two interacting fermions. For further simplicity, rather than consider an infinite isotropic three-dimensional periodic potential, we have taken a double-well with harmonic confinement in the transverse direction such that each well is isotropic near its minimum. From the two-body spectrum, we have determined the range of scattering lengths for which assumption (iii) is satisfied.

Furthermore, as long as the assumptions made in deriving the lattice model are valid, if one can choose the model parameters such that it reproduces the correct physics in some simple case (e.g., only two atoms on two sites) that can be treated exactly outside of the lattice model, then it should also reproduce the correct physics in more general cases that are very difficult to treat exactly. By matching the two-site

spectrum of the lattice model to the exact numerical spectrum obtained, we have determined the relationship between the experimental parameters and the model parameters. (In the case of the general Hubbard model, all the two-body parameters have been determined. The model contains one three-body process and one four-body process which cannot be fixed by a two-body calculation.)

Finally, we have demonstrated that an anharmonic external potential, such as an optical lattice, will induce additional Feshbach-type resonances in the atomic scattering due to the coupling between multiple molecular states with excited center-of-mass motion and the lowest scattering state with zero center-of-mass motion. We have found through explicit calculations for a double-well potential the avoided crossings in the bound states which are the signature of these induced resonances. Although the avoided crossings are quite narrow, we have determined that several are broad enough to transfer population from a given state to a variety of other states by performing an adiabatic ramp of the magnetic field, or a series of alternating adiabatic and diabatic ramps.

7.2 Outlook

Although most of the experiments examining quasi-low-dimensional ultracold gases to date have been performed with bosonic atoms, we anticipate that the prospect of direct observation of strongly correlated low-dimensional physics such as Luttinger liquid behavior or the Berezinskii-Kosterlitz-Thouless (BKT) transition will motivate further experiments with fermionic atoms as the state of the art progresses and allows sufficiently low temperatures to realize these phenomena. Our work in Chapters II and III may then be essential in understanding such experiments, since the multiband physics renormalizes the interaction parameters and modifies

the mapping between the parameters of a low-dimensional Hamiltonian and the experimental parameters. The necessity of our approach in order to obtain sensible predictions for the Thomas-Fermi radius of a quasi-two-dimensional fermionic gas has already been explicitly demonstrated [53], and the BKT transition temperature stemming from our approach differs appreciably from that obtained via a less subtle approach [55]. When the relevant experiments are performed, we expect they will confirm these predictions.

In three-dimensional optical lattices, progress is currently being made towards cooling fermionic gases to even smaller fractions of the Fermi temperature [90, 91]. These efforts are expected to soon open the door to exotic quantum magnetism, lattice supersolids, and other novel physics. Once this obstacle is broached, the effective lattice models laid out in Chapter V should become useful for understanding experiments performed near a Feshbach resonance. As there is great emphasis on cooling to the Néel phase, the ability to realize a $t-J$ model with the superexchange J tunable through zero is particularly interesting and relevant to ongoing research in the ultracold physics community. Also, the general Hubbard model we have derived near resonance – which includes dimer and occupation-dependent hopping – may well contain interesting physics not present in the usual Hubbard model realized far from resonance. This is a topic for future calculations.

In conclusion, we expect that the work presented in this dissertation will prove valuable in understanding experiments with strongly interacting fermions in optical lattices and provide a sound foundation for calculations of phase diagrams and other many-body considerations.

APPENDICES

APPENDIX A

Summations

In this appendix we perform the sum over the modes of a $(3-D)$-dimensional harmonic trap, $\mathbf{m}, \mathbf{n}$, and D-dimensional integration over the momentum, $\mathbf{k}$, in the untrapped directions

$$S\left(E, \mathbf{p}, \mathbf{p}'\right) \equiv \frac{1}{L^D} \sum_{\mathbf{mnk}} \frac{\gamma^*_{\mathbf{mnp}} \gamma_{\mathbf{mnp}'}}{E - 2\epsilon_{\mathbf{k}} - \varepsilon_{\mathbf{m}} - \varepsilon_{\mathbf{n}}} \,. \tag{A.1}$$

This important quantity appears in Eqs. (2.17), (3.5), and (B.8). Rewriting the numerator with the explicit definitions (2.7) and (2.9), and using the identity $\frac{1}{x} = -\int_0^\infty dt e^{tx}$ (valid for $x < 0$) to rewrite the denominator, the sum can be written as

$$\begin{aligned} S\left(E, \mathbf{p}, \mathbf{p}'\right) = & -2^{(3-D)/2} \frac{1}{L^D} \sum_{\mathbf{mnk}} \int_0^\infty dt e^{t(E - 2\epsilon_{\mathbf{k}} - \varepsilon_{\mathbf{m}} - \varepsilon_{\mathbf{n}})} \\ & \times \int d^{3-D}\mathbf{x} \langle \mathbf{x}|\mathbf{m}\rangle \langle \mathbf{x}|\mathbf{n}\rangle \langle \sqrt{2}\mathbf{p}|\mathbf{x}\rangle \int d^{3-D}\mathbf{y} \langle \mathbf{m}|\mathbf{y}\rangle \langle \mathbf{n}|\mathbf{y}\rangle \langle \sqrt{2}\mathbf{y}|\mathbf{p}'\rangle \\ = & -2^{(3-D)/2} \int \frac{d^D\mathbf{k}}{(2\pi)^D} \int_0^\infty dt e^{t(E-2\epsilon_{\mathbf{k}})} \prod_{i=1}^{3-D} \int dx_i \int dy_i e^{-2\left(x_i^2 + y_i^2\right)} \\ & \times \sum_{m_i n_i} \frac{e^{-m_i t} H_{m_i}(x_i)\, H_{m_i}(y_i)}{\sqrt{\pi} 2^{m_i} m_i!} \frac{e^{-n_i t} H_{n_i}(x_i)\, H_{n_i}(y_i)}{\sqrt{\pi} 2^{n_i} n_i!} \frac{H_{p_i}\left(\sqrt{2}x_i\right) H_{p'_i}\left(\sqrt{2}y_i\right)}{\sqrt{\pi 2^{p_i + p'_i} p_i! p'_i!}} \,, \end{aligned} \tag{A.2}$$

where $H_n(x)$ is a Hermite polynomial. Using Mehler's Hermite polynomial formula,

$$\sum_{n=0}^{\infty} \frac{w^n H_n(x)\, H_n(y)}{2^n n!} = \frac{\exp\left[\frac{2xyw - \left(x^2+y^2\right)w^2}{1-w^2}\right]}{\sqrt{1-w^2}} \,, \tag{A.3}$$

the sum over the trap modes can now be done analytically. After a little algebra and a change of variables, $\sqrt{2}x \to x$, we are left with

$$\begin{aligned} S\left(E,\mathbf{p},\mathbf{p}'\right) &= -\frac{1}{2^{(3-D)/2}\pi^{3(3-D)/2}}\int\frac{d^D\mathbf{k}}{(2\pi)^D}\int_0^\infty dt\frac{e^{t(E-2\epsilon_\mathbf{k})}}{\left(1-e^{-2t}\right)^{3-D}}\prod_{i=1}^{3-D}\frac{1}{\sqrt{2^{p_i+p_i'}p_i!p_i'!}} \\ &\quad\times\int dx_i\int dy_i\exp\left(\frac{2x_iy_ie^{-t}-x_i^2-y_i^2}{1-e^{-2t}}\right)H_{p_i}(x_i)\,H_{p_i'}(y_i) \\ &= -\frac{1}{(2\pi)^{(3-D)/2}}\int\frac{d^D\mathbf{k}}{(2\pi)^D}\int_0^\infty dt\frac{e^{t(E-2\epsilon_\mathbf{k}-\varepsilon_\mathbf{p})}}{\left(1-e^{-2t}\right)^{(3-D)/2}}\,\delta_{\mathbf{p}\mathbf{p}'}\,. \end{aligned} \tag{A.4}$$

Since the sum depends on the molecular modes $\mathbf{p}$ and $\mathbf{p}'$ only through a shift in the energy (which, of course, must be the case due to the separability of the center-of-mass motion), we will suppress those arguments and neglect $\varepsilon_\mathbf{p}$ below. The integral is divergent and we explicitly impose an energy cutoff on two dimensions by taking a lower limit $\epsilon = 1/2\pi E_c$ on the t-integration for $D \leq 1$ and an upper limit $K = \sqrt{2E_c}$ on the cylindrically radial k-integration for $D \geq 2$. However, the Hamiltonian parameters are renormalized in terms of this cutoff, so it can eventually be taken to infinity and nothing physical depends upon it. Performing the cutoff integral last, we obtain

$$S\left(E\right) = -\frac{1}{2^{3/2}\pi}\sqrt{E_c} - \frac{1}{2^{5/2}\pi}\begin{cases} -2\frac{\Gamma(-E/2)}{\Gamma(-E/2-1/2)} & D=0 \\ \zeta\left(1/2,-E/2\right) & D=1 \\ \int_0^\infty ds\left(\frac{\Gamma\left(s-\frac{E}{2}\right)}{\Gamma\left(s+\frac{1}{2}-\frac{E}{2}\right)}-\frac{1}{\sqrt{s}}\right) & D=2 \\ -\sqrt{-2E} & D=3 \end{cases} \tag{A.5}$$

where $\Gamma\left(x\right)$ is the gamma function and $\zeta\left(s,x\right) = \lim_{N\to\infty}\sum_{n=0}^N\left(n+x\right)^{-s} - \frac{(N+x)^{-s+1}}{-s+1}$ is the Hurwitz zeta function. For $D = 2$ we could not do the integral over $s \equiv k^2/2$ analytically, but we did separate out the divergence explicitly.

Strictly speaking, these results are valid only for $E < 0$, but they can be safely analytically continued to $E > 0$ for $D < 3$.

APPENDIX B

T-Matrix Calculations

In this appendix we derive the center-of-mass two-body T-matrix between atoms in arbitrary trap modes from the three-dimensional two-channel Hamiltonian, H, given in Eq. (2.5) for contact interactions. We use $|\mathbf{mnk}\rangle$ to denote an atomic pair state in trap modes $\mathbf{m}$ and $\mathbf{n}$ having relative momentum $\mathbf{k}$, and $|\mathbf{p}\rangle$ to denote a molecule in trap mode $\mathbf{p}$. The T-matrix is defined by

$$T(E) = H_I + H_I G(E)\, H_I = H_I + H_I G_0(E)\, T(E)\ , \tag{B.1}$$

where H_I is the interaction part of the Hamiltonian, $G(E) = (E^+ - H)^{-1}$ is the two-body propagator ($E^+ \equiv \lim_{\delta\to 0^+} E + i\delta$), and $G_0(E) = (E^+ - H_0)^{-1}$ is the non-interacting propagator. Putting the Hamiltonian in Eq. (2.5) into the Lippmann-Schwinger equation (B.1) and taking brackets yields

$$\begin{aligned}\langle \mathbf{mnk}|T|\mathbf{m'n'k'}\rangle = U_b\gamma_{\mathbf{mn}}^{\mathbf{m'n'}} + \sum_{\mathbf{p}} \frac{g_b\gamma_{\mathbf{mnp}}\langle \mathbf{p}|T|\mathbf{m'n'k'}\rangle}{E^+ - \varepsilon_{\mathbf{p}} - \nu_b} \\ + \sum_{\mathbf{m''n''k''}} \frac{U_b\gamma_{\mathbf{mn}}^{\mathbf{m''n''}}\langle \mathbf{m''n''k''}|T|\mathbf{m'n'k'}\rangle}{E^+ - 2\epsilon_{\mathbf{k''}} - \varepsilon_{\mathbf{m''}} - \varepsilon_{\mathbf{n''}}}\,,\end{aligned} \tag{B.2}$$

$$\langle \mathbf{p}|T|\mathbf{mnk}\rangle = g_b\gamma_{\mathbf{mnp}}^* + \sum_{\mathbf{m''n''k''}} \frac{g_b\gamma_{\mathbf{m''n''p}}^*\langle \mathbf{m''n''k''}|T|\mathbf{mnk}\rangle}{E^+ - 2\epsilon_{\mathbf{k''}} - \varepsilon_{\mathbf{m''}} - \varepsilon_{\mathbf{n''}}}\,, \tag{B.3}$$

$$\langle \mathbf{p}|T|\mathbf{p'}\rangle = \sum_{\mathbf{mnk}} \frac{g_b\gamma_{\mathbf{mnp}}^*\langle \mathbf{mnk}|T|\mathbf{p'}\rangle}{E^+ - 2\epsilon_{\mathbf{k}} - \varepsilon_{\mathbf{m}} - \varepsilon_{\mathbf{n}}}\,, \tag{B.4}$$

where we have suppressed the argument of T. Substituting Eq. (B.3) into Eq. (B.2) and using the identity $\gamma^{\mathbf{m'n'}}_{\mathbf{mn}} = \sum_{\mathbf{p}} \gamma_{\mathbf{mnp}} \gamma^*_{\mathbf{m'n'p}}$ [see Eq. (2.8)], we get

$$\langle \mathbf{mnk}|T|\mathbf{m'n'k'}\rangle = \sum_{\mathbf{p}} U_b^{\mathrm{eff}}\big(E^+ - \varepsilon_{\mathbf{p}}\big)\, \gamma_{\mathbf{mnp}} \Bigg[\gamma^*_{\mathbf{m'n'p}} + \sum_{\mathbf{m''n''k''}} \frac{\gamma^*_{\mathbf{m''n''p}}}{E^+ - 2\epsilon_{\mathbf{k''}} - \varepsilon_{\mathbf{m''}} - \varepsilon_{\mathbf{n''}}} \langle \mathbf{m''n''k''}|T|\mathbf{m'n'k'}\rangle \Bigg], \quad \text{(B.5)}$$

where

$$U_b^{\mathrm{eff}}(E) \equiv U_b - \frac{g_b^2}{\nu_b - E}\,. \quad \text{(B.6)}$$

Note that we can separate out the final state dependence on the right-hand side of the equation, so we can write the matrix element in the form:

$$\langle \mathbf{mnk}|T|\mathbf{m'n'k'}\rangle = \sum_{\mathbf{p}} U_b^{\mathrm{eff}}\big(E^+ - \varepsilon_{\mathbf{p}}\big)\, \gamma_{\mathbf{mnp}} \tilde{T}^{\mathbf{p}}_{\mathbf{m'n'k'}}\,. \quad \text{(B.7)}$$

Substituting this form into both sides of Eq. (B.5), we get

$$\tilde{T}^{\mathbf{p}}_{\mathbf{m'n'k'}} = \gamma^*_{\mathbf{m'n'p}} + \sum_{\mathbf{p'}} U_b^{\mathrm{eff}}\left(E^+ - \varepsilon_{\mathbf{p'}}\right) \tilde{T}^{\mathbf{p'}}_{\mathbf{m'n'k'}} \sum_{\mathbf{m''n''k''}} \frac{\gamma^*_{\mathbf{m''n''p}} \gamma_{\mathbf{m''n''p'}}}{E^+ - 2\epsilon_{\mathbf{k''}} - \varepsilon_{\mathbf{m''}} - \varepsilon_{\mathbf{n''}}}\,. \quad \text{(B.8)}$$

The inner sum is equal to $S\left(E^+ - \varepsilon_{\mathbf{p}}\right)\delta_{\mathbf{p'p}}$ (see Appendix A), where $S\left(E\right) \equiv S_p\left(E\right) - U_c^{-1}$ and $S_p\left(E\right)$ is defined as in Eq. (2.17), so we can solve Eq. (B.8) to obtain

$$\tilde{T}^{\mathbf{p}}_{\mathbf{m'n'k'}} = \frac{\gamma^*_{\mathbf{m'n'p}}}{1 - U_b^{\mathrm{eff}}(E^+ - \varepsilon_{\mathbf{p}})\, S(E^+ - \varepsilon_{\mathbf{p}})} \quad \text{(B.9)}$$

and, with $\left[U_p^{\mathrm{eff}}(E)\right]^{-1} \equiv \left[U_b^{\mathrm{eff}}(E)\right]^{-1} + U_c^{-1}$ as in Eq. (2.19),

$$\langle \mathbf{mnk}|T|\mathbf{m'n'k'}\rangle = \sum_{\mathbf{p}} \frac{\gamma_{\mathbf{mnp}} \gamma^*_{\mathbf{m'n'p}}}{\left[U_p^{\mathrm{eff}}(E^+ - \varepsilon_{\mathbf{p}})\right]^{-1} - S_p(E^+ - \varepsilon_{\mathbf{p}})}\,. \quad \text{(B.10)}$$

This is independent of the incoming and outgoing relative momenta due to the momentum independence of the contact interaction. For the special case of atoms asymptotically in the lowest mode of the trap, $\mathbf{m} = \mathbf{n} = \mathbf{m'} = \mathbf{n'} = \mathbf{0}$, we use the fact that $\gamma_{\mathbf{00p}} \propto \delta_{\mathbf{p},\mathbf{0}}$ to obtain Eq. (3.4) from Eq. (B.10).

We can also obtain the other matrix elements by substituting Eq. (B.10) back into Eqs. (B.3) and (B.4), which after some manipulation yields

$$\langle \mathbf{p}|T|\mathbf{mnk}\rangle = \frac{g_b \gamma^*_{\mathbf{mnp}}}{1 - U_b^{\text{eff}}(E^+ - \varepsilon_{\mathbf{p}})\, S(E^+ - \varepsilon_{\mathbf{p}})}\,, \tag{B.11}$$

and

$$\langle \mathbf{p}|T|\mathbf{p}'\rangle = \frac{g_b^2 S(E^+ - \varepsilon_{\mathbf{p}})}{1 - U_b^{\text{eff}}(E^+ - \varepsilon_{\mathbf{p}})\, S(E^+ - \varepsilon_{\mathbf{p}})}\, \delta_{\mathbf{pp}'}\,. \tag{B.12}$$

APPENDIX C

Stochastic Variational Method

In this appendix we outline the basic stochastic variational method employed in Chapters V and VI. This technique is quite powerful and in its general form is capable of handling several-fermion calculations, but we have only used it to perform calculations for two distinguishable fermions. Thus we describe below only a simple version of the method without some of the considerations necessary for a few-body problem. A detailed presentation of the more general n-body method is given in Ref. [76].

The variational wavefunction has the form

$$|\Psi\rangle = \sum_{i}^{N} \alpha_i |\phi_i\rangle \,, \tag{C.1}$$

where N is the size of the basis set, and $\{\alpha_i\}$ is a set of N linear variational parameters. Minimizing the variational energy, $E = \langle\Psi|H|\Psi\rangle/\langle\Psi|\Psi\rangle$, corresponds to solving the generalized eigenvalue problem, $\mathcal{H}\alpha = E\mathcal{B}\alpha$, where $\mathcal{H}_{ij} = \langle\phi_i|H|\phi_j\rangle$ and $\mathcal{B}_{ij} = \langle\phi_i|\phi_j\rangle$. The basis states in some set of coordinates $\mathbf{x}$ are taken as gaussians, or derivatives of gaussians, depending on the desired parity of the state,

$$\langle\mathbf{x}|\phi_i\rangle = \prod_j \left(\partial_{x_j}\right)^{1/2-P_j/2} \exp\left(-x_j^2/a_{ij}^2\right) \,, \tag{C.2}$$

where $\{a_{ij}\}$ is a set of $N \times \dim(\mathbf{x})$ nonlinear variational parameters which define the basis elements and $P_j = \pm 1$ is the parity of the state in x_j. Since the gaussians

form a complete set, the variational state can be made arbitrarily close to the exact state by taking N large enough and choosing the widths of the gaussians appropriately. Furthermore, the matrix elements of the Hamiltonian are easy to compute analytically in this basis space as functions of the a_{ij}'s.

The nonlinear variational parameters are selected from stochastically generated pools of candidates in such a way as to create an optimized basis in which to minimize the energy. The stochastic aspect allows the algorithm to escape local minima in the energy landscape and find the true global minimum. The algorithm is as follows: starting with a set of $N-1$ basis states,

1) a pool of (in our calculations) 25 new basis states is randomly generated, each defined by a given set of $\dim(\mathbf{x})$ values, $\{a_{Nj}\}$;

2) for each of the 25 possible N-dimensional basis sets formed by adding one basis state from the candidate pool, the energy is minimized with respect to α;

3) the new basis set that yields the lowest energy is kept and the previous steps are repeated until the basis size, N, has increased to the desired number.

In practice, linear independence of the basis set is also enforced and convergence is sped by randomly generating the gaussian widths within some predetermined physically reasonable range of values.

However, this process alone is not very efficient because some basis states which represent the best choice at a given basis size are not helpful in larger basis sets. As an extreme example, imagine that $\Psi_{\text{exact}}(x) = e^{-10x^2} + e^{-x^2/10}$. After one iteration, the algorithm will have chosen a compromise like $\Psi(x) = 2e^{-5x^2}$. Then several more iterations will be needed to approximate Ψ_{exact} with any accuracy, when only two basis states are really necessary. To reduce this sort of inefficiency, we implement a refining process to re-optimize the basis states as we increase the basis size. After

every addition of two new basis states following the process above, we make two refining passes, where each pass is as follows: starting with a set of N basis states and $n = 1$,

A) a pool of 25 replacement basis states is randomly generated, each defined by a given set of $\dim(\mathbf{x})$ values, $\{a_{nj}\}$;

B) for each of the 25 possible N-dimensional basis sets formed by replacing the n^{th} old basis state with a new one from the candidate pool, the energy is minimized with respect to α;

C) if the lowest of these 25 energies is lower than the current variational energy, the n^{th} old basis state is replaced by the new optimal one and the previous steps are repeated for $n = 1...N$.

Fortunately, during the refinement process, we do not need to solve the generalized eigenvalue problem for the $N \times N$ matrix $25N$ times, since the eigenvalues of the matrix with one basis state replaced can be obtained from the eigenvalues of the original matrix via a simple root-finding procedure [76].

BIBLIOGRAPHY

BIBLIOGRAPHY

[1] M. H. Anderson, J. R. Ensher, M. R. Matthews, C. E. Wieman, and E. A. Cornell. Observation of Bose-Einstein Condensation in a Dilute Atomic Vapor. *Science*, 269(5221):198–201.

[2] C. A. Regal, M. Greiner, and D. S. Jin. Observation of resonance condensation of fermionic atom pairs. *Phys. Rev. Lett.*, 92(4):040403, January 2004.

[3] M. Greiner, O. Mandel, T. Esslinger, T. W. Hansch, and I. Bloch. Quantum phase transition from a superfluid to a Mott insulator in a gas of ultracold atoms. *Nature*, 415(6867):39–44, January 2002.

[4] E. Timmermans, P. Tommasini, M. S. Hussein, and A. Kerman. Feshbach resonances in atomic Bose-Einstein condensates. *Phys. Rep.*, 315(1-3):199–230, July 1999.

[5] R. A. Duine and H. T. C. Stoof. Atom-molecule coherence in Bose gases. *Phys. Rep.*, 396: 115–195, June 2004.

[6] C. Chin, R. Grimm, P. Julienne, and E. Tiesinga. Feshbach Resonances in Ultracold Gases. *ArXiv e-prints*, arXiv:0812.1496v1, December 2008.

[7] J. Dalibard and C. Cohen-Tannoudji. Laser cooling below the doppler limit by polarization gradients: simple theoretical models. *J. Opt. Soc. Am. B*, 6(11):2023–2045, 1989.

[8] M. G. Prentiss. Bound by Light. *Science*, 260:1078–1080, May 1993.

[9] P. Jessen and I. Deutsch. Optical lattices. *Adv. Atom. Mol. Opt. Phys.*, 37(95), 1996.

[10] L. Guidoni and P. Verkerk. Optical lattices: cold atoms ordered by light. *Journal Of Optics B: Quantum and Semiclassical Optics*, 1:23–45, 1999.

[11] P. Berman. *Quantum Optics*. Physics 542 lecture notes, 2007.

[12] M. H. Szymanska, K. Goral, T. Kohler, and K. Burnett. Conventional character of the BCS-BEC crossover in ultracold gases of K-40. *Phys. Rev. A*, 72(1):013610, July 2005.

[13] W. Yi and L.-M. Duan. BCS-BEC crossover and quantum phase transition for Li-6 and K-40 atoms across the Feshbach resonance. *Phys. Rev. A*, 73(6):063607, June 2006.

[14] W. Zwerger A. Recati, P. O. Fedichev and P. Zoller. Fermi one-dimensional quantum gas: Luttinger liquid approach and spin-charge separation. *Journal of Optics B: Quantum and Semiclassical Optics*, 5(2):S55–S64.

[15] D. E. Sheehy and L. Radzihovsky. Quantum decoupling transition in a one-dimensional feshbach-resonant superfluid. *Phys. Rev. Lett.*, 95(13):130401, September 2005.

[16] A. Recati, J. N. Fuchs, and W. Zwerger. Boson-fermion resonance model in one dimension. *Phys. Rev. A*, 71(3):033630, Mar 2005.

[17] E. Orignac and R. Citro. Phase transitions in the boson-fermion resonance model in one dimension. *Phys. Rev. A*, 73(6):063611, June 2006.

[18] Han Pu Paata Kakashvili, S. G. Bhongale and C. J. Bolech. Signatures of strong correlations in one-dimensional ultracold atomic fermi gases. *Phys. Rev. A*, 78(4):041602, 2008.

[19] R. Jördens, N. Strohmaier, K. Günter, H. Moritz, and T. Esslinger. A Mott insulator of fermionic atoms in an optical lattice. *Nature*, 455(7210):204–207, 2008.

[20] D.B.M. Dickerscheid, U. Al Khawaja, D. van Oosten, and H.T.C. Stoof. Feshbach resonances in an optical lattice. *Phys. Rev. A*, 71(4):043604, April 2005.

[21] L. D. Carr and M. J. Holland. Quantum phase transitions in the fermi-bose hubbard model. *Phys. Rev. A*, 72(3):031604, Sep 2005.

[22] L.-M. Duan. Effective Hamiltonian for fermions in an optical lattice across a Feshbach resonance. *Phys. Rev. Lett.*, 95(24):243202, December 2005.

[23] L.-M. Duan. General Hubbard model for strongly interacting fermions in an optical lattice and its phase detection. *Europhysics Letters*, 81:20001, January 2008.

[24] J. P. Kestner and L.-M. Duan. Conditions of low dimensionality for strongly interacting atoms under a transverse trap. *Phys. Rev. A*, 74(5):053606, November 2006.

[25] J. P. Kestner and L.-M. Duan. Effective low-dimensional hamiltonian for strongly interacting atoms in a transverse trap. *Phys. Rev. A*, 76(6):063610, December 2007.

[26] J. P. Kestner and L.-M. Duan. Level crossing in the three-body problem for strongly interacting fermions in a harmonic trap. *Phys. Rev. A*, 76(3):033611, September 2007.

[27] B. Paredes, A. Widera, V. Murg, O. Mandel, S. Fölling, I. Cirac, G.V. Shlyapnikov, T.W. Hänsch, and I. Bloch. Tonks–Girardeau gas of ultracold atoms in an optical lattice. *Nature*, 429:277–281, 2004.

[28] T. Kinoshita, T. Wenger, and D. S. Weiss. Observation of a One-Dimensional Tonks-Girardeau Gas. *Science*, 305:1125–1128, August 2004.

[29] M. Köhl, H. Moritz, T. Stöferle, K. Günter, and T. Esslinger. Fermionic atoms in a three dimensional optical lattice: Observing fermi surfaces, dynamics, and interactions. *Phys. Rev. Lett.*, 94(8):080403, March 2005.

[30] T. Stöferle, H. Moritz, K. Günter, M. Köhl, and T. Esslinger. Molecules of fermionic atoms in an optical lattice. *Phys. Rev. Lett.*, 96(3):030401, 2006.

[31] Y. Castin. Simple theoretical tools for low dimension bose gases. *J. Phys. IV France*, 116:89, 2004.

[32] M. Olshanii. Atomic scattering in the presence of an external confinement and a gas of impenetrable bosons. *Phys. Rev. Lett.*, 81(5):938–941, August 1998.

[33] T. Bergeman, M. G. Moore, and M. Olshanii. Atom-atom scattering under cylindrical harmonic confinement: Numerical and analytic studies of the confinement induced resonance. *Phys. Rev. Lett.*, 91(16):163201, October 2003.

[34] T. Busch, B. G. Englert, K. Rzazewski, and M. Wilkens. Two cold atoms in a harmonic trap. *Found. Phys.*, 28(4):549–559, April 1998.

[35] D. S. Petrov, M. Holzmann, and G. V. Shlyapnikov. Bose-einstein condensation in quasi-2d trapped gases. *Phys. Rev. Lett.*, 84(12):2551–2555, March 2000.

[36] D. S. Petrov and G. V. Shlyapnikov. Interatomic collisions in a tightly confined bose gas. *Phys. Rev. A*, 64(1):012706, June 2001.

[37] P. O. Fedichev, M. J. Bijlsma, and P. Zoller. Extended molecules and geometric scattering resonances in optical lattices. *Phys. Rev. Lett.*, 92(8):080401, February 2004.

[38] C. Orzel, A. K. Tuchman, M. L. Fenselau, M. Yasuda, and M. A. Kasevich. Squeezed states in a Bose-Einstein condensate. *Science*, 291(5512):2386–2389, March 2001.

[39] D. Jaksch, C. Bruder, J. I. Cirac, C. W. Gardiner, and P. Zoller. Cold bosonic atoms in optical lattices. *Phys. Rev. Lett.*, 81(15):3108–3111, October 1998.

[40] M. W. Zwierlein, C. A. Stan, C. H. Schunck, S. M. F. Raupach, A. J. Kerman, and W. Ketterle. Condensation of pairs of fermionic atoms near a Feshbach resonance. *Phys. Rev. Lett.*, 92(12), March 2004.

[41] C. Chin, M. Bartenstein, A. Altmeyer, S. Riedl, S. Jochim, J. H. Denschlag, and R. Grimm. Observation of the pairing gap in a strongly interacting Fermi gas. *Science*, 305(5687):1128–1130, August 2004.

[42] R. B. Diener and T.-L. Ho. Fermions in Optical Lattices Swept across Feshbach Resonances. *Phys. Rev. Lett.*, 96(1):010402, January 2006.

[43] V. A. Yurovsky. Properties of quasi-one-dimensional molecules with Feshbach-resonance interaction. *Phys. Rev. A*, 73(5):052709, May 2006.

[44] D. B. M. Dickerscheid and H. T. C. Stoof. Feshbach molecules in a one-dimensional Fermi gas. *Phys. Rev. A*, 72(5):053625, November 2005.

[45] S. J. J. M. F. Kokkelmans, J. N. Milstein, M. L. Chiofalo, R. Walser, and M. J. Holland. Resonance superfluidity: Renormalization of resonance scattering theory. *Phys. Rev. A*, 65(5): 053617, May 2002.

[46] D. Blume and C. H. Greene. Fermi pseudopotential approximation: Two particles under external confinement. *Phys. Rev. A*, 65(4):043613, April 2002.

[47] Q. J. Chen, J. Stajic, S. Tan, and K. Levin. BCS-BEC crossover: From high temperature superconductors to ultracold superfluids. *Phys. Rep.*, 412(1):1–88, June 2005.

[48] M. Bartenstein, A. Altmeyer, S. Riedl, R. Geursen, S. Jochim, C. Chin, J. H. Denschlag, R. Grimm, A. Simoni, E. Tiesinga, C. J. Williams, and P. S. Julienne. Precise determination of Li-6 cold collision parameters by radio-frequency spectroscopy on weakly bound molecules. *Phys. Rev. Lett.*, 94(10):103201, March 2005.

[49] H. Moritz, T. Stoferle, K. Gunter, M. Kohl, and T. Esslinger. Confinement induced molecules in a 1D Fermi gas. *Phys. Rev. Lett.*, 94(21):210401, June 2005.

[50] J. K. Chin, D. E. Miller, Y. Liu, C. Stan, W. Setiawan, C. Sanner, K. Xu, and W. Ketterle. Evidence for superfluidity of ultracold fermions in an optical lattice. *Nature*, 443(7114):961–964, October 2006.

[51] Z. Hadzibabic, P. Kruger, M. Cheneau, B. Battelier, and J. Dalibard. Berezinskii-Kosterlitz-Thouless crossover in a trapped atomic gas. *Nature*, 441(7097):1118–1121, June 2006.

[52] E. L. Bolda, E. Tiesinga, and P. S. Julienne. Pseudopotential model of ultracold atomic collisions in quasi-one- and two-dimensional traps. *Phys. Rev. A*, 68(3):032702, September 2003.

[53] Wei Zhang, G. D. Lin, and L. M. Duan. BCS-BEC crossover of a quasi-two-dimensional Fermi gas: The significance of dressed molecules. *Phys. Rev. A*, 77(6), June 2008. ISSN 1050-2947.

[54] G.-D. Lin. Personal communication, 2008.

[55] Wei Zhang, G. D. Lin, and L. M. Duan. Berezinskii-Kosterlitz-Thouless transition in a trapped quasi-two-dimensional Fermi gas near a Feshbach resonance. *Phys. Rev. A*, 78(4), October 2008.

[56] D. S. Petrov. Three-body problem in Fermi gases with short-range interparticle interaction. *Phys. Rev. A*, 67(1):010703, January 2003.

[57] C. Mora, A. Komnik, R. Egger, and A. O. Gogolin. Four-body problem and BEC-BCS crossover in a quasi-one-dimensional cold fermion gas. *Phys. Rev. Lett.*, 95(8):080403, August 2005.

[58] M. Stoll and T. Kohler. Production of three-body Efimov molecules in an optical lattice. *Phys. Rev. A*, 72(2):022714, August 2005.

[59] F. Werner and Y. Castin. Unitary quantum three-body problem in a harmonic trap. *Phys. Rev. Lett.*, 97(15):150401, October 2006.

[60] S. Y. Chang and G. F. Bertsch. Unitary Fermi gas in a harmonic trap. *Phys. Rev. A*, 76(2): 021603, August 2007.

[61] M. W. Zwierlein, A. Schirotzek, C. H. Schunck, and W. Ketterle. Fermionic superfluidity with imbalanced spin populations. *Science*, 311(5760):492–496, January 2006.

[62] G. B. Partridge, W. H. Li, R. I. Kamar, Y. A. Liao, and R. G. Hulet. Pairing and phase separation in a polarized fermi gas. *Science*, 311(5760):503–505, January 2006.

[63] D. E. Sheehy and L. Radzihovsky. BEC BCS crossover, phase transitions and phase separation in polarized resonantly-paired superfluids. *Ann. Phys.*, 322:1790–1924, August 2007.

[64] W. Yi and L.-M. Duan. Trapped fermions across a Feshbach resonance with population imbalance. *Phys. Rev. A*, 73(3):031604, March 2006.

[65] T. N. De Silva and E. J. Mueller. Surface tension in unitary Fermi gases with population imbalance. *Phys. Rev. Lett.*, 97(7):070402, August 2006.

[66] K. Huang and C. N. Yang. Quantum-Mechanical Many-Body Problem With Hard-Sphere Interaction. *Phys. Rev.*, 105(3):767–775, 1957.

[67] J. L. Powell and B. Crasemann. *Quantum Mechanics*. Addison-Wesley, Reading, MA, 1961.

[68] J. von Stecher, C. H. Greene, and D. Blume. Energetics and structural properties of trapped two-component Fermi gases. *Phys. Rev. A*, 77(4):043619, April 2008.

[69] I. Stetcu, B. R. Barrett, U. van Kolck, and J. P. Vary. Effective theory for trapped few-fermion systems. *Phys. Rev. A*, 76(6):063613, December 2007.

[70] L.-M. Duan, E. Demler, and M. D. Lukin. Controlling Spin Exchange Interactions of Ultracold Atoms in Optical Lattices. *Phys. Rev. Lett.*, 91(9):090402, August 2003.

[71] D. Jaksch and P. Zoller. The cold atom Hubbard toolbox. *Ann. Phys.*, 315:52–79, January 2005.

[72] M. Lewenstein, A. Sanpera, V. Ahufinger, B. Damski, A. Sen, and U. Sen. Ultracold atomic gases in optical lattices: mimicking condensed matter physics and beyond. *Advances in Physics*, 56:243–379, March 2007.

[73] F. Werner, O. Parcollet, A. Georges, and S. R. Hassan. Interaction-Induced Adiabatic Cooling and Antiferromagnetism of Cold Fermions in Optical Lattices. *Phys. Rev. Lett.*, 95(5):056401, July 2005.

[74] A. Auerbach. *Interacting Electrons and Quantum Magnetism*. Springer-Verlag, New York, 1994.

[75] S. Fölling, S. Trotzky, P. Cheinet, M. Feld, R. Saers, A. Widera, T. Müller, and I. Bloch. Direct observation of second-order atom tunnelling. *Nature*, 448:1029–1032, August 2007.

[76] Y. Suzuki and K. Varga. *Stochastic Variational Approach to Quantum-Mechanical Few-Body Problems*. Springer-Verlag, Berlin, 1998.

[77] J. von Stecher and C. H. Greene. Spectrum and Dynamics of the BCS-BEC Crossover from a Few-Body Perspective. *Phys. Rev. Lett.*, 99(9):090402, August 2007.

[78] C. J. M. Mathy and D. A. Huse. Accessing the Neel phase of ultracold fermionic atoms in a simple-cubic optical lattice. *ArXiv e-prints*, arXiv:0903.0108v1, February 2009.

[79] I. Bloch. Ultracold quantum gases in optical lattices. *Nat. Phys.*, 1:23–30, October 2005.

[80] I. Bloch, J. Dalibard, and W. Zwerger. Many-body physics with ultracold gases. *Rev. Mod. Phys.*, 80:885–964, July 2008.

[81] R. Stock, I. H. Deutsch, and E. L. Bolda. Quantum State Control via Trap-Induced Shape Resonance in Ultracold Atomic Collisions. *Phys. Rev. Lett.*, 91(18):183201, October 2003.

[82] M. Krych and Z. Idziaszek. Controlled collisions of two ultracold atoms in separate harmonic traps. *ArXiv e-prints*, arXiv:0904.4203v1, April 2009.

[83] E. L. Bolda, E. Tiesinga, and P. S. Julienne. Ultracold dimer association induced by a far-off-resonance optical lattice. *Phys. Rev. A*, 71(3):033404, March 2005.

[84] J. Mentink and S. Kokkelmans. Two interacting atoms in an optical lattice site with anharmonic terms. *Phys. Rev. A*, 79(3):032709, March 2009.

[85] M. Anderlini, P.J. Lee, B.L. Brown, J. Sebby-Strabley, W.D. Phillips, and JV Porto. Controlled exchange interaction between pairs of neutral atoms in an optical lattice. *Nature*, 448(7152): 452–456, 2007.

[86] S. Trotzky, P. Cheinet, S. Folling, M. Feld, U. Schnorrberger, AM Rey, A. Polkovnikov, EA Demler, MD Lukin, and I. Bloch. Time-resolved observation and control of superexchange interactions with ultracold atoms in optical lattices. *Science*, 319(5861):295, 2008.

[87] C. Zener. Non-Adiabatic Crossing of Energy Levels. *Royal Society of London Proceedings Series A*, 137:696–702, September 1932.

[88] T. Goodman and L.-M. Duan. Test of particle-correlated tunneling for strongly interacting fermions in an optical superlattice. *Phys. Rev. A*, 79(2):023617, 2009.

[89] C. A. Regal, C. Ticknor, J. L. Bohn, and D. S. Jin. Creation of ultracold molecules from a Fermi gas of atoms. *Nature*, 424:47–50, July 2003.

[90] Tin-Lun Ho and Qi Zhou. Squeezing out the entropy of fermions in optical lattices. *Proceedings of the National Academy of Sciences*, 106(17):6916–6920.

[91] A. Georges L. De Leo F. Gerbier C. Salomon J.-S. Bernier, C. Kollath and M. Köhl. Cooling fermionic atoms in optical lattices by shaping the confinement. *Phys. Rev. A*, 79(6):061601, 2009.